The Energy Doubler

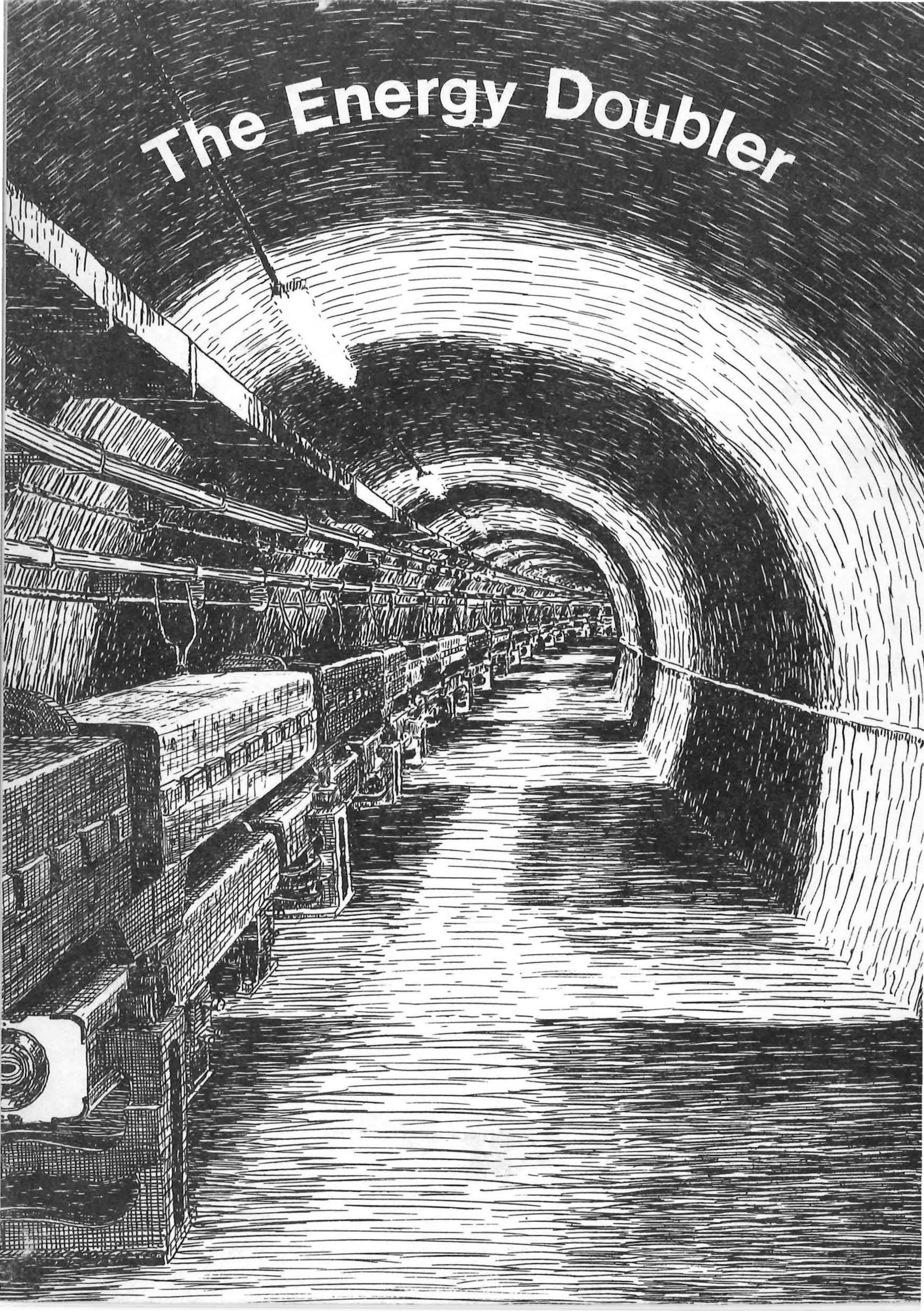

DRAFT VERSION

Prepared for the 1976 Summer Study
on Use of the Energy Doubler

Cover design by Angela M. Gonzales

THE ENERGY DOUBLER

A PROGRESS REPORT FOR THE ENERGY DOUBLER, SAVER, COLLIDER PROJECT

JUNE 1976

FERMI NATIONAL ACCELERATOR LABORATORY
BATAVIA, ILLINOIS

Operated by Universities Research Association, Inc., under contract with the U.S. Energy Research and Development Administration

TABLE OF CONTENTS

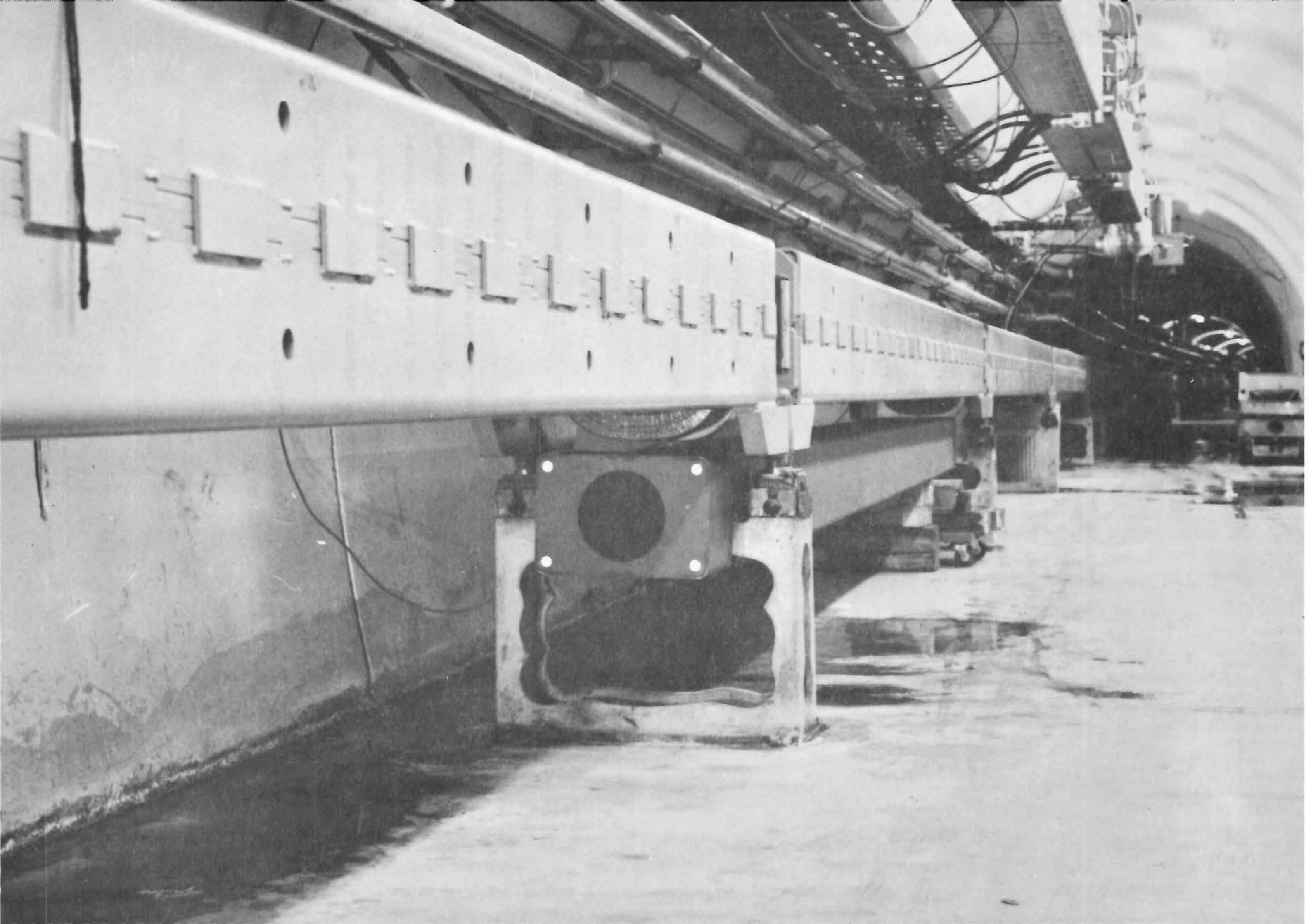

1. INTRODUCTION

The Energy Doubler is a 1000-GeV superconducting-magnet synchrotron to be installed in the existing Main-Ring tunnel of the Fermi National Accelerator Laboratory 500-GeV accelerator. The frontispiece shows a model of the proposed magnet installation under the existing Main-Ring magnets. The Main Ring will serve as injector for the Energy Doubler and accelerated beams from the Doubler will be extracted and transported to existing Fermilab experimental areas through the present Beam-Switchyard tunnels.

The use of the Energy Doubler in extending high-energy physics experiments is discussed in the next section and in more detail in Appendix I. The Doubler represents an inexpensive way of achieving higher energy while preserving the advantages of a fixed-target accelerator. Because two beams are present in the same tunnel, by reversing the direction of the beam, interesting colliding-beams experiments can be made.

It should not be forgotten that there are other significant advantages of the Energy Doubler. With the increasing awareness of a long-range energy shortage and with rising costs of electrical power, an important facet of a superconducting ring is its use as an "Energy Saver".

In routine Main-Ring operation at 400 GeV, a cycle that can be used has a 7-sec repetition rate, including a 2-sec flattop. This cycle entails a power consumption of approximately 90MW. The same cycling rate with the same flattop and intensity can also be produced using the Doubler at 400-GeV excitation. For example, protons can be accelerated to 275 GeV in the present accelerator, then transferred to the Doubler, where they can be further accelerated to 400 GeV at the rate of 50 GeV/sec; i.e., 2.5 sec up, 2 sec flattop, 2.5 sec down. The power consumption of the conventional system would then be only 23MW and that of the Doubler would be approximately 7MW. A total of 30MW instead of 90MW would bring a saving of up to $7.5 million per year at present rates, assuming that the accelerator pulsed continuously. The cost of the liquid nitrogen needed for the helium refrigerators which would be about $1 million, should be subtracted from this total. We intend to operate the present accelerator at higher energy in the coming year, up to 500 GeV, which we have recently achieved, so the saving could be considerably higher.

Use of the Saver to increase the maximum energy of the accelerator can be achieved with no additional operating cost and any energy up to 1000 GeV should be possible. It is also evident that the length of the flattop--a dominant cost factor for the present accelerator--can be extended without extra cost for the Doubler. As a result of this energy-saving aspect of the Energy Doubler, we sometimes use the name "Energy Doubler/Saver".

We have also investigated the use of the new Doubler ring as a beam stretcher. In this mode, there is no acceleration in the new ring. The beam is transferred from the Main Ring into the Doubler, which is held at constant field. Slow extraction from the Energy Doubler then lasts until the next pulse is available for injection. In principle, a duty factor of close to to 100% could result. For most experiments; i.e., those limited by counting rate, this is equivalent to a five-fold increase of intensity.

We have thus discussed three different possible modes of operation, but there is a continuous spectrum of energy, pulse rate, and flattop length lying between them.

More recently, there have been studies on colliding beams at Fermilab. It now appears that a step-by-step approach to colliding-beam experiments is feasible. Modest outlays of money are expected to give some of the important information expected of a storage-ring program, so that later, more-expensive steps can be better designed. As one example, it is crucial to know at what energy the mediating boson of the weak-interaction neutrino force manifests itself. Simple and relatively inexpensive experiments can be designed that have a good chance of answering this fundamental question. There are many other kinds of information that would unfold in the series of escalating steps that would eventually lead to a full-fledged colliding-beam facility such as POPAE.

One possible step would be a small storage ring (SSR) that will allow 25-GeV protons (or 50 to 60-GeV protons if the small ring uses supermagnets) to collide with the beam in the Main Ring without interference with regular use of the Main Ring. A center-of-mass energy of 200 GeV at a luminosity of about $10^{31} cm^{-2} sec^{-1}$ could be available in a few years from the time the experimenters have found the approximately $5 million that they have estimated is needed for its construction.

The completion of the Energy Doubler will provide for another step. Collisions could be made to occur between protons in the SSR and protons in the Doubler; then the c.m. energy would go up to about 300 GeV. The luminosity would be increased in that case, perhaps by a factor of ten, because the Doubler could also be used as a storage ring in which the beam from the Main Ring could be stacked. What has allowed the use of the Doubler as a storage ring is that the aperture has been increased to 7.6 cm in order to be able to extract the beam efficiently to the experimental areas.

An important and perhaps even more economical step than the one just described is inherent in the construction of the Doubler. It is feasible to bring about collisions between protons in the Main Ring with those in the Doubler. For this, the direction of the beam in the Main Ring must be reversed for reversed injection into the Doubler. We can make it possible to do this reversal by adding a small length of tunnel near the Booster injector, so that the beam can be reversed upon injection and then accelerated to full energy.

In order to facilitate bringing the two beams into collision, the position of the Doubler has been moved from the top of the tunnel to just below the Main Ring, as shown in the frontispiece and in the drawing of Fig. 1. Thus, for a very modest extra expense; i.e., the reversing tunnel, which might cost a few hundred thousand dollars, important exploratory experiments could be made at luminosities of about $10^{31} cm^{-2} sec^{-1}$ and at c.m. energies of up to approximately 1000 GeV. This energy corresponds to 250 GeV in the Main Ring incident on 1000 GeV in the Doubler. Higher energies could be reached by pulsing the Main Ring, but at the cost of duty cycle.

With such a program, it would be possible to have a significant colliding-beam facility at Fermilab that would be able to explore the deepest part of the proton at c.m. energies well above 1 TeV and at luminosities up to $10^{31} cm^{-2} sec^{-1}$.

Since September 1972, when Energy-Doubler effort by Fermilab began, substantial technological progress has been achieved in the areas of superconducting magnets and cryogenic-system development. This work has benefited by the ERDA-supported programs at the other labs, such as BNL and LBL. An important milestone was reached on March 12, 1976, when the first full-size Energy-Doubler prototype magnet successfully achieved its design field. This success established the

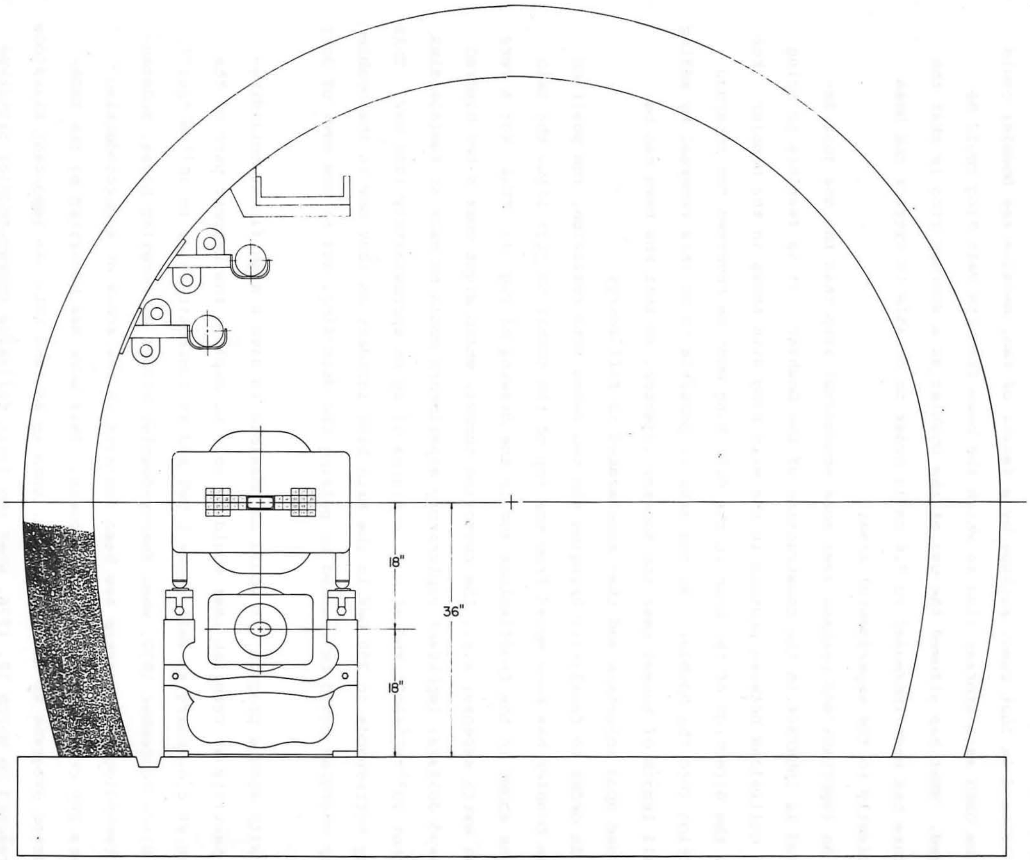

Fig. 1. The Energy Doubler installed in the Main-Ring tunnel.

technical feasibility of the Energy Doubler and provided a strong basis for confidence in the cost estimates, because simplified techniques applicable to production magnets were used in the prototype. There are still other objectives that must be satisfied, such as the ultimate magnetic-field quality, but the potential stumbling blocks of satisfactory "training" behavior and ramping capabilities have already been overcome.

We conclude that the technology has reached an appropriate state for initiation of Energy-Doubler magnet production. By July 1976, six magnets are scheduled to have been wound and a rate of one magnet every two weeks achieved. With high priority given to the Energy Doubler in FY 1977, there should be sufficient progress to complete the accelerator in FY 1978, provided the funds are available.

This report records the progress in the design and development work and the considerations underlying design decisions. The work reported here depends on the earlier Energy Doubler reports[1-4], but this report is written to be understood without reference to the earlier reports.

2. THE ENERGY DOUBLER IN PHYSICS RESEARCH

The Energy Doubler can be used as a colliding-beam device, as described above, but its primary use is expected to be as fixed-target accelerator. A fixed-target accelerator may not be as efficient as colliding beams in producing large available center-of-mass energies, but it does have the great advantage of large interaction rate; its luminosity is of the order of a million times greater than that of a colliding-beams device.

The large interaction rate allows the production of intense secondary beams of various particle types, which uniquely allows the study of strong interactions of π-mesons, K-mesons, neutrons, and so forth. Only in this way can the inner structure of hadrons other than the proton be explored. It is of utmost importance to exploit the ability of the fixed-target accelerator to produce very high-energy neutrino, electron, muon and photon beams. For example, with 1000-GeV protons, useful fluxes of neutrinos at 750 GeV would be produced, allowing a sensitive test of $W^{\pm}$ masses up to 60 GeV/c^2.

Progress in elementary-particle physics has been characterized and guided by advances toward higher-energy beams. Higher energies means shorter wave lengths and shorter wave lengths mean higher resolving power with which to examine the internal structure of the proton and the neutron. There are many ways in which an increase in energy can contribute to studies of the elementary particles. Three of the most important are the following:

1. New and massive particles have been postulated to play an important role in the structure and interactions of matter. In order to produce such particles, an energy commensurate with the mass of the heavy particle is required. Thus, if particles such as quarks, intermediate bosons, or magnetic monopoles exist beyond the range of present explorations, it is of the utmost importance to extend the available bombarding energies in order to further our understanding about the possible existence of such particles.

2. To explore the deepest parts of a nucleon, glancing collisions are not enough. It is necessary to have intimate collisions between a bombarding particle and the target particle. In such collisions, large amounts of momentum are transferred between bombarding and bombarded particle. Large momentum transfers occur with much greater frequency for high-energy bombarding particles than for low. Thus, higher-energy beams provide a more effective probe of the inner structure of fundamental particles.
3. Much of the important work in exploring the structure of matter is carried out through the use of beams of secondary particles such as pions, kaons, muons, neutrinos, electrons, photons, and hyperons. The intensity of such secondary beams, as well as their energy, is an extrement important factor in the capability they provide for studying some of the most unusual and often the most interesting interactions. The higher the energy of a beam of primary protons, the greater the multiplicity of secondary particles that is produced in a primary proton interaction. The higher the multiplicity, the greater the intensity of the secondary beams of particles, at lower secondary energies as well as higher.

Now, although a fixed-target accelerator is inefficient compared with colliding beams in producing large center-of-mass energies between colliding particles, the energy remaining in the moving center of mass is by no means wasted. Even if the secondary particles are produced in the c.m. system at relatively low energy, in the laboratory system they will still share all the incident particle energy. In this sense, a fixed-target accelerator is unique in that it can be considered a "c.m. accelerator" of the secondary particles.

Neutrino physics has become particularly exciting. Because the intensity and energy of the neutrino beam at Fermilab are vastly increased over what previously had existed and because the interaction cross section has also increased with energy, we are now able to observe thousands of neutrino interactions where only tens could be seen at lower energy. Thus neutral-current interactions, indicative of a unification of electromagnetic and weak forces, have been seen in abundance. By now, many dimuon events have also been observed, not, as had been expected, as a clear signal of the intermediate boson, but rather as an unexpected indication of a new particle that very likely carries with it a new kind of quantum number.

Effects indicative of granularity in the proton also become more prominent as energy increases. Thus, had we stopped at 200 GeV, the unexpectedly high frequency of particles of large momentum transfers resulting from collisions would barely have been observable, while at 400 GeV the effect is very large. That the high luminosity of a fixed-target accelerator is important is evident in Fermilab experiments in which it was possible to exceed momentum transfers observed at the CERN ISR.

In summary, the proposed addition of a new superconducting ring at Fermilab offers the possibility of the study of a very broad range of fundamental questions in particle physics in a new and presently inaccessible energy region. The profound discoveries made with the present accelerator leads us to expect new phenomena to be uncovered when the Energy Doubler becomes operational. The new experiments, together with the complementary experiments at other facilities, such as PEP, offer great promise of leading to a new depth of understanding of elementary particles and the fundamental laws of physics.

3. PROGRESS TO DATE

During the period in which the present Fermilab accelerator was being designed, we considered but reluctantly rejected the possibility of building it with superconducting magnets--the state of that art was just too primitive then. In choosing conventional magnets, however, we realized that when superconducting techniques were eventually developed, we could double the energy of our accelerator by replacing the conventional magnets in the existing ring by "supermagnets".

A better opportunity would be to use the present Main-Ring accelerator as the injector into a second complete ring of superconducting magnets. Then the injection energy of protons into that ring could be more than ten times the energy of the present booster injection into the Main Ring. In addition, the Main Ring would then continue to operate. A significant economy could be made by placing the superconducting ring in the Main-Ring tunnel. Because such a synchrotron using superconducting magnets could be designed to reach about twice the energy of the protons in the conventional Main Ring, the project was originally called the "Energy Doubler".

Presented by this opportunity of reaching as much as 1000 GeV, we have been careful to maintain the Main-Ring tunnel clear of obstructions or interferences. The 24 service buildings were also designed so that space is left clear for the installation of refrigeration and other ancillary equipment necessary for the supermagnets. The present magnet power supply has the electrical capability and is flexible enough to energize both the Main Ring at 300 GeV and the Doubler up to 1000 GeV at the same time. Indeed, at first we had hoped to be able to build the Doubler within our original $250 million authorization, in the same spirit that we were able to produce 500 instead of 200 GeV. Our work has been in parallel with and has taken advantage of the efforts and experience with supermagnets at other laboratories such as LBL, Brookhaven, and Rutherford.

On March 9, 1971, R. R. Wilson introduced during his testimony before the Joint Committee on Atomic Energy the concept of a superconducting ring in the

Fermilab Main-Ring tunnel to be used to double the energy of the accelerator. Until September 1972, the Laboratory staff was fully occupied in completion of the accelerator and the equipment necessary for its utilization. Beginning at that time, it was possible to devote some attention to the Doubler idea.

For the past four years, work has been in progress at Fermilab to demonstrate the feasibility of constructing the Energy Doubler - an accelerator employing superconducting magnets which would increase the energy of protons available at the Laboratory by at least a factor of two above that provided by the present accelerator system; i.e., 1000 GeV.

At the outset, a number of tentative design principles were established, among which are:

(i) The Doubler cycle time was picked with the realization the first ramping supermagnets to be developed would ramp more slowly than conventional magnets. It was deemed that a desirable goal would be to achieve an average intensity of about 10^{12} protons/sec, which implies a cycling time of about one minute. At this cycling rate, the thermal load originating from induced currents should not be a major contributing factor to the refrigeration load. It should be emphasized that there is always the option of increasing the repetition rate and hence the average proton intensity by increasing the refrigeration capacity.

(ii) The magnet dewars would themselves play the role of transfer lines carrying coolant from and back to the refrigerators located in the service buildings.

(iii) The magnets would have a cold beam tube, since the relatively low proton beam current will not have stringent vacuum and surface cleanliness requirements.

(iv) The magnet iron used to enhance the magnetic field would be at room temperature and would be always below saturation, thus insuring linearity with excitation.

(v) The superconducting material would be NbTi. (See Appendix V.)

(vi) The current in the conductor would be consistent with utilization of existing Main-Accelerator power supplies for Doubler excitation at the highest practical current density.

(vii) The protons would be extracted and transported into the present experimental areas.

Magnets have been designed with both 2.5-in. and 3-in. bore, which give a good-field circular aperture of 1-2/3 in. and 2 in. respectively. In September 1975, the 2.5-in. magnet series was terminated and 3 in. was chosen as the bore size for the Energy Doubler dipoles. It is prudent to have as large an aperture as is necessary to give sufficient allowance for closed-orbit variations and for optimum slow-extraction efficiency. Clearly, the 3-in. bore is more desirable for bringing the Doubler into operation and it was possible to overcome the problems of additional cost, higher magnet voltage, more difficult magnet protection, and larger refrigerators.

By now, we have built more than 50 magnets. We have demonstrated that the difficulties presented when we began have been overcome to an extent that we initiated in January 1976 the fabrication of full-size Doubler magnets. We still expect to go through further production of model and prototype magnets in order to optimize our present design. Production problems are to be worked out in parallel by winding coils for six 22-ft long magnets by July 1976. At that time the winding rate will be one set of coils for a 22-ft magnet every two weeks.

4. TECHNICAL DESCRIPTION OF THE ENERGY DOUBLER

The Energy Doubler consists of the following major systems:

(i) An extraction system from the present accelerator using electrostatic septa and Lambertson magnets to extract the proton beam from the accelerator, probably at 100 GeV, and inject the protons into the Energy Doubler magnets.

(ii) Approximately 800 22-ft long superconducting dipole magnets capable of being connected together into 48 subsystems, together with 240 quadrupole magnets.

(iii) An rf system and its associated power supplies capable of accelerating the protons up to 1000 GeV at a rate of 50 GeV/sec.

(iv) Power supplies, magnet-protection, vacuum system, and instrumentation and control system required to operate the Energy Doubler.

(v) Helium-refrigeration and transport system required to provide the approximately 4K temperature needed for superconducting magnets.

(vi) Modification of the internal-target station at the C-0 long straight section for experiments using the circulating proton beam.

(vii) An extraction system for the Energy Doubler that allows slow or fast beam to be brought from the Doubler magnets through electrostatic septa, Lambertson magnets and superconducting beam-transport magnets into the present Beam-Switchyard system for use in the Neutrino and Proton experimental areas.

The location of a typical Doubler magnet is shown in Fig. 1. The proton orbit of the Doubler is exactly aligned horizontally with the Main-Ring orbit and 16 in. below. This location facilitates beam transfer into and out of the Doubler and opens the possibility of colliding the Doubler proton beam with the Main-Ring beam. Since we are using the present Main-Ring tunnel, only limited variation from the disposition of magnets in the present accelerator is possible for the Doubler lattice. For example, the presently conceived Doubler geometry will duplicate the six long and six medium straight sections of the Main Ring. It is possible to use a centerline-to-centerline dipole magnet length for the Doubler magnets of 22 ft rather than the 20 ft of the Main Ring. This keeps the junction for Doubler magnets away from the area where Main Ring magnet junctions occur, in most cases, thereby reducing interferences.

5. MAGNET DESIGN AND FABRICATION

We present here a summary of work on dipole-magnet design and fabrication. A cross-sectional view of a dipole is given in Fig. 2. Further details of design philosophy and design parameters appear in Appendices II, III, VI, and VII. Earlier considerations are discussed in References 1, 2, and 3. Our work has been concentrated on superconducting magnet development and we have carried out this development with dipole magnets. Nonetheless, we have also worked on quadrupole design and a cross section of a quadrupole is shown in Fig. 3.

Beam Tube. A 0.025-in. thick non-magnetic stainless-steel tube, elliptically shaped to give a horizontal aperture of 2.8 in. and a vertical aperture of 2 in., serves as the separation between the beam vacuum space and the two-phase helium coolant.

Two-Phase Liquid-Helium Channel. The two-phase, liquid-gaseous (4.4K) helium coolant is contained between the stainless steel beam tube on the inside and the single-phase concentric tube on the outside. These two tubes touch on the horizontal axis and have 0.25 in. clearance vertically at the top and bottom.

Inner Single-Phase Helium Tube. A 0.025-in. thick non-magnetic stainless-steel tube elliptically shaped, 2.9 in. horizontally and 2.6 in. vertically and concentric with the beam tube. The heat exchange between the warmer single-phase and the cooler two-phase helium occurs over the surface area of this tube. The heat flows through the wall of the tube.

Wire Development. For our first full-scale magnets, we wanted conductor that could be wound by somewhat conventional techniques and therefore settled on a solid conductor insulated with Formvar. Since then, interest in magnet systems cycling faster than the somewhat arbitrarily selected 100-sec cycle time has increased. At these higher repetition rates, the ac losses in the solid conductor with its large filaments become unacceptable. We have now moved toward Rutherford-style cable construction, which has smaller filaments. This style of conductor is described in Appendix V. We have recently received large

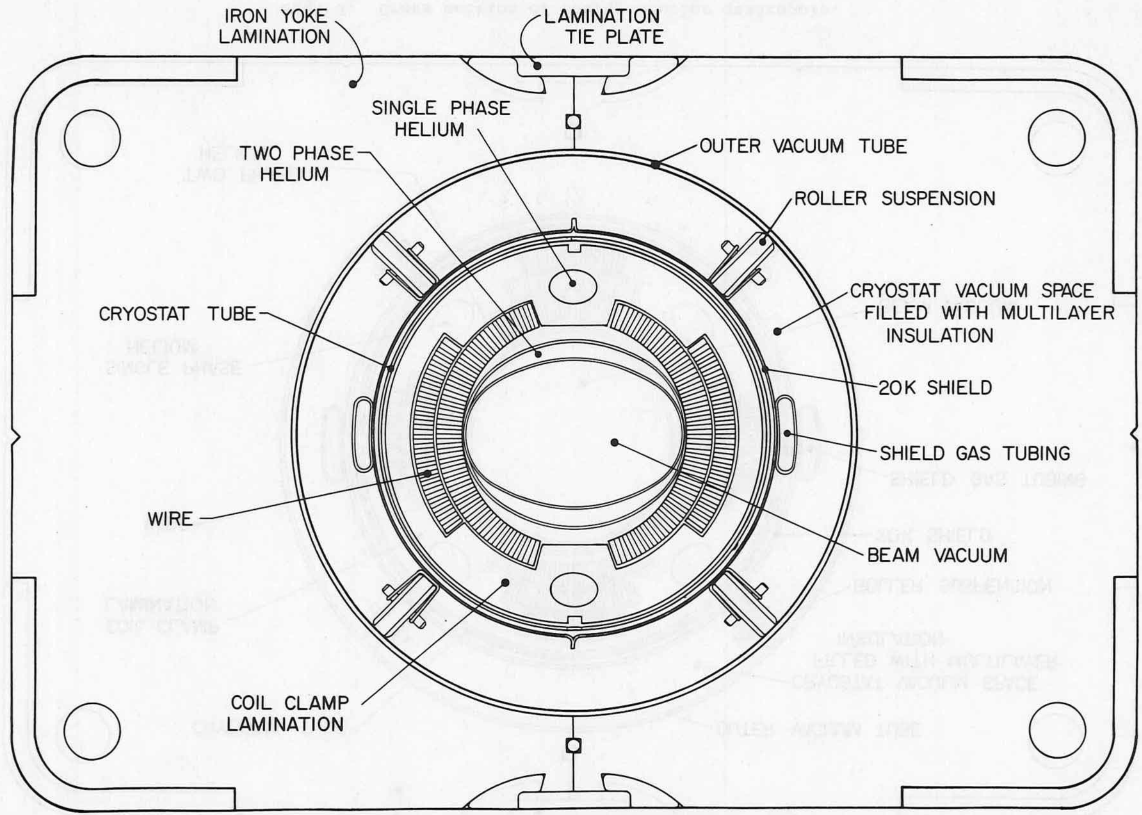

Fig. 2. Cross section of Energy Doubler dipole.

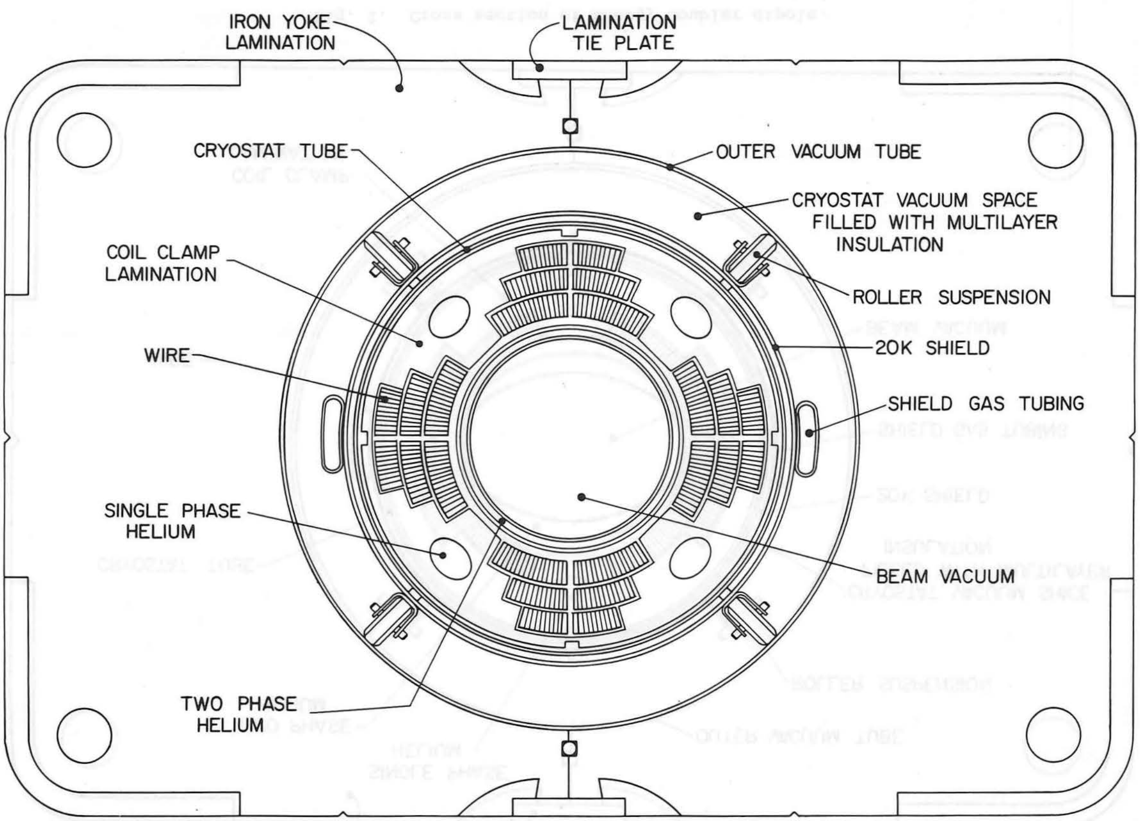

Fig. 3. Cross section of Energy Doubler quadrupole.

deliveries (some 7000 pounds) of cable. The performance of this material exceeds our critical current-density specifications, it has filament size less than 12μ, and it stands up well to handling during winding.

We have also pursued other avenues of wire development. We were able to purchase a large mill run of high resistivity-ratio copper, as well as enough NbTi alloy to fabricate one-sixth of the ring.

Since we decided on the cable style of construction, we have placed essentially identical orders for cable from all commercial manufacturers in order to qualify them with respect to ability to meet delivery requirements and superconducting properties. All conductor in this program is being fabricated with the Fermilab NbTi and copper, so that starting materials are identical. A parallel program, using the same materials, will test certain construction and other processing parameters pertaining to billet extrusion.

Coils. The coils are wound in concentric shells, with overall conductor placement calculated to provide a field uniform to 0.1% over 67% of the area of the bore tube (see Fig. 2). Prior to winding, the wire is cleaned and spiral-wrapped with Mylar tape (0.001-in. thickness) to provide electrical insulation of 1000V. A one-third width longitudinal tape helps to form an approximate trapezoid or "Keystone" shape for better packing of the turns. Finally a fiberglass-epoxy tape (0.008-in. thickness) is spiral-wrapped with 0.060-in. gaps giving open areas for cooling. Thirty-four turns are placed on each inner shell half coil and twenty-one turns are placed on each outer half shell.

Coil Collars. Previous coil-banding methods used in conjunction with bore tubes or bore rings showed coil distortion during excitation and the support of the coils has therefore been recently changed to look more like a cold-iron magnet design. In our case, these close fitting collars are laminations of Nitronic 33 stainless steel half rings 0.062-in. thick. These laminations are compressed into place by external clamps and glued with epoxy or welded. The coils, when collared, appear to be inside a 5-1/8-in. diameter pipe made up out of the collars, with a minimum wall thickness of 3/8 in. Test magnets fabricated with this coil-support system show minimum training and coil distortion during excitation well within acceptable limits.

Cryostat. The helium vessel inside the coil bore is made up of the beam tube and the single-phase inner tube described above. Outside the coil collars, another 0.025-in. thick round stainless steel tube forms the separation between the single-phase liquid helium and the cryostat vacuum space.

A heat shield kept at 20K by flow of cold helium gas surrounds the magnet and in turn is wrapped with 15 layer pairs of Dimplar superinsulation to minimize heat leak. Finally, a close fitting 7-1/2-in. diameter tube that is in intimate contact with the round hole in the magnet iron yoke serves as the cryostat's outer vacuum wall. At the ends, quick-disconnect couplings that are good for low-temperature operation connect the flow circuits from magnet to magnet. End bells and bellows complete the cryostat, with the exception of the support system to hold the cold parts centered in the structure. This system is described in more detail in Appendix VI. For the metal parts of the vessels, we are adapting production sheet-metal techniques for fabrication in order to minimize the number of machined parts.

6. HELIUM-REFRIGERATOR STUDIES - PUMP LOOP

The design principles upon which the magnet cooling system is based are reported elsewhere.[5,6] Basically, subcooled liquid helium is to be circulated by means of pumps located in service buildings distributed around the Main Ring. At a point midway between any two service buildings, the liquid will pass through a Joule-Thomson valve and counterflow back to the pump as boiling liquid helium in an annular space between the subcooled liquid that surrounds the coils and the beam tube.

To verify this concept, a liquid-helium pump loop has been constructed and tested. The loop consists of two lengths of coaxial pipe, each 200 ft long, and associated valving. A large helium refrigerator with a production rate of about 150 ℓ/hr provides liquid. The loop is fully instrumented and a large number of experiments have been carried out.

To date, the basic cooling concept has been verified, as well as the performance of two different circulating pumps. The flow characteristics of helium under these conditions have been measured and several experiments pertinent to the operation of the Doubler have been performed. (See Appendix XI.) The operation of a 20-ft magnet in the loop showed improved performance over a single dipole operated in a pool-boiling helium.

7. REFRIGERATION

In order to provide the large amount of liquid-helium temperature refrigeration required by the Energy Doubler magnets, we have decided on the use of a central helium-liquefier facility that will provide liquid helium for distribution to "satellite" units located around the ring. The central helium plant will utilize "surplus" compressors that we are obtaining from the Santa Susana rocket-engine test center. The capacity of the central liquefier will be 4000 ℓ/hr of liquid helium, which will accumulate in a tank truck of 10,000 gal (40,000 ℓ) capacity. The satellite stations will receive liquid helium from the tanker approximately one a day. By the use of a "reliquefier" principle (see Appendix XI), each satellite will be able to provide the refrigeration needed by the magnets in its portion of the ring and to return high-pressure helium gas via a small pipeline to the central liquefier location. The central liquefier will be provided with a liquid-nitrogen-temperature precooler, which is also to be brought from the Santa Susana plant. This will reduce the requirements of the individual refrigerators for liquid nitrogen, saving about $500,000 annually in operating cost for the Energy Doubler refrigerators.

So far, the three large compressors have been removed from the California installation and protected against corrosion. A reconditioning plan is being drawn up and foundations are being installed at Fermilab. A 50-ft by 180-ft pre-engineered building has been contracted for to house the equipment and will be installed as soon as compressor foundations are complete. The 4000 ℓ/hr helium-liquefier cold box has been under contract since February 1976 and should be delivered by August 1977, the time of the commissioning of the plant. This helium-refrigeration plant will be the largest in the world by more than a factor of two.

We have also designed and constructed a prototype satellite refrigerator station, which is under test. This unit will be installed in a service building and used to cool the first string of Energy Doubler magnets to be installed in the Main Ring tunnel during the summer of 1976.

8. INSTALLATION

One of the tasks that has received the most serious consideration during the design study has been the planning of the installation of the new ring of superconducting magnets into the Main-Ring tunnel without serious interference with normal accelerator operation. We have developed a magnet and cryostat design that we believe will permit efficient installation. Individual magnets are to be moved into the tunnel while the accelerator is in use. During an accelerator down period, the Energy Doubler magnets that are already in the tunnel are lowered to carts, moved into position, and the connections and alignment completed. When the string of magnets is complete and connected to the cryogenic service boxes (there will be a total of 48 independent strings of magnets) pumping, purge and cooldown operations can be accomplished from the service buildings, again during normal accelerator operations.

In order to prove our concepts, a second beam-extraction system has been installed in the Main Accelerator in the B-0 long straight section. With this system, a few percent of the protons can be extracted at an energy of 100 GeV for injection into Doubler magnets. We have already been successful in installing 2.5-ft long and 10-ft long model supermagnets in this beam and operating them in a superconducting mode without interference with the accelerator.[7]

Because of the change of position of the Energy Doubler from the top of the tunnel to 16-in. underneath the Main-Ring magnets, we are relocating this extraction system and our program now is to install a string of ten regular supermagnets in this beam and hence to test our ideas about installation, alignment, and operation under actual conditions in the tunnel.

9. MAGNET PROTECTION

A serious problem could arise should one of the magnets in the ring accidentally undergo a quench if no provision has been incorporated to handle this occurrence without damaging equipment. Of course, quenches occur many times in the course of testing individual magnets, but the magnets are not damaged because we have developed electronic devices to detect the incident quench. When a quench is detected, the magnet current is immediately shunted through an external resistor by means of a thyristor, while at the same time the power supply is disconnected.

One is justifiably concerned when 800 magnets are connected in series, for it is conceivable that the whole energy in the magnet ring, about 300 MJ, or even some small fraction of this, might be deposited explosively in one or more of the magnets.

The magnets are connected in 48 separate groups of 17 magnets each; at the end of each group or string the leads are brought to room temperature and then to 24 power supplies. Thyristors connected to these leads will, upon command from an electronic quench detector, isolate the group in which the quench occurred from the rest of the magnets.

We have several different solutions for isolating the quenched magnet from the 16 other magnets in the group. The surest, but probably most expensive, solution is to bring out a small warm lead at each magnet (it need not carry the full current continuously). Then the current in the quenched magnet can be bypassed through an external individual thyristor, thus isolating it from the other magnets. The power supplies at the adjacent service buildings can then be used to pull the energy out of the quenched magnet and the adjacent magnets to minimize the loss of coolant. Other possibilities that are under study include various schemes of having the protective circuitry within the cryogenic systems to a greater or lesser degree.

10. MAGNET TESTS

Over the past year we have been testing a series of magnets that were constructed with different parameters in order to correlate the effects of various construction techniques with magnet performance.[8] The following areas have been and continue to be under investigation: types of wire, stranding techniques, number of strands, types of insulation, banding techniques, structural restraints, and problems of fabrication.

Most of the testing work has been aimed toward obtaining high-field magnets. Field quality has not been explored in depth in the past year, but both early and recent work indicate that field quality can be made acceptable and reproducible from magnet to magnet.[9]

11. COST AND SCHEDULE

The Energy Doubler is being built as a research and development project utilizing operating funds, following the recommendation of the Low Committee on High Energy Physics Facilities of the High Energy Physics Advisory Panel. Details concerning the definitions and funding assumptions are given in Appendix XIV. It is estimated that fabrication and installation of all Doubler magnets will be completed in fiscal year 1978 and protons will be accelerated to 1000 GeV at a slow repetition rate. The 1000-GeV proton beam will be extracted and transported to experimental area for use in experiments in fiscal year 1979. To meet this schedule, 270 dipoles will be completed in the mini-year and FY 77 and 530 in FY 78. All 240 quadrupoles will be built in FY 78, with the exception of extracted beam components and their controls, which will be built in FY 79.

Anticipated R&D funding for FY 77 and FY 78 which will achieve a circulating beam is shown below. The cost of a central helium liquefier is not included because we have acquired most of the equipment as surplus and will utilize it for not only the Doubler but also for the rest of Fermilab.

(All amounts in thousands of dollars)

	FY 77	FY 78
Dipoles	5,400	11,600
Quadrupoles	0	1,800
Other Components	150	4,400
Satellite Refrigeration System	450	2,200
Contingency	0	0
Annual R&D	4,000	5,000
Total	10,000	25,000

REFERENCES

[1]Some Preliminary Concepts of the Energy Doubler, P. J. Reardon and B. P. Strauss, Fermilab Report TM-421, May 1973.

[2]The Energy Doubler Design Study, March 1, 1974, FN-263.

[3]D. A. Edwards et al., Progress Report on the NAL Energy Doubler Design Study, Proceedings of the IXth International Conference on High Energy Accelerators, SLAC, May 2-7, 1974, p. 184.

[4]Energy Doubler/Saver Proposal, June 1975.

[5]P. C. VanderArend et al., Cooling of a System of Superconducting Magnets by Means of Pumped Liquid Helium, Proceedings of 1974 Applied Superconductivity Conference.

[6]P. C. VanderArend et al., A Large Scale Pumped Subcooled Liquid Helium Cooling System, to be published in Advances in Cryogenic Engr., Vol. 21, (1976).

[7]C. Rode et al., Operation of an Energy Doubler Magnet in the Extracted Beam of the Fermilab Accelerator, IEEE Trans. Nucl. Sci., Vol. NS-22 (1975).

[8]B. Strauss et al., Results of Magnet Prototype Evaluation for the Fermilab Energy Doubler Project, ibid.

[9]D. Drickey et al., Performance Studies of Superconducting Dipoles for the Fermilab Energy Doubler, ibid.

BIBLIOGRAPHY SINCE REF. 3

1. Synchronous Transfer of Beam from Main Ring to Energy Doubler, L. C. Teng, TM-489, May 1, 1974.

2. Energy Doubler Dipole Mark II: Nonlinearity and Tolerance Requirement, S. Ohnuma, TM-502, June 14, 1974.

3. Short Sample Test of Some Superconducting Wires, R. Yamada et al., TM-523, September 20, 1974.

4. Some Short Sample Test Data, P. Price et al., TM-538, November 23, 1974.

5. Losses in Superconductors for the Energy Doubler, J. H. Murphy et al., TM-545, February 17, 1975.

6. Thermal Conductance Measurements of Mechanical Supports for Superconducting Magnets, Particle Accelerator Conference, M. Kuchnir and P. Sanger, TM-552, March 1975.

7. Electrical Protection of Superconducting Magnet Systems, D. F. Sutter et al., TM-559, March, 1975.

8. Short Sample Test Data III, P. Price et al., TM-567, March 24, 1975.

9. Energy Doubler/Saver Radiofrequency Acceleration System, L. C. Teng, TM-574, April 30, 1975.

10. Fermilab Energy Doubler Magnets--Magnetostatics, S. C. Snowdon, TM-575, April 29, 1975.

11. Short Sample Test Data IV, M. E. Price et al., TM-587, June 26, 1975.

12. Power Economies for the Fermilab Energy Doubler/Saver, R. Cassel et al., TM-590, July 17, 1975.

13. Superconducting Magnet Systems at Fermilab, J. R. Heim, TM-591, July 1975.

14. Third-Integer Resonant Extraction from the Energy Doubler/Saver, L. C. Teng, TM-593, June 30, 1975.

15. Fabrication of Cryogenic Electrical Feedthroughs, M. Kuchnir, TM-596, August 8, 1975.

16. Superconducting Wire Test at Fermilab, R. Yamada et al., TM-598, July 1975.

17. Fabrication of Multi-Filament NbTi Composite Wire for Accelerator Applications, B. P. Strauss et al., TM-606, August 1975.

18. A Discussion of Aperture and Space Allocation in the Energy Doubler/Saver, T. Collins, et al., TM-614, September 1975.

19. Mechanical and Thermal Stresses in Doubler Dipole Magnets, S. C. Snowdon, FN-284, October 1975.

20. Forced Flow Heat Load Measurements, D. Richied and C. Rode, TM-624, November, 1975.

21. Summary of the First 5 Months at B12, R. Norton, et al., TM-625, November 1975.

22. Small Solenoid Test of Insulation Method, M. E. Price et al., TM-634, December 1975.

23. AC Loss in Flat Transposed Superconducting Cable, H. Ishimoto et al., TM-636, October 1975.

24. AC Loss Test of D-10-3 Magnet, R. Yamada et al., TM-638, December 30, 1975.

25. Hysteresis Loss Test of Superconducting Wires, M. E. Price et al., TM-639, December 15, 1975.

26. Method for Measurement of Thermal Conductance, M. Kuchnir, to be published in Advances in Cryogenic Engr., Vol. 21 (1976).

27. Superconducting Wire Stability Workshop/7-22-74, TM-641, January 30, 1976.

28. Heat Leak Measurements on a D-10' Cryostat, M. Kuchnir, TM-645, February 17, 1976.

29. Carbon Resistance Thermometers, M. Kuchnir et al., TM-647, March 9, 1976.

30. Operational Test and Field Measurement of D-10-3 Magnet, R. Yamada et al., TM-651, March 26, 1976.

APPENDIX I. PHYSICS OF THE DOUBLER

J. Peoples

A. Introduction

Whenever a new accelerator is proposed, one of the first questions an experimentalist asks is, "Is the energy range appropriate for interesting experiments?" An answer can be given for the Fermilab Energy Doubler by selecting the most significant experiments that have been done in elementary-particle physics since 1972 and then seeing how the Energy Doubler will be an appropriate facility to follow up on the most promising leads that these experiments have uncovered. Four experimental discoveries of unquestioned importance are:

1. Weak neutral currents[1]
2. Narrow resonances[2]
3. Dilepton production by neutrinos[3]
4. Unexpectedly large cross sections for particle production at large transverse mementa in hadron collisions.[4]

Although each of these discoveries came as a surprise, there were theoretical ideas that predicted the gross features of the phenomena. For example, gauge theories predicted the existence of weak neutral currents.[5] This type of theory, which unifies electrodynamics and the weak interactions, establishes a mass scale for the weak interactions since it predicts the mass of the intermediate vector boson. Clearly this is a promising and exciting lead that should be further investigated.

The results of experiments that have already followed up on the above discoveries have not always been in harmony with the theoretical ideas that were initially advanced to explain the discovery. For example, the explanation of the narrow resonances as bound states of a charmed quark-antiquark is both appealing and consistent with many of the facts,[6] but the theory of charmed quarks predicts that charmed particles should exist with masses between 2 and 3 GeV/c^2.[7] Production of these particles should be possible at presently available energies at Fermilab, the ISR, and SPEAR. That they have not been discovered presents a serious difficulty to that theory.

The physical laws that describe these new phenomena could well be even more complex than the theoretical framework that now exists. These results suggest that a new scale of masses has been reached. The present energy of the Fermilab accelerator, 400 GeV, certainly extends into that domain, but it does not span it, as the following example shows: Gauge theories predict that the mass of the charged intermediate vector boson, $W^{\pm}$, is greater than 37 GeV/c^2.[5] Experiments using 150-GeV neutrinos, produced by 300-GeV protons, have ruled out the existence of a $W^{\pm}$ particle less massive than 10 GeV/c^2.[6] Improvements in those experiments that can now be done with neutrinos produced with 400-GeV protons will raise the limit to 30 GeV/c^2. On the other hand if 1000-GeV protons were available at an intensity of 10^{12} protons/sec, then a useful flux of 750-GeV neutrinos could be obtained. The same type of experiment would be sensitive to the existence of the $W^{\pm}$ if its mass were 60 GeV/c^2. The possibilities presented by neutrinos, although they are exceptionally rich, are by no means the only possibilities that an Energy Doubler will provide to follow up the aforementioned discoveries.

B. Experimental-Area Utilization

It is proposed to extract beams of 1000-GeV protons to both the Neutrino Area and the Proton Area. Ninety percent of the protons could be transmitted to the Neutrino Area as a sequence of millisecond spikes, while the remainder of the beam could be slow-extracted to the Proton Area. The fast beam would be used with either a proposed high-energy dichromatic beam or a broad-band focusing system to produce neutrino beams for the 15-ft Bubble Chamber and for electronic detectors. The remainder of the beam, slow-extracted to the Proton Area, could in turn be split and transported to targets in the P-West, P-Center and P-East branches of that area.

The Neutrino Area presents three new opportunities with the Doubler. The most important would be the use of higher-energy neutrino beams with the existing 15-ft Bubble Chamber and the massive toroidal spectrometers in Lab C and Lab E. With a triplet focusing system that would be a simple extension of the present triplet focusing system, physics could begin as soon as an extracted beam was available. Measures to harden the first half of the shield to 500 GeV with iron magnets are underway as part of the present experimental program. These techniques could easily be adapted to 1000 GeV.

The second opportunity would be the use of the present 500-GeV hadron beam with either electronic detectors or the 30-in. Bubble Chamber. The third would be the use of the muon beam at its present peak energy of 300 GeV. In both cases, straight-forward substitution of superconducting magnets would make it possible to double the energy of each beam. These latter possibilities will have to be deferred to a later phase of Doubler utilization.

A high-energy, high-intensity pion beam is scheduled for construction this year. It will achieve a peak energy of 1000 GeV when all the superconducting magnets are in place. Upstream of the secondary-beam production target there will be a transmission-target station, which is presently being used to study inclusive particle production and elastic scattering.

The pion beam will also have the capability of operating as a high-purity electron beam. This option, together with the broad-band photon beam and the tagged-photon beam in the P-East branch, will provide an excellent set of facilities for studying electron-photon physics.

The P-Center branch can be used for the study of p-p interactions with the primary proton beam. In addition plans have been developed to expand this area to include a charged- or neutral-hyperon beam and associated experimental facility.

One of the most exciting possibilities is the possibility of colliding the Doubler with the Main Ring or a newly proposed small storage ring. The former can provide an equivalent laboratory energy of 400,000 GeV at a luminosity of 10^{31} $cm^{-2} sec^{-1}$.

Finally, a wide variety of measurements can be made with the internal target at C-0 during the acceleration cycle. The experiments must be modest in size in order to fit either in the Main-Ring tunnel or in the new spectrometer room that has been built to accommodate a 6-GeV spectrometer. This spectrometer can be used for observing recoil protons from various p-p scattering processes. Threshold effects can be detected because the processes can be studied at any energy between 300 and 1000 GeV. Very-low-momentum recoils can be measured with solid-state recoil spectrometers. In turn, this permits very precise measurements of p-p elastic scattering and related exclusive and inclusive processes.

The use of the Meson Laboratory with the Energy Doubler appears quite feasible. It appears possible to construct one 800-GeV beam (the present M2 beam), one 400-GeV beam (the present M6 beam), and one 600-GeV beam (the present M1 beam). The last two beams would be relatively rich in K^- and $\bar{p}$'s. This project will be deferred until a later phase of the Doubler utilization.

Rather than consider the many possible experiments that can be done at energies up to 1000 GeV, the following paragraphs will deal only with the experiments and facilities that bear on the discoveries mentioned earlier.

C. Neutrino Physics

W Particles. As mentioned before, the discovery of weak neutral currents makes it plausible that some type of gauge theory is correct. On the basis of these theories, the $W^{\pm}$ mass is expected to be between 40 and 60 GeV/c^2. This mass range will be accessible to a 1000-ton electronic detector. In a typical six-week running period with the Doubler, it will be possible to target 2×10^{16} 1000-GeV protons. On the basis of the extrapolation of pion and kaon production at present Fermilab energies up to energies of 1000 GeV, the neutrinos produced by such exposure would produce about 1000 events with a total energy greater than 750 GeV in the detector. The measurement of the q^2 dependence of the neutrino cross section obtained from these events will be sensitive to the existence of $W^{\pm}$ bosons if the W mass is less than 60 GeV/c^2.

As significant as the $W^{\pm}$ is, the search for the W^0 is just as important. Although its mass is expected to be higher, neutrino experiments using a narrow-band beam can search for propagation effects in the neutral-current interaction.

The possibility of colliding the Main Ring with the Energy Doubler allows one to search for the presence of W of much larger masses. With a center-of-mass energy of 900 GeV and a luminosity of $10^{31}\,cm^{-2}\,sec^{-1}$, it would be possible to detect these particles if their mass were less than 200 GeV/c^2.

Narrow Resonances and New Particles. Gauge theories predice that either a strangeness-changing neutral current exists or that additional quarks conspire to suppress the strangeness-changing neutral currents.[9] Experimentally, the strangeness-changing neutral currents, if they exist, are several orders of magnitude weaker than the strangeness-nonchanging neutral currents. Therefore, new particles such as charmed hadrons should be expected. The narrow resonances may well be related to such a family of particles.

The energy dependence of the neutrino total cross section can also be a good indicator of such new phenomena. In the energy range of 1 to 100 GeV, the cross section is proportional to the energy; the constant of proportionality is 0.78×10^{-38} cm^2/GeV.[8] If a family of charmed particles with masses between 2 and 3 GeV/c^2 exists, this proportionality constant will increase significantly in the energy range between 100 GeV and 750 GeV.

The 15-ft Bubble Chamber filled with either liquid H_2 or D_2 should be an excellent detector for these new particles. The neutrino can transform a proton or a neutron into a charmed baryon very cleanly. Other than the outgoing μ^-, there are no extra particles. In hadron production of charmed particles, it is necessary to produce these particles in pairs. Moreover, there will probably be a few more pions produced, making such an event complicated and difficult to interpret. On the other hand, the neutrino-induced event in H_2 or D_2 will be simple and straightforward to interpret.

Dilepton Phenomena. The neutrino-induced dilepton events seen in the present electronic detectors need to be studied in much more detail. Measurements of the dynamics of their production over the full range of neutrino energies can be provided by the Doubler. Such measurements may present a few surprises, since the source of these events is not yet known. Because of the increase in the flux of neutrinos above 50 GeV, some of these phenomena will be accessible to investigation in the 15-ft Bubble Chamber filled with neon and hydrogen.

It is worth stressing that in many instances the neutrino is the most energy-economical probe to search for new particles, because all its energy can go into producing such a particle. This is particularly true when the search is for a heavy "gauge" lepton.

D. Hadron Physics

Experiments with hadrons can be expected to reveal more about narrow resonances and large transverse-momentum phenomena. The center-of-mass energy afforded by the Doubler is comparable to that available at the ISR, while the available luminosity is five orders of magnitude larger.

Hadron Jets. Results from the ISR suggest that hadron jets that carry away a large amount of transverse momentum may exist. Nevertheless, the limited interaction rate makes it difficult to establish this phenomenon conclusively. To observe this phenomenon, each jet must have at least 6 to 8 GeV/c transverse momentum, perhaps with one leading particle having half of the transverse momentum. The requirement that the transverse momentum must balance implies that 16 GeV of energy is in the jets. This in turn requires 60% of the available center-of-mass energy when the present accelerator is run at 400 GeV. That energy is too low to see those effects because of the constraint that momentum conservation imposes on the amount of available phase space. When the experiment is done with 1000-GeV protons, the center-of-mass energy has increased by another 16 GeV. This should be enough to see these processes without the distorting effects resulting from constraints of momentum conservation.

Does the Doubler provide enough intensity? The answer is yes. The precursors of these experiments have been done or will be done in the existing Proton Area. Those experiments have rarely used more than 10^{11} protons/sec, since the detectors could not handle higher instantaneous counting rates. Because the Doubler offers the prospect of an intensity of the order of 10^{12} protons/sec and of a 30% to 40% duty cycle with a factor of two finer rf structure, this type of experiment will be easier with the Doubler than with the present accelerator.

Massive Dilepton Pairs. The production of a particle or jet of particles that has a transverse momentum of more than 6 GeV can be thought to be a consequence of the parton or quark structure of hadrons. In the parton model, the hadronic granularity can manifest itself in other ways. The production of massive dilepton pairs is such an example.[10] Experiments exploring this possibility are now in progress at Fermilab. The sensitivity of an experiment to large masses, for example from 5 to 20 GeV/c^2, is limited in the first instance by the counting rate that the experiment can handle. The available beam intensity has usually been two orders of magnitude greater than what can be used. If the protons were 1000 GeV, the dilepton mass range could be extended to 40 GeV. The sensitivity would be at least two orders of magnitude greater than for a comparable experiment at the ISR.

This type of experiment has been a particularly exciting area of study since it was in such an experiment that the narrow resonances appeared quite unexpectedly.[2] One must be prepared for more surprises.

Narrow Resonances. The study of the production of the known narrow resonances, and perhaps some unknown ones, will be an important measurement in the 400- to 1000-GeV range by protons and in the 300- to 750-GeV range by negative pions. If charm or the new degree of freedom connected with these resonances has not been discovered by the time the Doubler is operating, investigation of the energy dependence and the $p_\perp$ dependence of the production of the narrow resonances at higher energies could be a clue to what would be, by that time, a rather deep mystery. These experiments are quite simple to do at Fermilab. An experiment at Fermilab that followed the original BNL experiment was run quite easily in a neutron beam of only 10^6 interacting neutrons per 7-sec pulse of 300-GeV protons.[11] The event rate was approximately two per hour. Follow-up experiments at 400 GeV are underway; they have event rates one or two orders of magnitude higher. The reason for the ease of measurement is that the production cross section has risen by two orders of magnitude between 30 GeV and 300 GeV.

E. Other Physics

It is important to measure the production of the narrow resonances in secondary beams. For example, the photoproduction of the $\psi(3.1)$ and $\psi(3.7)$, which was done at first at Fermilab[12] in the broad-band beam, can be extended to photon energies of 600 GeV. In a similar manner, the value of the tagged-photon beam is enhanced, although for it to use the Doubler energy, it would have to be upgraded from 300 to 600 GeV. Of more importance is the fact that the flux of photons in the range of 75 to 225 GeV will be sufficiently intense that the applicability of vector dominance to the ψ photoproduction can be tested. Because of the design of these experiments, it is not sufficient to produce more protons at 400 GeV to get the answer; the spectrum must be hardened. The first experiment was limited to 10^{11} protons/sec by the accidental counting rate. The better duty factor of the Doubler will make it possible to make substantial improvements in the counting rate of these experiments.

The P-West pion beam, because of its large acceptance, will be able to provide fluxes of more than 10^7-negative pions/sec at 400 GeV even when the production target is illuminated with only 5×10^{10} protons. This is a better average intensity than that of any existing pion beam in the Meson Area. At the expense of reduced intensity in the Neutrino Area, the pion flux in the P-West beam could go up by an order of magnitude and thus the study of massive dilepton production by pions could be carried out in such a beam. The comparison of pion and proton production of those pairs is very important. Of considerable significance is the fact that production of narrow resonances can be carried out in this beam. One could also study jet phenomena induced by meson-nucleon collisions. It is important to stress again that a comparison of these processes that probe the granularity of the hadrons when they are done with different projectiles is very significant, because the quark or parton content is quite different in each case. As long as free-quark beams are not available, the only way to test for their effects will be using beams of bound quarks with different quark and antiquark composition. Of course, one will also look for the production of free quarks.

References

[1]F. Hasert et al., Phys. Lett. 46B, 138 (1973); A. Benvenuti et al., Phys. Rev. Lett. 32, 800 (1974); B. Augert et al., Phys. Rev. Lett. 32, 1454 (1974); B. Barish et al., Phys. Rev. Lett. 34, 538 (1975).

[3] J. J. Augert et al., Phys. Rev. Lett. 33, 1404 (1974); J. E. Augustin et al., Phys. Rev. Lett. 33, 1046 (1974).

[4] A. Benvenuti et al., Phys. Rev. Lett. 33, 419 (1975).

[4] B. Alper et al., Phys. Lett. 44B, 521 (1973); M. Banner et al., Phys. Lett. 44B, 537 (1973); F. W. Busser et al., Phys. Lett 46B, 471 (1973); J. W. Cronin et al., Phys. Rev. Lett. 31, 1426 (1973).

[5] S. Weinberg, Phys. Rev. Lett. 19, 1264 (1967); Phys. Rev. Lett. 27, 1688 (1971); A. Salam, Elementary Particle Theory, edited by N. Svartholm, p. 367 (1968).

[6] T. Appelquist and D. H. Politzer, Phys. Rev. Lett. 34, 43 (1975); A. De Rujula and S. L. Glashow, Phys. Rev. Lett. 34, 46 (1975); T. Appelquist et al., Phys. Rev. Lett. 34, 365 (1975); E. Eichten et al., Phys. Rev. Lett. 34, 369 (1975).

[7] M. K. Gaillard, B. W. Lee, and J. L. Rosner, Rev. Mod. Phys. 47, 277 (1975).

[8] Proceedings of the XVII International Conference on High Energy Physics, London, P. IV 141 (1974).

[9] S. L. Glashow, J. Iliopoulos, and L. Maiani, Phys. Rev. D2, 1285 (1970).

[10] J. H. Christenson et al., Phys. Rev. D8, 2016 (1973); S.D. Drell and T.M. Yan, Phys. Rev. Lett. 25, 316 (1970).

[11] B. Knapp et al., Phys. Rev. Lett. 34, 1044 (1975).

[12] B. Knapp et al., Phys. Rev. Lett. 34, 1040 (1975).

APPENDIX II. MAGNET LATTICE AND DYNAMICS

L. C. Teng

A. Ring Geometry and Magnet Lattice

The Energy Doubler will be placed directly underneath the Main Accelerator, with the Doubler orbit 16 in. below and parallel to the Main-Accelerator orbit. The possibility of a future addition of a superconducting ring in this location was anticipated during the design of the Main Accelerator and care was taken to leave this space relatively free of obstructions. Except for some minor modification of the support stands of the Main-Ring magnets, there will be no interference between the installation of the Doubler ring and the Main Accelerator.

This choice of location for the Doubler has two important advantages. First, the orbit geometry and the magnet lattice of the Doubler ring will be identical to those of the Main Ring. Thus the focusing and accelerating properties of the Doubler beam will be the same as those of the Main-Ring beam. This means that the experience gained in aligning, tuning, and operating the Main Ring can be applied directly and in detail to the Doubler. Second, the small separation of 16 in. between the Main Ring and the Energy Doubler implies that one can bring the two orbits together for colliding beams with minimum effort. Colliding-beam operation, which will be discussed in more detail below, is clearly a natural and extremely useful mode of operation whenever there are two rings (and hence two beams) existing in the same tunnel. In addition, the proximity of the Doubler orbit to the Main-Ring orbit makes it easy to transport the beam extracted from the Doubler to the present Main-Ring extracted-beam line and hence to the present experimental areas and facilities.

As will be discussed later, no deviation from the Main-Ring lattice is necessary for injection, acceleration, or extraction of beam in the Doubler. Some unessential but desirable minor modifications of the magnet lattice are made to take advantage of the higher injection energy (100 GeV) into the Doubler. Higher injection energy means smaller required aperture, hence higher attainable quadrupole field gradient relative to the dipole field. The design quadrupole gradient

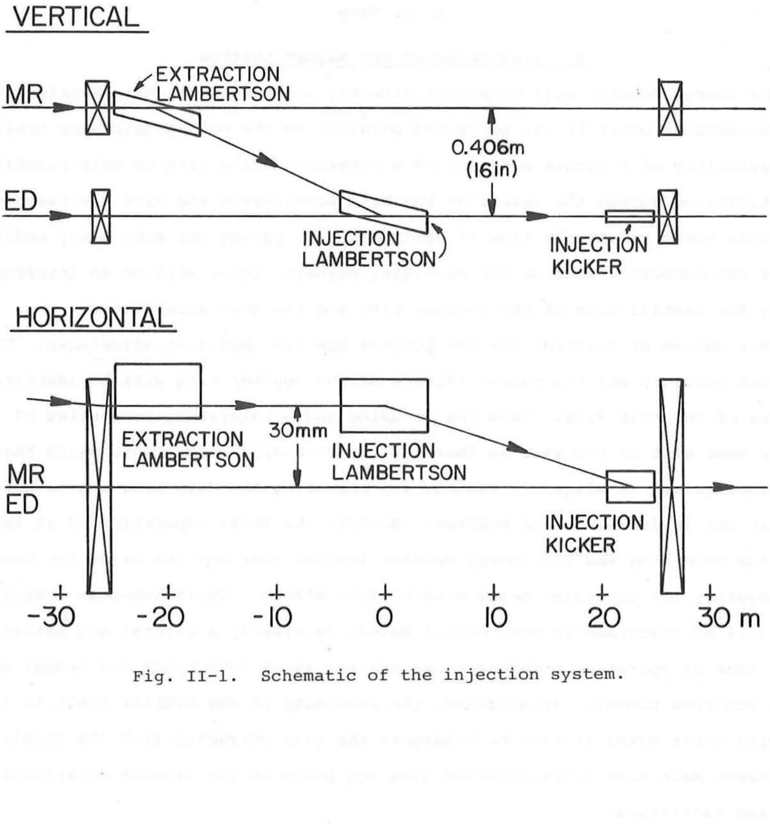

Fig. II-1. Schematic of the injection system.

at 1000 GeV is 24.1 kG/in. compared with the equivalent 15.3 kG/in. of the Main Ring. Operating at this gradient and at the same betatron oscillation tune of $\nu = 19.4$ as the Main Ring, the gradient length of normal-cell quadrupoles need only be 53 in. compared with 84 in. for the Main Ring. Furthermore, experience in the Main Ring indicates that the length of the mini-straight section can be reduced. The length gained in these ways is to be added to the dipole, so that one can reach higher energy with the same peak dipole field strength, or conversely, the same energy at lower dipole field. The effective length of a Doubler dipole is 252 in., 13 in. longer that a Main-Ring dipole. For 1000 GeV, one therefore needs a field strength of only 42.3 kG. The Doubler will contain a total of 774 dipoles, as does the Main Accelerator.

It might be possible to increase the quadrupole gradient further. This would further reduce the necessary gradient length of the quadrupoles, which could be added to the mini-straight section, which has been reduced from 83 in. in the Main Ring to 62 in. in the Doubler.

The long straight sections in the Main Ring are matched for a betatron tune of 20.25. At a tune of 19.4, these long straight sections are slightly mismatched. In the Doubler, matching across the long straight section is restored for a tune of 19.4 by minor readjustment of the matching quadrupoles. The total number required is 192 normal-cell quadrupoles and 48 long straight-section matching quadrupoles, as in the Main Accelerator.

B. Beam-Transfer System

The beam in the Main Ring will be transferred at 100 GeV to the Energy Doubler in one revolution. The beam-transfer system is located in the 50.8-m long straight section B (LB). It may be noted that some small amount of beam loss is unavoidable during transfer. This stray beam hitting a superconducting magnet might cause it to quench and hence only conventional magnet elements will be used in the beam-transfer system.

Extraction from the Main Ring will be accomplished by fast-kicking the beam horizontally outward across a Lambertson iron-septum magnet (the extraction Lambertson) located at the upstream end of LB. This entire system is shown in Fig. II-1. The fast kicker is located in the mini-straight section at station A46. It has a length of 1.5 m, a peak field of 1 kG, and a rise time less than 0.2 μsec. This kicker will kick the 100 GeV beam by an angle of 0.44 mrad. The corresponding displacement at the extraction Lambertson septum is 3 cm, ample for clearing the septum. The Lambertson is 8 m long, has a field of 9.16 kG, and bends the beam downwards by 22 mrad. The beam arrives at the Doubler level (16 in. below) at the midpoint of LB, where a second Lambertson magnet (the injection Lambertson) bends the beam back up 22 mrad to a horizontal orbit. At the injection Lambertson, the beam will be 3 cm horizontally outside the central orbit of the Energy Doubler. The injection Lambertson is tilted slightly so that in addition to the 22-mrad upward bend, it also deflects the beam horizontally inward by 1.32 mrad. This brings the beam inward to cross the Doubler orbit horizontally near the downstream end of LB, where a 4.5-m long fast kicker will kick the beam horizontally outward by 1.32 mrad. The beam will then travel along the Doubler orbit.

Since no quadrupole is added or bypassed in the transfer line, betatron matching should be perfect throughout the transfer. The horizontal dispersion is also properly matched. The vertical dog-leg introduces, however, a mismatch in the vertical dispersion equal to the vertical displacement, namely 16 in. or 0.41 m. But since the momentum spread in the beam at transfer is $\Delta p/p = 0.5\times10^{-3}$, this mismatch increases the beam height by only 0.2 mm, which is entirely negligible. With kicker rise and fall times shorter than 0.2 μsec and a Lambertson septum thickness less than 3 mm, the beam loss on the septum should be less than 0.1% and the transfer efficiency should be better than 99.9%.

Two special features of this beam-transfer scheme deserve mention. The Energy Doubler magnets are designed with a cold bore. Unless absolutely necessary, the cold bore should continue uninterrupted for as long as possible. Indeed, both the correction-magnet packages and the beam-position monitors that will occupy the mini-straight sections are designed to operate cold so that most, if not all, of the mini-straight sections will have a cold bore. It should be possible to continue the cold bore through a complete sextant of the ring. Only long straight sections will then have a warm bore with cold-warm transition sections at either end. It is therefore desirable to locate all injection, acceleration, and extraction elements in long straight sections. The scheme described is designed to satisfy this criterion.

The injection Lambertson located at the midpoint of LB serves equally well for injection of beam in the reverse direction. For colliding beam between the Main Ring and the Energy Doubler, one must be able to operate both accelerators in the reverse direction. This can be done by reversing the dipole fields and leaving the quadrupole fields unchanged. The focusing actions of all the quadrupoles on the beam circulating in the opposite direction will then be reversed so that the focusing sequence on the beam will remain unchanged. An identical but reversed injection system, using the same injection Lambertson with field reversed, will transfer the beam from the Main Ring to the Energy Doubler in exactly the same manner but in the reversed direction. Of course, it is not really necessary to use the same Lambertson for injection in both directions. One can move the Lambertson downstream and install two such magnets with opposite fields, one on each side of the midpoint of LB. For injection in a given direction, only one of the magnets is to be used; the other one is turned off. Alternatively, one can transfer the reversed beam in a different long-straight section using an entirely independent system. For either arrangement, moving the injection Lambertson downstream will reduce the required bending strength of both the injection and the extraction Lambertson magnets.

C. Beam Dynamics and Aperture Considerations

1. Magnetic-field corrections. The Energy Doubler has a magnet lattice that is essentially identical to the Main Accelerator, and the beam-dynamical effects arising from constructional errors are therefore the same for the two accelerators and have, thus, already been determined (see Section 4.4 of NAL Design Report 1968). Furthermore, the tuning and operating experience gained from the Main Ring is applicable in detail to the Doubler. Finding and improving the closed orbit with a properly instrumented beam position-monitoring system is a well-understood problem. Given good magnetic-measurement data, a careful survey, and reliable means for beam steering, it is likely that a circulating beam can be obtained without unusual difficulty insofar as effects due to magnetic-length and placement errors are concerned.

Harmonic multipole errors excite resonances. Low-order resonancs cause excessive growth in beam size and must be avoided. But with reasonable care in the fabrication of magnets, the widths of these resonances caused by harmonic errors can be held down to tolerable values, and with proper regulation of the power supplies these resonances can be avoided. This is especially true with a superconducting magnet system, for which the response of the field to power-supply ripple is small and slow. It is therefore likely that no harmonic correction will be necessary.

The chromaticity, the variation of betatron tune with momentum, must be adjusted to ensure that the ring has a reasonably large momentum aperture. The natural kinematic chromaticity of the ring is $\frac{\Delta\nu}{\Delta p/p} \simeq 22$. To first order, ignoring space-charge instability problems, this chromaticity can be reduced to zero. Landau damping of coherent space-charge instabilities introduces other requirements on chromaticity. An average sextupole field is provided by the trim-magnet packages located in the ministraight sections to adjust chromaticity to the desired value. Higher-order dependences of ν on $(\Delta p/p)^2$, $(\Delta p/p)^3$, etc., can be corrected by higher-order average multipoles, but in all likelihood these corrections will not be necessary. Dependence of tune on amplitude limits the betatron aperture of the ring. This dependence is compensated by average octupole fields produced also by the trim-magnet packages.

2. Aperture. The most severe aperture requirement is imposed by the operation of an efficient slow beam-extraction system. In a resonant-extraction scheme, the aperture has to be large enough in the extraction plane to permit an unstable betatron oscillation of sufficient amplitude to develop so that the amplitude-dependent step size becomes sufficiently large to jump across an extraction septum with high efficiency. The half-integer resonant extraction system currently in use on the main accelerator takes up about 2 in. of aperture for the unstable betatron oscillation to build up and another0.75 in. (step size 0.375 in.) to accommodate the stepped-over beam that enters the septum aperture at the proper phase of oscillation. At present, the extraction efficiency is close to 99% and is limited by the effective thickness of the electrostatic septum.

For a superconducting magnet ring with negligible field ripple it is more advantageous to employ a third-integer scheme. In such a scheme, the stable betatron amplitude is not enlarged near resonance as in the half-integer scheme, so that more of the available aperture can be used for the buildup of unstable betatron amplitude. Moreover, the step size is the accumulation of the amplitude growth in 3 turns instead of 2. Thus, one can obtain larger step size for the same available aperture or the same step size with a smaller total aperture. The slow-extraction system for the Doubler described below requires a horizontal good-field aperture of 2.25 in.

3. Space-charge effects. The incoherent space-charge tune shift for a beam intensity of 5×10^{13} proton/pulse is negligible at energies above 100 GeV.

Intensity-dependent collective effects in the Energy Doubler can be estimated by scaling from knowledge of the same effects in the Main Ring. We can expect longitudinal as well as transverse coherent instabilities to occur in the same manner as they do in the Main Ring. Since both the tune spread and the momentum spread in the beam decrease roughly linearly as energy increases, the tolerable transverse and longitudinal coupling impedances of the beam enclosure for the Doubler will be about half those for the Main Ring. Conversely, for the same coupling impedances, the 1000-GeV beam in the Doubler can be expected to be twice as unstable as the 500 GeV Main-Ring beam.

Longitudinally, the tolerable impedance in the Main Ring is given by $Z/n \sim 10\Omega$, where n is the mode number. The major contribution to this coupling impedance comes from parasitic modes in the rf cavities. This instability was cured after these parasitic modes were properly damped and the inactive cavities were properly shorted on the flat-top. Similar precautions will be taken in the design of the Doubler rf cavities. In addition, a wide-band longitudinal feedback damper may be necessary for the full intensity of 5×10^{13} protons/pulse. Such a damper is being designed for the Main Ring.

On the other hand, since both the aperture and the rf of the Doubler can contain much larger momentum spread, it should be possible to increase the momentum spread intentionally as the beam is being accelerated. One can keep the momentum spread at 1000 GeV as large as or even larger than that at 500 GeV. The larger momentum spread, in addition to maintaining stability through Landau damping, will make slow extraction easier and smoother.

Transverse coherent instabilities in the Doubler must be cured in the same manner as those in the Main Ring by using a wide-band feedback damper. This technology is well-developed and straightforward. In addition to the damper, which will take care of the lower modes, the chromaticity of the machine must be adjusted by the trim sextupoles to positive values throughout the acceleration cycle to insure instability of the higher head-tail modes.

D. RF Accelerating System

It is expected that the ring magnet of the Energy Doubler will be capable of being operated at a wide range of ramp rates, depending on the requirements of the application. The highest ramp rate considered is 100 GeV/sec. The rf system is therefore designed to have the capability of accelerating 5×10^{13} protons at the rate of 100 GeV/sec. With a revolution period of 21 μsec, this corresponds to an energy gain of 2.1 MeV/turn and a power to the beam of 800 kW.

The position of the Doubler directly underneath the Main Ring is such that its circumference can be adjusted to be precisely equal to that of the Main Ring. This will enable synchronous transfer of the beam from the Main Ring to the Doubler. After transfer to the Doubler, the beam bunches from the Main Ring are captured directly into accelerating rf buckets without debunching and rebunching. The process of debunching and rebunching would require a front porch in the Doubler magnet ramp and would always incur some beam loss.

1. Choice of frequency. For synchronous beam transfer, the rf harmonic number of the Doubler should be an integral multiple of 1113, corresponding to a frequency that is an integral multiple of 53.1 MHz. The choice of frequency depends on (1) consideration of beam dynamics, (2) consideration of physical dimensions of the cavities, and (3) availablility of power-amplifier tubes for supplying the rf power.

It is desirable to have the rf cavities small. In our case, the placement of the Doubler directly underneath the Main Ring restricts the diameter of the cavities to less than 0.8 m. For multi-gap cavities the gaps are generally spaced at intervals corresponding to multiples of 180° rf phase. Hence, higher accelerating voltages can be achieved per unit length of cavity at higher frequencies. These considerations favor the choice of a high frequency.

On the other hand, the shorter wave length at higher frequency means shorter rf buckets, and hence a restriction on the maximum beam-bunch length that can be contained. The beam in the Main Ring is most tightly bunched at the extraction energy when the magnetic field is constant (flat-topped) and the rf is full-on at some 3.5 MW. At 100 GeV, the measured longitudinal emittance of 0.1 eV-sec per beam bunch in the Main Ring gives under these conditions, a bunch length of 0.5 m and a momentum spread of 0.25 eV-sec/m. This bunch length is short for 53.1 MHz rf buckets, but is long compared with buckets at frequencies more than twice this value. At three times this frequency, to obtain rf buckets matched in shape to these beam bunches would already require a rather low synchronous phase angle and hence a rather high cavity voltage. As a compromise, we have chosen an rf frequency twice that of the Main Ring, or 106.2 MHz for the Energy Doubler. This corresponds to a harmonic number of 2226.

With this harmonic number and an acceleration rate of 100 GeV/sec or 2.1 MeV/turn, we can operate at a reasonably high synchronous phase angle of 50°. This gives a required cavity voltage of 2.75 MV/turn and a bucket area of 0.25 eV-sec, which is adequate to contain the beam-bunch longitudinal emittance of 0.1 eV-sec. To match the shape of the beam bunches to that of the buckets, so that there will be no dilution during transfer, the beam should be extracted from the Main Ring on the flattop at 100 GeV with the Main Ring rf operating at the full voltage of 3.5 MV/turn. Only every other bucket in the Energy Doubler is filled by a beam bunch. At the frequency of 106.2 MHz, the cavity diameter can be made smaller than 0.8 m and several tetrodes are commercially available for use as the rf power amplifier.

Initially, when the Doubler is operating at an acceleration rate of 37.5 GeV/sec (100 GeV to 1000 GeV in 24 sec) or 0.786 MeV/turn, we have to lower the synchronous phase angle to 42° to obtain the same bucket area. This gives a required cavity voltage of 1.17 MV/turn. For bunch-shape matching under these conditions, the beam should be extracted from the Main Ring on the 100 GeV flattop with the rf operating at 1.75 MV/turn.

2. Cavity and power amplifier. Because of the very small frequency-modulation range needed, one can consider high-Q, high shunt-impedance cavities. Simple double-gap drift-tube cavities will have adquately high Q and shunt impedance. The cavity shown in Fig. II-2 has a Q of 22000 and a shunt impedance R_{sh} of 1.0 MΩ. The gaps are spaced at 140° instead of 180° of rf phase. This allows the addition of inductance coming from stems extending laterally outward from the midpoint of the cavity for power input and for tuning. This cavity can sustain a gap voltage of 0.5 MV or a total accelerating voltage of (2 sin 70°) x 0.5 MV = 0.94 MV per cavity. Three such cavities will be sufficient to produce the 2.74 MV needed. For the initial low acceleration rate of 37.5 GeV/sec the required voltage of 1.17 MV/turn can be supplied by two or perhaps even one cavity.

The most convenient location for the cavities is in long straight-section F where the Main-Ring rf cavities are housed (the RF Hall). A total length of 4 m is adequate for the three cavities. This space is now avilable near the downstream end of the straight section. In any case, ample space can be made available by removing some of the Main-Ring cavities, which will not be needed for acceleration to only 100 GeV.

In order to accelerate 5 x 10^{13} protons at a rate of 100 GeV/sec, the required rf-power input to the beam is 800 kW or 267 kW per cavity. To this one has to add the power consumed by the cavity, which is

$$\frac{1}{2}\frac{V^2}{R_{sh}} = \frac{(0.46\text{x}10^6)^2}{2\text{x}1.0\text{x}10^6}\ \text{W} \cong 106\ \text{kW}, \tag{1}$$

when operating at a gap voltage of 2.74/6 MV = 0.46 MV. Hence, the power amplifier must deliver 373 kW to the cavity. Each cavity will be powered by four 4CW50,000 tetrodes, each of which is capable of supplying 100 kW power at 106 MHz. A tube of

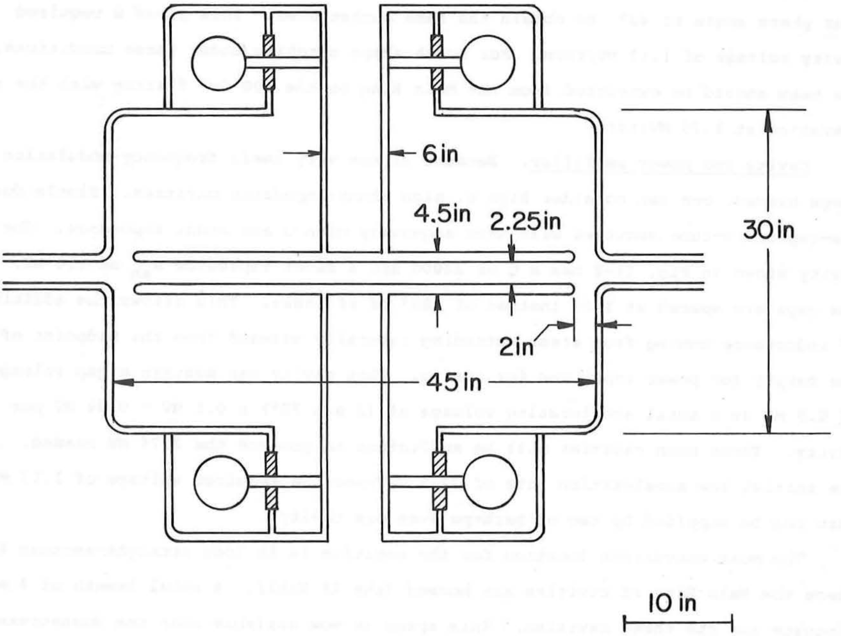

Fig. II-2. Double-gap rf cavity.

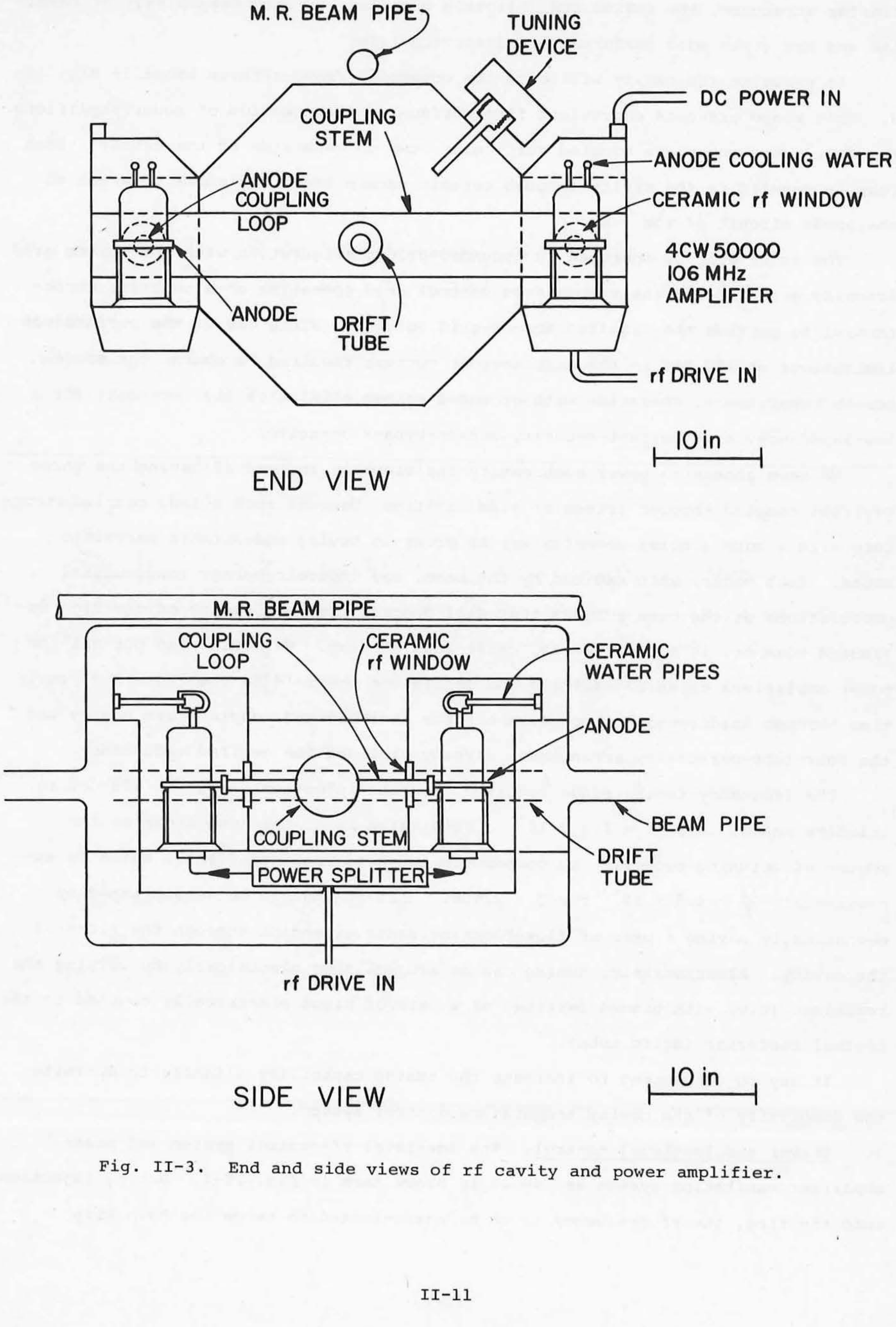

Fig. II-3. End and side views of rf cavity and power amplifier.

similar structure, the 4CW100,000 (slightly modified) is used extensively at Fermilab and has given good performance and service life.

In practice the cavity will have the octagonal cross-section shown in Fig. II-3. This shape presents convenient flat surfaces for connection of power amplifiers. The four power tubes are mounted vertically, two on each side of the cavity. Each tube is coupled to the cavity through ceramic vacuum seal rf windows adjacent to the anode circuit of the tube.

The tubes will be operated in grounded-grid configuration with the screen grid actually grounded and the rf-bypassed control grid operating at a negative dc potential to provide the required screen-grid voltage. Since one of the performance limitations at 100 MHz is the displacement current required to charge the anode-screen capacitance, operation with grounded screen eliminates the necessity for a low-impedance, high current-capacity screen-bypass capacitor.

We have chosen to power each cavity individually instead of having the three cavities coupled through irises or side cavities, because such a long coupled structure with a more complex geometry may be prone to having undesirable parasitic modes. Such modes, when excited by the beam, may induce coherent longitudinal oscillations of the beam bunches that will degrade the duty factor of the slow extracted beam or, in extreme cases, cause loss of beam. We could also put all the power amplifiers on an rf manifold and couple the manifold to the individual cavities through unidirectional couplers, but the manifold and couplers are costly and the four-tube-per-cavity arrangement already provides the desired redundancy.

The frequency tuning range required from the injection energy of 100 GeV to infinite energy is $\Delta f/f = 4.3 \times 10^{-5}$. This value is of the same order as the amount of detuning necessary to compensate for beam-loading effects, which is approximately $\frac{\Delta f}{f} \sim 4.5 \times 10^{-5}$ for $Q \sim 22000$. This tuning can be accomplished by mechanically moving a pair of flux-blocking vanes extending through the sides of the cavity. Alternatively, tuning can be accomplished electrically by varying the reactance (e.g., with biased ferrite) of a pair of plugs electrically coupled to the central conductor (drift tube).

It may be convenient to increase the tuning capability slightly to minimize the complexity of the cavity temperature-control system.

3. <u>Driver and low-level control</u>. The low-level rf-control system and power-amplifier excitation system are shown in block form in Fig. II-4. During injection into the ring, the rf frequency is to be phase-locked to twice the Main Ring

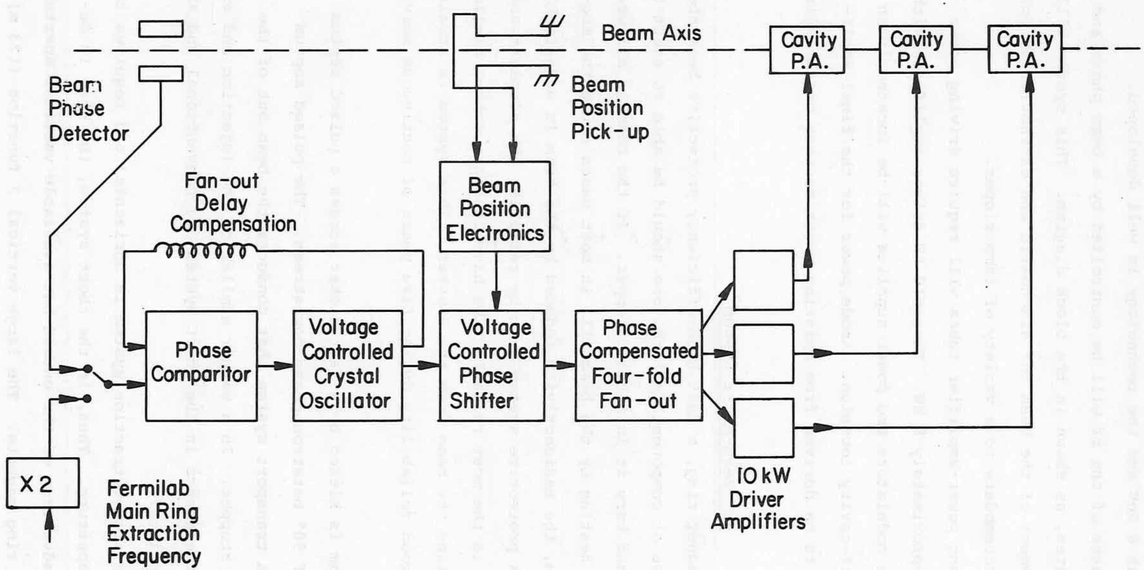

Fig. II-4. Low-level rf system.

extraction frequency. Such a system is presently employed for injection from the booster into the Main Ring at 8 GeV and the technology is well developed.

After injection, the phase of the rf will be controlled by a beam phase and radial-position feedback system, as shown in the block diagram. This system will make possible arbitrary movement of the beam for diagnostic and extraction purposes and it will automatically accommodate to a variety of ramp slopes.

Each cavity with its four power-amplifier tubes will require driving power (in grounded-grid service) of approximately 8 kW. Three-10 kW driver amplifiers with their associated series-tube modulators and power supplies will be located in an existing gallery above the rf-cavity location. Anode power for the final amplifiers is presently expected to be derived from existing power sources of the Main-Ring rf system.

E. Beam-Abort System

In a superconducting magnet ring, a fast high-efficiency protective beam-abort system is important. In case of component failure, one should be able to eject the beam from the ring rapidly and bury it in a beam stopper. If the beam is allowed to strike the ring magnets, heating by the beam will in most cases cause the magnets to quench. In addition, the radioactivity induced by the beam is undesirable.

1. General description. A protective system must be reliable; the simplest and most straightforward scheme is the most reliable. We have chosen a scheme similar to that employed for extracting the beam from the Booster. This system is straightforward and has shown very good reliability during five years of continuous service in the Booster.

In this scheme, the beam is kicked by a fast kicker across a pulsed septum placed at an odd multiple of 90° betatron phase downstream. The pulsed septum forms the first element of a transport system that conducts the beam out of the accelerator and onto a beam stopper. In a manner similar to the injection and extraction systems, all magnet elements in the abort system are conventional and are located in long straight sections.

As described below, the slow-extraction system is horizontal and requires the use of the full horizontal aperture. Thus, in the abort system, the beam is deflected vertically to take advantage of the unused but available vertical aperture in the circular bore of the ring magnets. The large vertical β function (123 m) at the upstream end of a long straight section where the septum is located also favors vertical deflection.

At the moment of an emergency abort, the horizontal position of the beam is unpredictable. For total protection, the septum must extend over nearly the full horizontal aperture of the ring. The iron septum of a Lambertson magnet cannot be uniformly thin over this width. Hence a current-carrying septum is used. The septum is pulsed to avoid the need of cooling. The rise time of the pulse should be short compared with the time it takes for the beam to strike the bore-pipe following a component failure. A rise time of 50 μsec is adequate.

2. Components.

a. Kicker. The kicker is located at the upstream end of long-straight section D and is composed of six sections of ferrite-core window-frame magnets. Each section has a length of 1 m and an aperture of 6 cm (h) x 3 cm (v), and is properly terminated in its characteristic impedance. These kickers are pulsed to a peak field of 1 kG with a rise time of about 0.2 μsec. They will kick a 1000-GeV beam downward by an angle of 0.18 mrad.

b. Septum. The series of septum magnets has a total length of 10 m, an aperture of 4 cm (h) x 2 cm (v), and a septum thickness of 2 mm. The cores will be stacked from 0.1-mm thick laminations so that the magnets can be pulsed to a half-sine wave with a half-period of 100 μsec, corresponding to a quarter-wave rise time of 50 μsec. The peak field is 10 kG and the total bending angle for a 1000-GeV beam is 3 mrad. Since the revolution time of the Doubler is only 21 μsec, during that time the variation of the field near the top of the sine wave is only approximately 0.5% and is quite tolerable. At the entrance of these septum magnets, which is located at the upstream end of long-straight section E, the downward displacement of the beam produced by the kicker is about 2 cm, ample to clear the septum. At the end of these septum magnets, the beam will be 3.5 cm below and at a downward angle of 3 mrad with respect to the Doubler orbit. These septum magnets are followed by sections of higher-field (say, 20 kG) dc magnets that deflect the beam further downward onto a beam stopper buried underneath the tunnel floor.

c. Beam stopper. A simple steel cylinder 3 m long and 1 m diameter will suffice. For added safety, it may be advisable to insert from the front end an aluminum (low-Z) core 1.5 m long and 10 cm in diameter to reduce the thermal shock in case the beam is very narrowly focused. To supply more efficient shielding against neutrons, one may want to surround the stopper with 0.5 m thick concrete. More than 90% of the energy contained in a 1000-GeV beam will be deposited in this stopper.

3. Trigger, timing sequence, and efficiency. The beam-abort system should

normally be triggered every pulse at the end of the beam spill to clean out any small amount of beam remaining in the ring. This will also keep the whole system in proper working condition. Emergency triggers could come from:

(i) Ring-magnet quench

(ii) Loss of rf

(iii) Excessive radiation around the ring

(iv) Excessive horizontal or vertical excursion of the beam.

Other types of triggers may be added as one gains experience in operation.

When an abort trigger is received, the septum is pulsed immediately. This is followed 36 μsec later by the pulsing of the kicker. To keep the geometry of the deflected beam to the stopper fixed during the accelerating ramp, the power supplies of all the magnets must be ramped accordingly, reaching the values given above only at 1000 GeV.

The kicker displaces the beam downward across the septum at a rate of 20 mm/0.2 μsec = 100 mm/μsec. The fraction of beam hitting the 2-mm septum is, therefore, 2 mm/(21 μsec x 100 mm/μsec) $\cong$ 0.1%. Even for a full-intensity beam of 5×10^{13} protons, this amounts to only 5×10^{10} protons hitting the septum, which is entirely tolerable.

Immediately following an emergency abort, injection from the Main Ring will be inhibited until the faulty condition is rectified.

F. Colliding Beams Between Main Ring and Energy Doubler

With both the Main Ring and the Energy Doubler in the same tunnel, it is possible to obtain colliding-beam operation between the two beams. To do this one would inject the 8 GeV beam from the Booster backward into the field-reversed Main Ring. This beam circulating counterclockwise in the Main Ring would be accelerated to 100 GeV, then transferred to the Doubler, also with field reversed. The beam would then be accelerated to say 1000 GeV in the Doubler and stored there. In the meantime, the field in the Main Ring would be returned to its normal direction and a normal clockwise-circulating beam accelerated to some desired energy in the Main Ring. The oppositely circulating beams would then be brought together by steering magnets to collide in a long straight section.

In the following we examine the component systems needed and the performance capabilities of this colliding-beam operation.

1. <u>Operating the Main Ring and the Doubler in the reversed direction</u>. Some slight modifications in the power supplies and the controls are needed to reverse

the current in the Main-Ring dipole circuit. After the current is reversed, the magnets should be pulsed to full current several times to retrain their remanent fields.

To inject the 8-GeV beam from the Booster backward into the Main Ring, one can either turn the beam 180° at the end of the Transfer Hall by some high-field (approximately 65 kG) dipoles and inject backward into the same long straight section A or perhaps more realistically, one can add a second independent backward 8-GeV beam-transfer system. Reversing the excitation current in the Doubler and transferring the beam from the Main Ring to the Doubler in the reversed direction is not difficult. The transfer process was discussed in Section B of this Appendix.

2. Geometry of the colliding beams. The beams are parallel-displaced by dipoles to collide head-on in the middle of a 51-m long straight section, it is most advantageous to position the two rings so that their orbits are as close as possible. This has been a major consideration in locating the Doubler 16 in. underneath and running parallel to the Main Ring. The geometry of the two beams in the long straight section is shown in Fig. II-5. For this geometry, the highest center-of-mass energy is obtained when the Doubler beam is at its full energy of 1000 GeV and the Main-Ring beam is at the highest energy permitted by the strength of the dipoles that displace the beams to collide. The level arm on either side of the colliding-beam region depends on the length ℓ in the middle of the long straight section taken up by the colliding beams. If one assumes 6-m long dipoles with peak field of 42.344 kG, the same field as the Doubler dipole, one finds

Main-Ring beam energy (GeV)	300	400
Beam colliding length ℓ (m)	10.0	3.8
Beam separation at end of common dipoles s (in.)	4.2	3.4

These results show that 1000 GeV on 300 GeV is reasonable, provided the inboard dipoles that are used in common by both beams have an aperture larger than 4.2 in. This geometry gives 10 m for the length over which the beams collide, which may be longer than necessary. If the peak dipole field can be extended to 60 kG, the corresponding values are:

Main-Ring beam energy (GeV)	400	500
Beam colliding length ℓ (m)	13.3	9.5
Beam separation at end of common dipoles s (in.)	4.8	4.1

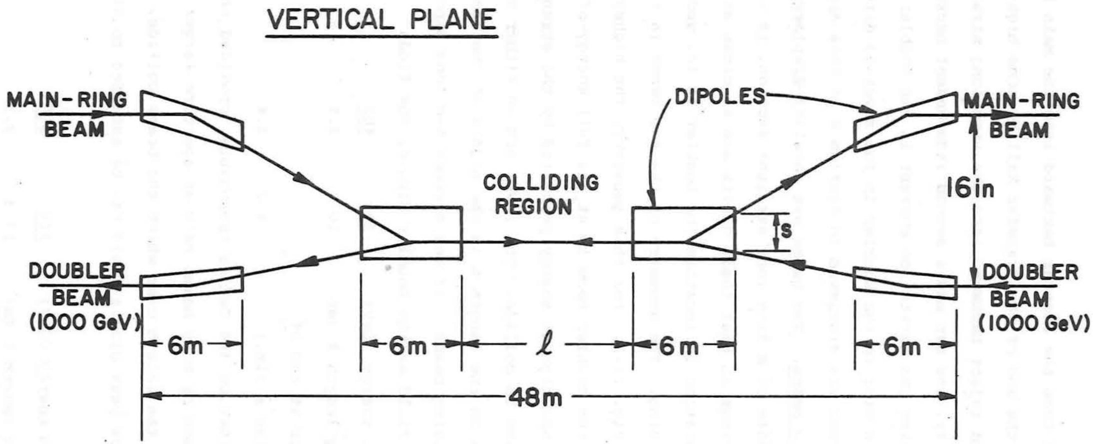

Fig. II-5. Geometry of colliding beams.

This shows that 1000 GeV on 500 GeV can be reasonably managed with 60-kG fields.

Displacing the beams vertically produces a vertical dispersion over the colliding-beam region, but the increase in beam height from this dispersion is small. More detailed study is needed on the step-by-step procedure of arriving at these beams and the colliding configuration.

3. Luminosity and tune shift. The luminosity of two beams with currents I_1 (in A) and I_2 (in A), and identical cross-sectional area a (in mm^2) colliding head-on over a length ℓ (in m) is given by

$$L = (0.26 \times 10^{32}\ \mathrm{cm}^{-2}\ \mathrm{sec}^{-1})\ \frac{I_1 I_2}{a}\ \ell. \tag{2}$$

For an estimate of the lower limit for, say, 1000 GeV on 300 GeV, we take the radius of both beams to be 1.5 mm (that at 300 GeV) and the current of both beams to be 0.15 A, corresponding to 2×10^{13}p/p. Over a 10-m colliding length, the total luminosity will be $0.8 \times 10^{30}\mathrm{cm}^{-2}\mathrm{sec}^{-1}$. If we take a beam intensity of 5×10^{13}p/p and a beam radius of 1 mm (roughtly that at 1000 GeV) we get an upper limit which is $(2.5 \times 1.5)^2 = 14$ times larger of $1.1 \times 10^{31}\mathrm{cm}^{-2}\mathrm{sec}^{-1}$.

Assuming a Gaussian beam profile, the beam-beam tune shift of beam 1 due to beam 2 is given by

$$\Delta\nu_1 \cong 0.096\ \frac{\beta_1}{\gamma_1}\frac{I_2}{a_2}\ , \tag{3}$$

where β_1 and γ_1 are respectively the amplitude function in the colliding region and the energy in mc^2 units of beam 1. The larger tune shift is that of the 300 GeV beam ($\gamma_1 = 321$, $\beta_1 = 70$ m). For the lower and upper limits of luminosity given above, we find for $\Delta\nu_1$ the values 0.004 and 0.025. The larger value is higher than the conventionally assumed tolerable limit of 0.005, but the real limit still remains to be determined empirically.

We not examine the various possibilities of increasing the luminosity beyond the upper limit given above. We can increase the 300-GeV beam current I_1. This will leave the tune shift of this beam unchanged. Continued effort is spent in improving the Main-Ring beam intensity.

The current I_2 of the 1000-GeV beam in the Doubler can be substantially increased by momentum stacking in the manner of the CERN ISR. But if the luminosity is indeed limited by the tune shift of the 300-GeV beam, increasing I_2 will not help, because both the luminosity and the tune shift have the same linear dependence on I_2.

One can reduce a by reducing the amplitude function in the colliding region. This can be done by retuning the matching quadrupoles in the long straight section. Assuming both β_1 and β_2 are reduced by a factor 10 from 70 m to 7 m, a(=a_1 = a_2) will be reduced by a factor 10. This leaves the tune shift unchanged, but improves the luminosity by a factor 10.

Because the wavelengths of both the Main-Ring rf (5.6 m) and the Doubler rf (2.8 m) are shorter than the beam-colliding length (10 m), bunching the beams will not increase the total luminosity. This bunching will, however, localize the luminous region, which may be advantageous for certain experiments.

We conclude, therefore, that it is feasible in principle to collide the 1000-GeV Doubler beam with the Main-Ring beam at 300-500 GeV. The maximum luminosity obtainable over a 10-m length can be in the range of 10^{30} - 10^{31}cm^{-2}sec^{-1}. As mentioned above, there are many operational problems, such as beam stability, beam switching, vacuum, duty factor, and so forth, that must be further studied in detail.

G. Extraction System

Both slow and fast modes of beam extraction are required for the Energy Doubler in order to optimize its use for physics experiments with fixed targets. As in the design of the beam-transfer system, we take as a design criterion that all magnet elements that may be sprayed by stray beams should be conventional and should be located in long straight sections where the vacuum pipe bore is warm. In addition, the extraction channel is designed to transport the extracted beam to the existing Main-Ring external-beam line. The present beam switchyard will be modified to transport the 1000-GeV beam to various existing experimental areas and facilities.

1. Slow extraction. As stated in Section C of this Appendix, the horizontal third-integer resonant-extraction scheme operation at ν = 19-1/3 will be used for slow extraction from the Doubler. In this scheme, the horizontal width of the beam is resonantly excited by a sextupole to grow at an increasing rate per turn. The outer part of the beam then steps across an electrostatic wire septum and is deflected by the septum to enter an extraction channel, which begins at the upstream end of long-straight section A (LA).

The sextupole is placed in long straight section D 10 m downstream of the midpoint D0. The electrostatic septum is located at the downstream end of long-straight section F and positioned so that the septum is 2 cm outside the central orbit. For the third-integer resonance, the oscillations of the particles return to the same phase every three revolutions but with larger amplitudes. With a sextupole strength of $B''\ell = 2.4 \times 10^4$ kG/m and a betatron tune of $\nu = 19\text{-}1/3$, the beam half-width at the septum will grow from 2.0 cm to 2.9 cm in three turns. The 0.9-cm wide part of the beam that is inside the aperture of the electrostatic septum is deflected 0.06 mrad by the septum. To deflect the 1000-GeV beam by 0.06 mrad, the electrostatic septum must be 6 m long and operate at a field of 100 kV/cm. As it arrives at the entrance of the extraction channel, this deflected beam will be 0.42 cm wide and separated from the undeflected part of the beam by a gap of 0.32 cm. This separation is adequate to clear the iron septum of the Lambertson magnet that constitutes the first element of the extraction channel. The part of the beam passing just outside the channel aperture will continue to circulate around the ring and be extracted three turns later.

The largest beam excursion in normal cell-dipoles is ±2.8 cm and occurs in sector F between the electrostatic septum and the extraction channel. The aperture radius 1.125 in. = 2.86 cm of the ring dipole is thus just adequate. The largest beam excursion anywhere is ±3.1 cm and occurs in quadrupoles immediately downstream of the long straight sections. Quadrupoles should therefore have an aperture radius larger than 3.1 cm or about 1.25 in.

With a step size of 9 mm and an effective electrostatic septum thickness of, say, 0.1 mm, the extraction efficiency should be close to 99%. During extraction, the horizontal betatron tune is shifted from 19.4 to 19-1/3 either by the normal-cell quadrupole or by a conventional extraction quadrupole located in a long straight section at proper betatron phase relative to the electrostatic septum.

This system can also be employed for the medium-fast extraction (coherent extraction) in the same manner as is done on the Main Ring.

2. Fast (one-turn) extraction. Fast extraction is accomplished simply by a fast kicker located at the downstream end of LA. The kicker has a length of 3 m, a peak field of 1 kG and a rise time less than 0.2 μsec. It will be able to kick the beam 0.09 mrad. The displacement at the entrance to the extraction channel from this kick will be 6.6 mm, adequate to clear the channel septum.

3. Extraction channel. Beginning at the upstream end of LA, the first elements are sections of Lambertson iron-septum magnets totalling 20 m in length and operating at an average field of 8.9 kG. The entire beam channel is shown in Fig. II-6. These magnets bend and beam vertically upward by 5.35 mrad. After the Lambertson

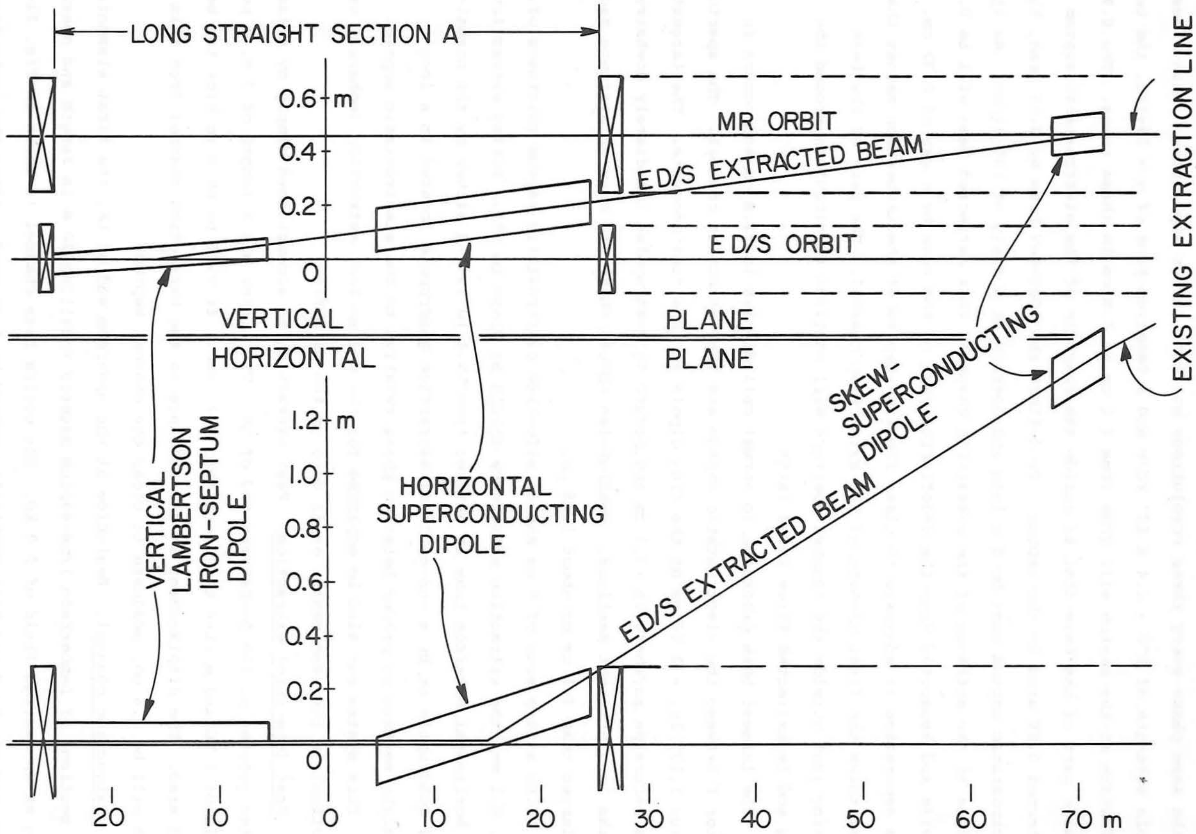

Fig, II-6. Vertical and horizontal views of Energy Doubler extraction channel.

magnets, the beam drifts for 10 m, then enters a series of superconducting dipoles with a total length of 20 m and an average field of 40 kG. These dipoles are far enough downstream from all the septa so that there is no danger of their being sprayed by stray beam. These dipoles deflect the beam horizontally outward by 24 mrad. The combination of 5.35 mrad up and 24 mrad out will make the beam cross the present extracted-beam line about 5 m from the end of the Transfer Hall, where sections of superconducting dipole with a total length of 4.8 m and an average field of 40 kG tilted at a 20° angle from the horizontal will deflect the beam vertically downward by 5.35 mrad and horizontally inward by 2 mrad to follow the existing beam line. Superconducting quadrupoles will be installed in the transport line after the 20-m dipole to produce the desired beam optics.

With the 4.8-m dipoles turned off, the existing extraction channel can be operated for the beam extracted from the Main Ring without modification or interference. If desired, the 4.8-m section of superconducting dipoles can be replaced by a longer section of conventional dipoles having the same bending strength. These conventional dipoles can be turned on and off rapidly to switch between the Doubler and Main-Ring pulses.

The extraction system described here was discussed in Ref. 1. In addition, the work of Collins and Edwards[2] has led to a better understanding of the aperture, extraction system, and correction elements. The work reported in this appendix depends on their calculations.

REFERENCES

1. Third-Integer Resonant Extraction from the Energy Doubler/Saver. TM-593. L. C. Teng, June 30, 1975.
2. A Discussion of Aperture and Space Allocation in the Energy Doubler/Saver. TM-614. T. L. Collins and D. A. Edwards, September, 1975.

APPENDIX III. MAGNET CALCULATIONS

S. C. Snowdon

Optimized parameters for the 45-kG dipole are summarized in Table III-I. The two-shell geometry is shown in Fig. 2 of the main text. Conductor positions are given in Table III-II and magnetic forces in Table III-III. An additional displacement force of 10 lb/in. would be generated if the coil package were displaced from the center of the iron by 0.010 in.

The shell locations given optimize the central-field integral including end effects (3D) as shown in Table III-IV, which also gives the homogeneity of the central field (2D) resulting from this optimization.

The optimized parameters for the 25.7 kG/in. quadrupole are summarized in Table III-V. Note that three shells were required, as shown in Fig. 3 of the main text, to give the required strength using the same conductor and conductor current as in the dipole. Tables III-VI and III-VII contain the conductor locations and magnetic forces in the first octant. An additional displacement force of 11 lb/in. would be generated if the coil package were displaced from the center of the iron by 0.010 in.

The shell locations given optimize the central-field integral including end effects (3D) as shown in Table III-VIII, which also gives the homogeneity of the central field (2D) resulting from the optimization.

Table III-I. Design Data for Dipole Magnet

Central Field	45 kG
Effective Length	252 in.
Conductor Current	4609 A
Total Number of Turns	110
Conductor Size - 23-strand cable (no insulation)	0.304 in. by (0.052/0.050) in.
Effective Current Density	297.3 kA/in.^{2}
Maximum Field at Conductor	49.1 kG
Inner Conductor Radius	1.500 in.
Inner Iron Radius	3.750 in.
Weight of Iron	7375 lb
Weight of Conductor	285 lb
Inductance	0.043 H
Stored Energy	0.51 MJ

Table III-II. Location of Conductor in First Quadrant

Layer	Turns	θ_s (Deg)	θ_f (Deg)	R_0 (in.)	R_1 (in.)	Wrap (in.)	Spacer (in.)
1	34	.1729	72.9489	1.500	1.814	.005	.00093
2	1	.1437	2.0114	1.835	2.153	.007	.00000
3	20	2.0098	37.0405	1.835	2.149	.005	-.00011

Table III-III. Forces on Each Conductor

Layer	Cond.	1	2	3	4	5	6	7	8
1	F_x(lb/in.)	71.2	71.5	71.8	72.3	72.9	73.5	74.3	75.2
		76.1	77.2	78.2	79.4	80.5	81.6	82.5	83.1
		83.3	82.9	82.1	81.4	81.1	81.2	81.8	82.7
		84.1	85.8	87.9	90.4	93.3	96.8	101.0	106.0
		112.3	120.3						
1	F_y(lb/in.)	.4	-1.2	-2.8	-4.4	-6.0	-7.6	-9.3	-11.0
		-12.8	-14.6	-16.5	-18.6	-20.8	-23.1	-25.6	-28.3
		-30.9	-33.4	-34.9	-35.8	-36.1	-36.0	-35.7	-35.2
		-34.5	-33.9	-33.1	-32.3	-31.5	-30.7	-29.8	-29.1
		-28.4	-28.1						
2	F_x(lb/in.)	-11.1	-10.5	-10.2	-9.7	-9.0	-8.1	-7.0	-5.7
		-4.1	-2.4	-.4	1.8	4.3	7.0	10.1	13.5
		17.4	21.8	26.8	32.8	40.1			
2	F_y(lb/in.)	-.4	-3.9	-7.6	-11.3	-14.9	-18.4	-21.9	-25.4
		-28.9	-32.4	-35.9	-39.4	-43.0	-46.5	-50.2	-54.0
		-58.0	-62.3	-67.0	-72.5	-79.1			

Net x-Force on Current in First Quadrant 2953 lb/in.

Net y-Force on Current in First Quadrant -1565 lb/in.

Table III-IV. Field Homogeneity (B_n/B_1 at 1-in. Radius)

	Unsaturated		Finite Permeability	
	(2D)	(3D)	(2D)	(3D)
Dipole	1.00000	1.00000	.99725	.9980
Sextupole	.00119	-.00002	.00130	.0001
Decapole	.00022	.00008	.00032	.0002
14-pole	.00051	.00047	.00014	.0001
18-pole	-.00116	-.00116	-.00054	-.0005
22-pole	.00038	.00037	-.00168	-.0002

Table III-V. Design Data for Quadrupole Magnets

Central Gradient	25.7 kG/in.
Effective Length	53 in.
Conductor Current	4609 A
Total Number of Turns (4-poles)	156
Conductor Size - 23-strand cable	
(no insulation)	0.304 in. by (0.052/0.050) in.
Effective Current Density	297.3 kA/in.^{2}
Maximum Field at Conductor	46.9 kG
Inner Conductor Radius	1.625 in.
Inner Iron Radius	3.875 in.
Weight of Iron	1330 lb
Weight of Conductor	85 lb
Inductance	0.0065 H
Stored Energy	93 kJ

Table III-VI. Location of Conductors in First Octant

Layer	Turns	θ_s (Deg)	θ_f (Deg)	R_0 (in.)	R_1 (in.)	Wrap (in.)	Spacer (in.)
1	16	1.2861	32.2763	1.625	1.939	.005	-.00081
2	13	1.0826	22.4571	1.960	2.274	.005	-.00027
3	1	.9339	2.4515	2.295	2.613	.007	.00000
4	9	2.4511	15.2720	2.295	2.609	.005	-.00004

Table III-VII. Forces on Each Conductor

Layer	Cond.	1	2	3	4	5	6	7	8
1	F_x(lb/in.)	73.2	73.9	74.5	75.0	75.2	75.4	75.3	75.2
		74.7	74.1	73.1	72.1	71.8	72.5	74.4	77.9
1	F_y(lb/in.)	3.4	-3.7	-10.6	-17.3	-23.8	-30.2	-36.7	-43.0
		-49.3	-55.5	-61.5	-66.8	-71.7	-76.4	-81.8	-88.1
2	F_x(lb/in.)	17.4	17.8	18.2	18.8	19.4	20.0	20.6	21.1
		21.5	22.2	23.8	26.5	30.7			
2	F_y(lb/in.)	2.7	-5.7	-14.0	-22.3	-30.7	-39.2	-47.7	-56.0
		-64.3	-72.0	-79.6	-87.6	-96.7			
3	F_x(lb/in.)	-34.4	-34.0	-33.5	-32.6	-31.1	-29.2	-26.5	-23.1
		-18.9	-13.8						
3	F_y(lb/in.)	1.8	-6.7	-15.2	-23.4	-31.8	-40.3	-49.1	-58.4
		-68.7	-80.4						

Net x-Force on Current in First Octant 1189 lb/in.

Net y-Force on Current in First Octant -1698 lb/in.

Table III-VIII. Field Homogeneity (B_n/B_2 at 1-in. Radius)

	Unsaturated		Finite Permeability	
	(2D)	(3D)	(2D)	(3D)
Quadrupole	1.00000	1.00000	.99995	.9999
12-pole	.00096	.00000	.00096	.0010
20-pole	-.00115	-.00115	-.00115	-.0012
28-pole	.00005	.00005	.00005	.0001

APPENDIX IV. RADIATION-DAMAGE CONSIDERATIONS

P. A. Sanger

The effects of radiation on the superconducting magnets may be an important factor in both the operation and the long-term reliability of the Energy Doubler. Studies of these effects have been concentrated in two main areas, effects of beam heating on magnet performance and long-term degradation of materials such as insulations and conductors.

A problem in the understanding of radiation-heating effects is the lack of detailed theoretical and experimental investigations in this area. It can, however, be concluded that the response of a system to radiation heating is strongly dependent on the details of construction, notably the enthalpy of the magnet-coil materials and the heat-transfer capabilities of the conductor.[1] The approach adopted for the Energy Doubler has been to correlate experimentally the quench current of our magnets under simulated loss conditions to a simple calorimeter under the same loss conditions. This correlation then allows us to evaluate the performance of our magnets at other locations without the complications of installing a cryogenic magnet at that location. Preliminary data indicate that radiation heating will probably not be a serious limitation to the normal operation of the Energy Doubler. Nevertheless, tuning will have to be accomplished at the lowest possible intensity. The use of superconducting elements in the extraction, injection, and abort systems is questionable and has been avoided. (See Appendix II.)

The sensitivity of polymeric materials to ionizing radiation varies greatly depending on their composition. Usable limits range from 10^5 rads (Teflon) to 10^{11} rads (mineral-filled epoxy). Energy-Doubler magnets will utilize epoxies as structural adhesives and as part of the conductor insulation, various polymers as high-voltage electrical insulation for instrumentation leads, and Mylar in the thermal insulation. Reasonable choices for each application can be made based on typical dose rates in the present accelerator. Measurements are in progress to determine dose levels at locations comparable to those planned for the superconducting magnets. Dose rates of the order of 10^8 rads/yr are expected.[2,3]

Radiation effects on the metallic components of the magnets are also being investigated. The resistivity of the stablizing copper matrix of the conductor is the most sensitive to radiation.[4] Sizable resistivity increases have been measured and are being studied. It has been found that the effect of these changes can be minimized by periodic room-temperature anneals.

References

[1]G. T. Danby, Radiation Heating: Experience and Projections, Proc. 1975 Isabelle Summer Study, BNL-20550, Vol. 2, p. 631

[2]M. Awschalom et al., Radiation Measurement Around the Fermilab 300 GeV Main Accelerator, TM-516, September 1974.

[3]J. H. McCrary et al., Radiation Levels in the Fermilab Main Ring Enclosure During Accelerator Operation, TM-623, November 1975.

[4]P. Sanger, Displacement Damage for 300 GeV Protons, Proc. 1975 Isabelle Summer Study, BNL-20550, Vol. 2, p. 626.

APPENDIX V. SUPERCONDUCTING WIRE

B. P. Strauss

A. Introduction

Many of the operating characteristics of a superconducting magnet, as well as the cost, are strongly dependent on the specific design and construction of the superconducting wire. In this section we describe the choice of conductor and its construction, as well as some of the trade-offs that were made.

B. Superconductor Parameters

Superconductors can be characterized by their critical temperature, critical field, and critical current. High critical-current density is required in order to minimize the total amount of wire and cost. It is also required in order to stabilize the conductor for successful magnet operation. This stabilization is accomplished by providing a high-conductivity copper or aluminum matrix around the superconducting alloy. The stabilizing matrix serves two purposes. First, it provides a parallel conduction path shunting any excess current above the critical current of the superconductor. The criterion of stability is that the I^2R losses in the matrix are less than the total capacity for local heat transfer to the helium bath. Second, high-conductivity metals such as copper have low magnetic diffusivities. This means that the movement of flux lines is slowed down, thus limiting the occurrence of flux jumps. A flux jump is a change in flux within the conductor that could cause a quench if the magnetic energy change exceeded a critical level.

By examining the physics of a single superconducting filament in a copper matrix, we can solve the diffusion equations for a finite local temperature rise at the surface of the superconducting alloy. This gives the following criterion for stability:

$$\frac{d}{D} \lesssim \frac{138}{\pi^2} \frac{k_s}{\rho_{cu}} \frac{1}{J_c^2} \frac{J_c}{\partial J_c/\partial T} , \qquad (1)$$

where k_s is the thermal conductivity of the superconductor, ρ_{cu} is the resistivity of the copper matrix, d is the diameter of the filament, D is the overall diameter of the strand, and J_c is the critical current density. This criterion and the

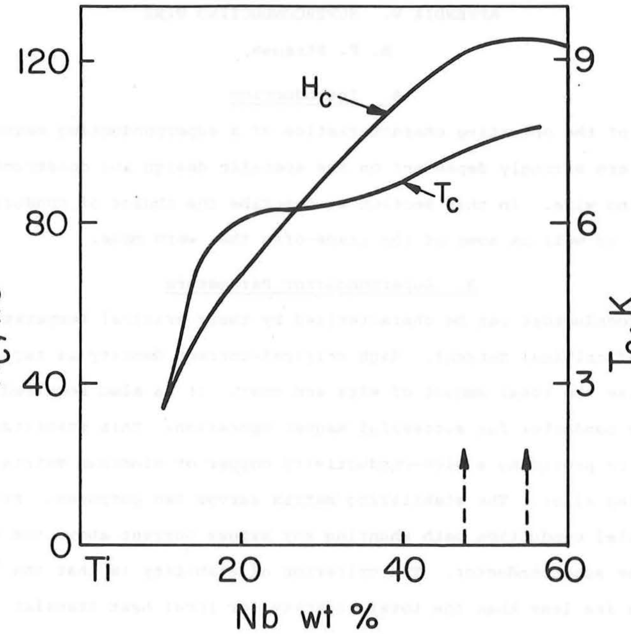

Fig. V-1. T_c and H_{c2} as a function of composition.

adiabatic stability criterion of magnetic stored energy in an individual filament require that the individual filament size be smaller than 10 μm. It should be noted that these models, as well as the ac loss models to be discussed later, require that the individual filaments be electrically decoupled from each other. Decoupling is accomplished by twisting the wire around its axis, thus forcing the individual filaments to assume a helical path within the stabilizing matrix. Thus, to attain stability, one must fabricate a conductor with small twisted filaments and one must provide a high-conductivity matrix.

C. Fabrication Techniques

With present technology, one is limited to niobium-titanium alloys in order to be able to fabricate conductors with all the above properties. Niobium-titanium has the ductility (as compared with, say, NbZr solid-solution) to permit the large-scale reductions necessary in production. For typical conductors, one starts by assembling alloy rods into hex-o.d., round-i.d. copper (ASTM Spe. B-170-1) tubes. These tubes are then stacked in a hexagonal array until the required number of filaments is reached. To attain the small filament sizes discussed above, more than 2000 composite rods are required. An extrusion can is then slipped over the stacked assembly and filler rods are inserted to help increase the packing density. The nose and tail pieces are then electron-beam welded into the can as it is pumped out.

The assembled can is then extruded at about a 16 to 1 reduction in area. Rod drawing then follows. In this process, the composite is reduced to approximately 0.30 in. diameter. Standard wire-drawing techniques are used to reduce the diameter of the wire further. At several points during this process, the wire is annealed to soften the copper.

D. Thermal and Mechanical Processing

In order to optimize the superconducting properties, the choice of alloy and the heat-treatment schedule during reduction are important. The critical temperature T_c and upper critical field H_{c2} are not very sensitive to composition, as shown in Fig. V-1.[2] On the other hand, critical current is not an inherent property of the material and benefits from treatment. Microscopically, magnetic flux penetrates a type-II superconductor in the form of fluxons or quantized flux lines. These fluxons interact with the transport current by means of the Lorentz force, JxH. During flux motion or change, voltages are induced by Faraday's Law and the superconductor becomes normal. Thus one must limit the motion of the flux lines by

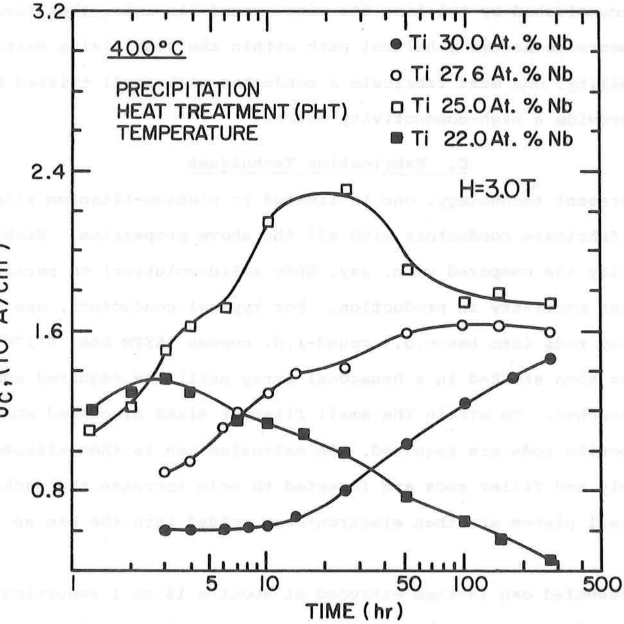

Fig. V-2. J_c (3T) as a function of heat treatment time for several alloys.

"pinning" in order to optimize the critical current. Effective pinning sites are normal regions within the superconductor, which can be inhomogeneities, dislocations, precipitates or voids. In the following, the effects of mechanical and thermal processing are discussed.

For high-titanium alloys (those with greater than 50% Ti by weight), superconducting properties are optimized by a precipitation heat treatment (PHT) to form a fine distribution of normal flux-pinning particles. Figure V-2 shows parametric J_c curves for several alloys as functions of time for fixed heat-treatment temperature.[3] Here one can see typical effects that would be evident in plotting, say, mechanical properties in a PHT alloy. For example, the effects of over-aging are plainly evident. The amount of prior cold work also affects the current density, because dislocations usually provide nucleation centers for precipitation growth.

Figure V-3 is a plot of the critical temperature as a function of PHT.[2] These data suggest that heat treatment may change the chemistry of the matrix phase because critical temperature is a function of composition.

For low-Ti alloys (Nb44-48Ti), cold work is the predominant factor in attaining high H_c. Figure V-4 shows the effect of heat treatment on a cold-worked Nb45Ti alloy.[2] The ideal structure has the dislocation networks in a cellular structure with an average cell-wall separation of a few hundred Angstroms. In this work, the authors found that both the J_c and the α-phase precipitate increased with cold work.

Figures V-5 and V-6 are from work by Neal et al.[4] Here one can see the effects of cold work and heat treatment on the Lorentz or pinning force. In Fig. V-5, one can see J_c increasing with working and in fact there is a minimum amount of working at which the pinning force takes a large jump. In Fig. V-6, one sees the effect of heat-treatment time. Heat treatments in the range of 300°C for one hour produce a large increase in J_c. At higher temperatures, gain growth was obviously too high and properties began to fall. Heat treatment in the 350°C range for times exceeding one hour also improved the critical current capacity.

<u>Intermediate Heat Treatments</u>. The timing of the heat treatments can produce changes in J_c for the equivalent amount of cold work. An intermediate heat treatment will result in recovery and cell-wall rearrangement and perhaps some precipitation within the highly deformed structure. Additional cold work after the heat treatment will produce new dislocations that tend to tangle around the precipitates and cell walls and result in more effective pinning centers. Figure V-7 illustrates

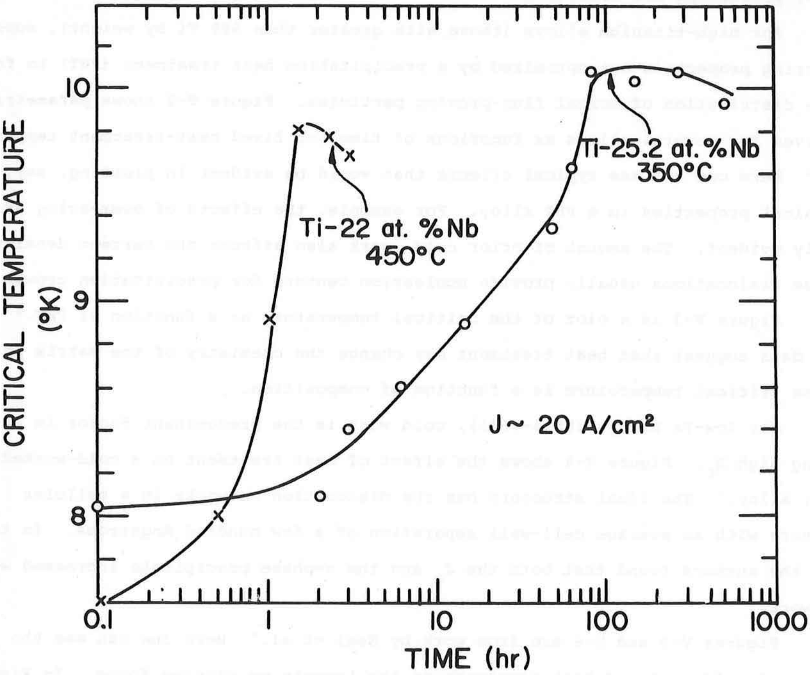

Fig. V-3. T_c vs. heat treatment time.

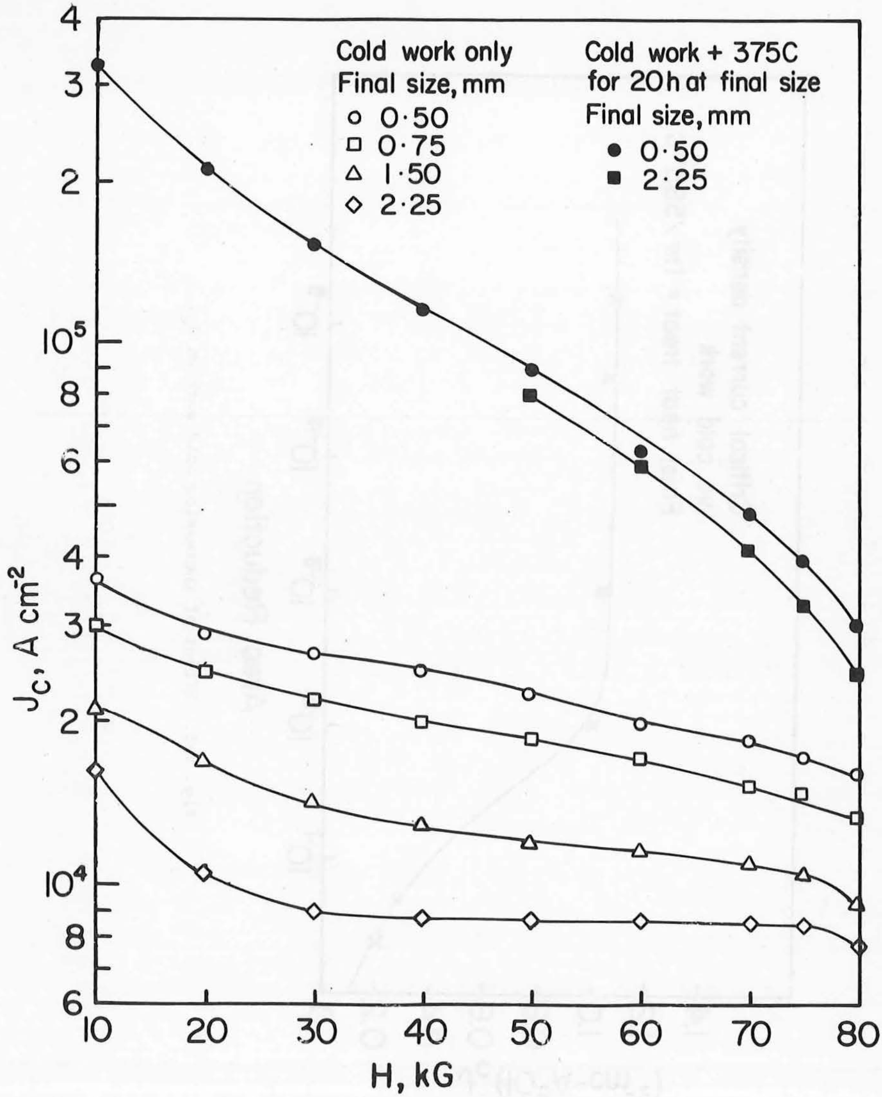

Fig. V-4. Effect of increasing cold work on J_c.

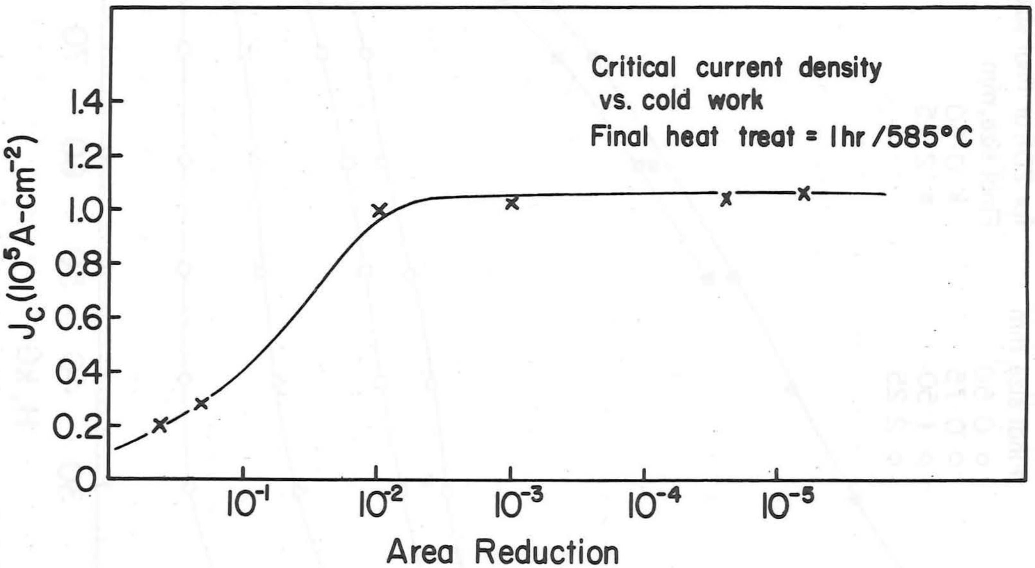

Fig. V-5. Effect of increasing cold work on J_c.

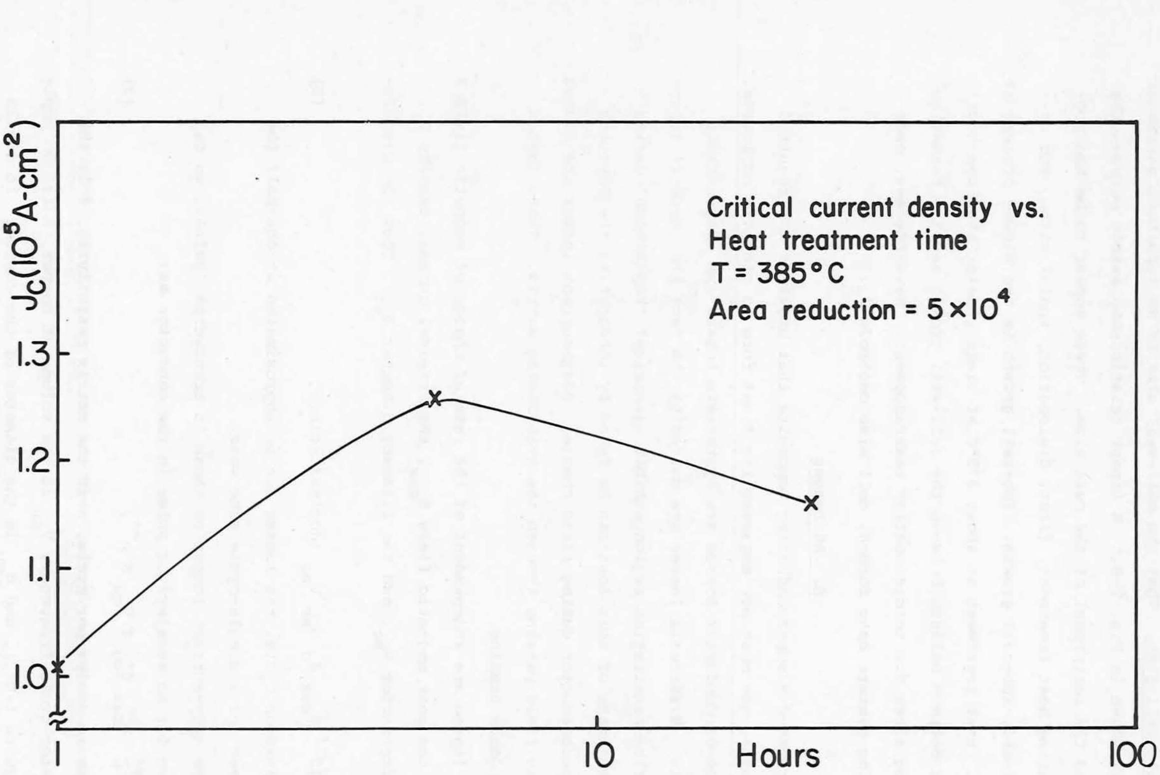

Fig. V-6. Effect of heat treatment time on J_c.

the effects of increasing cold work after heat treatment at an intermediate state.

Pinning Force vs Cell-Wall Size. That the cell-wall size is an important parameter in determining J_c is shown in Fig. V-8.[4] A linear relationship exists between the critical current and the reciprocal of the cell size. There appear to be two processes occurring during heat treatment, first, dislocation, annihilation, and rearrangement, and second, sub-cell growth. Sub-cell growth is the slower process at lower temperatures. Heat treatment at about 375°C at times greater than one hour seems to provide an optimum balance between the cell-wall growth and the formation of effective pinning sites due to dislocation rearrangement. Nevertheless, once the effective pinning centers have formed, cell size controls J_c.

E. AC Losses

Having fabricated a superconducting composite that provides the required number of ampere turns, one must now engineer its final form to minimize ac losses. The dominant sources of conductor losses are hysteresis losses and eddy-current losses in the matrix. Hysteresis losses are caused by the fact that type-II superconductors in the flux-penetration region exhibit electrical "resistance" during field change. An estimate of this loss can be found by integrating the Poynting Vector over the superconductor during field change. Eddy-current losses are caused by changing magnetic field passing through the stabilizing matrix. These losses appear as ordinary Joule heating.

Hysteresis losses are independent of the rate of change of magnetic field $\dot{B}$ and depend only on the peak magnetic field B_{max}, the critical current density J_c, the volume of superconductor V_{sc}, and the filament diameter d_{sc}. Thus the hysteresis energy loss is

$$W_H = 10^{-8} B_{max} J_c d_{sc} V_{sc} \text{ (Joules/cycle)}.. \tag{2}$$

For a typical accelerator cycle, the losses can be approximated at one-half the above, which is given for a single-cycle sine wave.

Modeling the eddy-current losses on those in transverse laminae, we can formulate the losses for an accelerator pulse in the conductor as:

$$W_E = \frac{\pi^2}{4} B_{max}^2 d_{cu}^2 f V_{cu} K \rho^{-1}, \tag{3}$$

where W_E is the loss in Joules per cycle, ρ is the matrix resistivity, f is the equivalent accelerator-cycle frequency, V_{cu} is the volume of copper, K is an empirical coefficient (with $1<K<2$), and d_{cu} is the diameter of the copper. It should be noted that the eddy-current losses are a function of the ramp rate and frequency

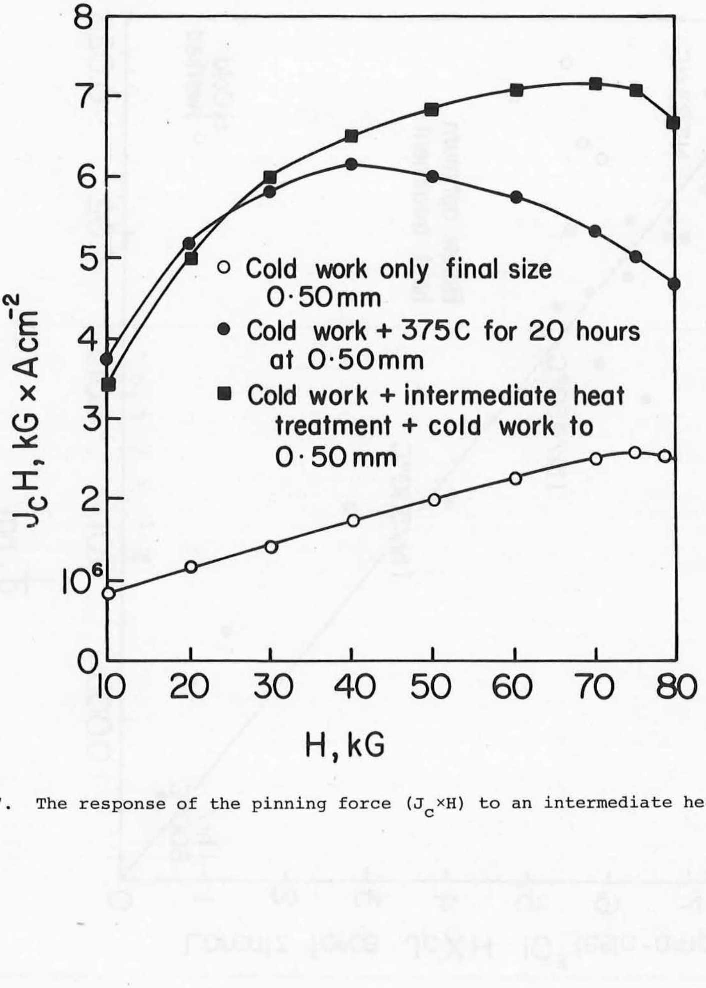

Fig. V-7. The response of the pinning force (J_c×H) to an intermediate heat treatment.

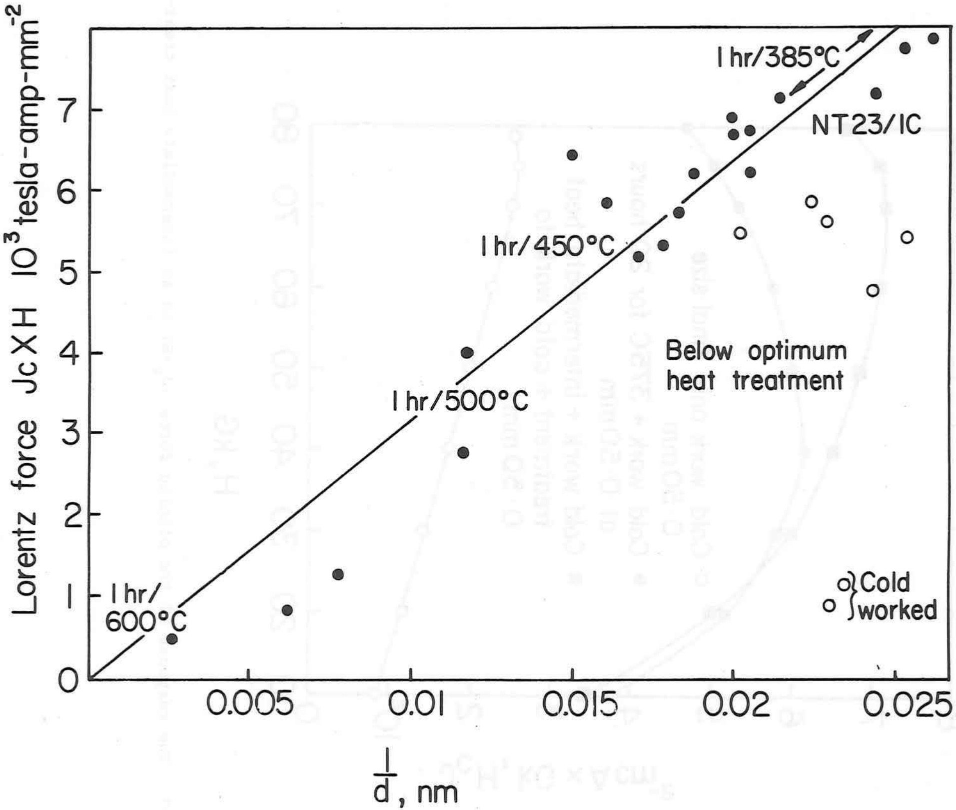

Fig. V-8. The pinning force as a function of cell size.

as well as the physical size of the conductor. The eddy-current losses dominate at the higher ramp rates, but can be minimized more readily by specific conductor design. In particular, d_{cu} and ρ can be changed easily.

F. Present Doubler Conductor

Based on the loss criteria, a requirement that total conductor losses be less than 1 W/m of magnet, the stability criteria and production limitations, we have chosen a Rutherford style of cable. Shown in Figs. V-9 and V-10, this cable is made with a Nb-46.5 wt/0 Ti alloy and has a 1.8 to 1 copper to superconductor ratio. Each of the twenty-three strands of 0.027-in. diameter in the cable has 2100 filaments of 8 μm diameter. This filament size is small enough to insure stability, as well as low ac hysteresis loss, and represents somewhat of a lower limit on size. A coating of Sn-5wt/0 Ag solder is used on each strand to provide a high resistivity layer in order to reduce the strand to strand coupling and hence reduce eddy-current losses.

Early in the program, the Laboratory purchased 300,000 lbs of copper. With this purchase we were able to bring up the average resistivity of the delivered material to better than 240:1. The resistivity ratio is a good measure of the impurity content of the copper and, in particular, the iron content. For stability reasons, it is necessary to have this ratio as high as possible. This copper has since been fabricated into enough copper hex tube and extrusion cans to produce 260 billets of material.

In placing large orders for the copper components and the NbTi parts described below, we have observed that the quality of the parts has shown significant improvement. Fabrication costs for the copper components have also dropped significantly.

Of the 15,000 lbs of NbTi purchased, most has been used in development programs and in the fabrication of production billets. Finished quality of the NbTi rods has improved over the past two years.

G. Vendor Qualification

By placing orders with domestic fabricators of superconductor, we have found that all are able to meet our specified electrical properties. There are differences in production rates, but these are not significant at present. We find that the differences in electrical properties vary more over a single billet than from fabricator to fabricator.

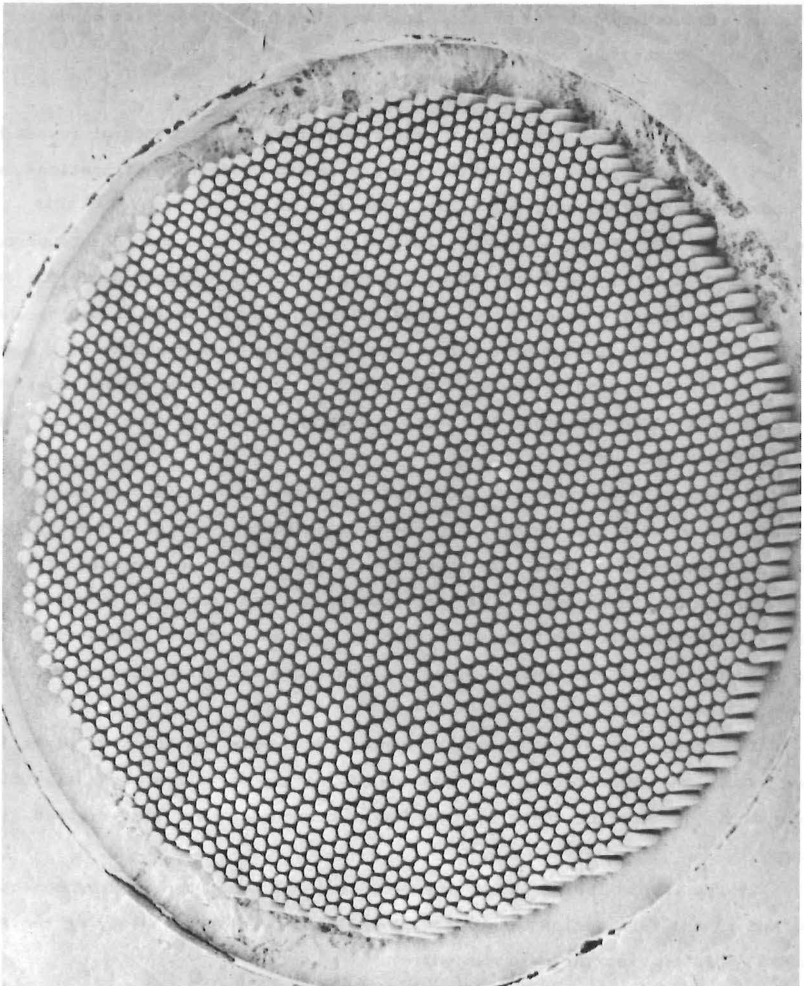

Fig. V-9. Superconducting strand (2100 filaments).

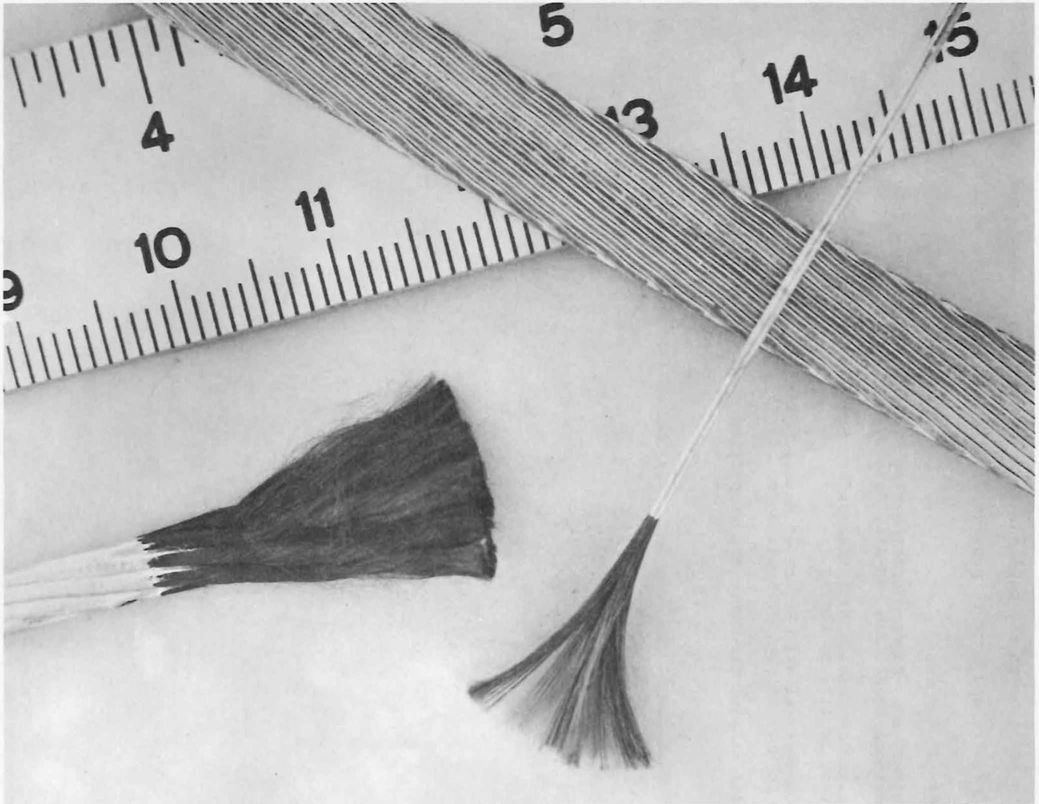

Fig. V-10. Superconducting cable (23 strands).

Three firms have been able to provide us with 23-strand cable of varying quality. This process is rapidly attaining high quality levels overall and seems to depend strongly on technique.

In addition to the cabling, we are developing cleaning and taping capabilities in industry and hope to provide finished cable ready to wind in the magnets.

References

[1]D. F. Sutter, ed., Superconducting Wire Stability Workshop - July 22, 1974 Fermi National Accel. Lab. TM-641, January 1976.

[2]P. R. Critchlow et al., Multifilamentary Superconducting Composites, Cryogenics, 11 (1), 3, (1971).

[3]A. D. McInturff et al., Effect of Metallurgical History on Critical Current Density in NbTi Alloys, J. Appl. Phys., 44 (5), 2378, (1973).

[4]D. F. Neal et al., Structure and Properties of Nb44%Ti Wire, Acta Met., 19, 6, (1971).

APPENDIX VI. MAGNET SYSTEM

G. H. Biallas

A. Introduction

This section describes the mechanical design of the Doubler superconducting-magnet system. This topic includes the magnet-string concept, the dipole, quadrupole and trim-magnet designs, and the magnet-support design.

The foremost system choice was to build a separated-function accelerator with a duplicate lattice to the Main Ring. Our early efforts convinced us that superconducting pure dipoles and quadrupoles would be preferable to combined-function magnets. Inherent in the latter magnet is a large coil-bundle to iron-shield force. In a no-saturation warm-iron design, this force causes excessive heat conduction through the support to helium and excessive deflection-caused field inaccuracy.

We know from our Main-Ring experience that less trim magnet space is required and we believe that we can make a greater-strength quadrupole. These conditions allowed us to lengthen the dipole slightly to 22 ft center-to-center and shorten the quadrupole to 4 ft. (The Main-Ring dipoles are 20 ft 11 in. center-to-center and quads are 7 ft.) The design calls for 778 dipoles and 240 quadrupoles. Most of our effort has been directed towards the dipoles and they will be treated first in this report, with quadrupoles and trim magnets discussed in less detail.

B. Magnet Strings

The remaining over-all system choice was to group the magnets into 48 subsystems each made of 16 dipoles, 4 quadrupoles and trim magnets. All magnets in these strings share a common current (except the trims), common helium supply (one-hase helium and return two-phase helium), common beam and thermal-insulation vac- - and common 20K-shield helium flow. The magnets are made as identical modules connected at their ends in junction boxes to form strings. The strings ex- rom every tunnel service entrance independently in each direction halfway to entrance.

The string choice was made at the project start and follows from the simplifying philosophy of seeking the smallest number of penetrations from room temperature to cold helium. The primary penetrations to minimize were the 4500-A current leads. At least one set per string is required because the power supplies are warm. Our design holds to this minimum. These penetrations are located in the service buildings where there is easy access to the refrigerator and where it is easy to connect to the power supplies. Calculations to investigate replacing these leads with a superconducting-secondary transformer proved the replacement to be impractical. The transformer is too large at our ramp rate. A superconducting transmission bus inside the helium supply pipe carries the current down to the magnets, which act as their own bus and transfer the current downstream from one magnet to the other. The current handoff to the next independent string halfway in the tunnel is made cold and superconducting. The only remaining active leads are the low current (200-A) trim-magnet leads coming out at the individual magnets. Every dipole and quadrupole has an inactive gas-cooled safety lead.

The remaining features of these strings, such as the liquid-helium coolant and gaseous-helium shield, as well as the vacuum systems, are discussed in Appendices XI and XII.

Connections between magnets take place at junction boxes. Over-pressure relief and magnetic-energy withdrawal safety leads are placed in these and are the major penetrations. Magnets will all be made as standard modules, with the end functions of every system handled entirely within the separate clamp-on end boxes.

C. Dipoles

Coils are the heart of the magnets. They are made of wire that is a twisted and flattened cable (0.300 x 0.050 in.) of twenty-three, 0.027-in. dia. strands. As discussed in Appendix V, the strands are made of 2300 filaments of Niobium Titanium coextruded in a copper matrix with the proportions of one part superconductor to 1.8 parts copper. Once the individual strands met the stability criteria of Appendix V, we selected the number of strands in the cable and hence the operating current by the following reasoning. A coil package of two layers with few turns is easiest to build and has the smallest inductance. The smallest cabl to let this geometry reach 45 kG with a small factor of safety is the 23-str operating at 4500 A. This many strands had never been made up in a flat cab working with our vendors, we were finally able to produce it reliably.

The dipole coil package is formed as a top and a bottom coil, each two layers or shells forming saddle-shaped coils. In double-layer winding, the conductor winds out from the center in a flat spiral on one level and after a transition to a second level, out from the center in the opposite-hand spiral. The leads end up conveniently on the outer edges of the coil and no internal splice need be made; the entire double layer can be made of one length of conductor. Thirty-four turns are wrapped into the inner spiral and 21 in the outer. In the top coil, the last half turn in the outer shell is left out to form a lead at the back end of the coil. An additional wire is then placed into the void created and becomes the bus conductor. The coil bundle has a lead set at each end.

Superconducting wire has no resistance to electric current and can be made about one-hundredth the size of a comparable copper conductor. This allows the magnet designer to use almost unlimited current and turns without economic hesitation and allows placing them into a small enough package that high fields can be achieved. An additional construction difference from conventional magnets is that the iron has been removed from the active-field area. In conventional magnets, the contour of the iron pole tip determines the field quality. In superconducting magnets, the sole determinant of field quality is the wire position. This position dependence requires a new precision on the part of coil fabricators, which in the past had only to be concerned with external coil dimensions and not positions of individual turns.

Field calculations to determine the position of these wires are discussed in Appendix III. Manipulating the inner coil edges of our simple geometry allows fields good to one part in 10^4 at 1 in. from the center at the mid-plane.

The insulation system for the coils has several requirements. The conductors have to be isolated turn-to-turn to withstand voltages of the order of 10V. Extreme parts of the coils must withstand thousands of volts to either ground, companion top or bottom coils, or the bus conductor. For turn-to-turn protection, the conductor is covered in a spiral-wrapped overlapped 0.001-in. thick Mylar tape. Before this wrapping, the cable is ultrasonically cleaned in Freon solvent to remove fabrication-induced metallic slivers. No adhesive is used on the tape because of our experience that any adhesive bonded to the cable causes degraded coil characteristics. The cable should have a keystone or trapezoid shape to fit well into the Roman arch-like shell geometry. Since it is actually a rectangle, a layer of 0.003-in. 1/3-width Mylar tape is applied along the outer edge to fill the void. (Experiments are underway to form the cable as a trapezoid.) Over this taped cable is wrapped a 0.007-in. lightly epoxy-impregnated 0.25-in. wide glass tape. It is wrapped like a barberpole with 1/16-in. gaps to aid helium permeation. When the coil is formed in its mold, there is just enough epoxy to hold the coil together but not enough to drip or seep into the cable itself.

The insulation from inner to outer shells is by intermediate banding. This epoxy-impregnated 1/4-in. wide glass tape, 0.021-in. thick, spaced 3/8-in. apart, is applied in a herringbone pattern down the length of the inner layer or shell. The second shell is then wound on top of this spacer. The gaps form helium convection passages to aid in cooling the outer shell. At the coil ends, the spacer is placed in a chevron pattern to support the coil wraparounds uniformly. Upper-coil to lower-coil insulation is provided by an extra layer of 0.010-in. Kapton at the midplane where they meet. Short-to-ground insulation is provided by a 0.030-in. built-up mat of Dacron-Mylar-Dacron sheet.

It might be noted that cable is available to a size tolerance of ±0.001 in. In 34 turns this can result in a 0.068-in. difference in build-up. We have found that the 0.007-in. glass tape barberpole is mushy enough before curing to take up this difference with ease.

Because the superconducting wire is sensitive to field strength, there should be no regions in the coil where the field is unnecessarily high. This would quench the conductor. Such a weakest-link region exists at the inner hairpin turnarounds of the inner shells. Our design spaces out the inner ten turns with crescent-like spacers. This diffuses the magnetic field to bring it down to the average coil field.

To produce the abrupt transition from layer to layer at the center of these double-layer coils, the twisted cable is untwisted one half pitch. The strands are then parallel and able to be jogged easily between the layers in the 0.75-in. length provided.

The coils can be molded very accurately in a mold after winding, but they will not stay that way without some filler to complete the circular arch. We have designed these fillers or keys into the coil-clamp-collar coil supports to be discussed below. At the half-circular ends of the coils, the coil-clamp collars cannot perform this function. Machined G-10 keys with matched coefficient of thermal expansion fill the gap. They also house the guide and support slot for the layer-to-layer transition mentioned above.

To complete the cylindrical coil package, curved wedge-shaped pieces are pushed in and clamped against the coil ends. These maintain a definite end geometry and resist the magnetic forces.

In our designs we have concentrated on keeping the wire constrained at all times to prevent frictional heating caused by motion. Through our testing it has become evident that adhesives like epoxy bonding the wire can make coils quench prematurely. When the strong bond cracks, the heat generated by the resultant motion is great enough to cause a quench. When we switched to the present Mylar-covered wire, the magnets performed better, as if the Mylar was also acting as a thermal insulation preventing the cracking epoxy heat from reaching the wire. The epoxy is still necessary to assemble the coil. Associated with this adhesive cracking and frictional heating is the training process. The coils are finally trained and the highest currents achieved when all wires have jockeyed to their lowest-energy positions.

In our past reports we proposed a form of banding to restrain the coils against the 6000-lb/in. outward force. The moment tending to flatten the coil was taken by a stiff bore tube or stiff rings. This system amounted to an internal skeleton. It was successful in that our coils were able to reach 95% of the maximum attainable current, but we found the deflections of the coil bundle to be too large to maintain the proper conductor placement required for field quality.

Our present solution is an external skeleton scheme known as "coil-clamp collars". They are a lamination made of stainless steel. Instead of inserting the coils in a finished yoke, as in a conventional magnet, these non-magnetic laminations are built up around the coil. They are fastened by a combination of a dovetail epoxy lap joint and a series of welds. They have cut the deflection of the coil by a factor of two. They show less training and they have a built-in potential to produce a more accurate coil bundle.

The collar is a single lamination that performs many functions. Two laminations complete the circular wrap around the coil with the keyed joint at a plane 20° to the vertical. The adjoining pairs in the buildup are flipped such that a 40°-wide overlap for an epoxy lap joint is seen by every lamination. The laminations have key surfaces on the inside that butt up against the edge insulation of the two shells. The laminations are registered to each other by notches in the outside circular surface. During assembly, the tooling squeezes the laminations down while registering them with respect to one another as the epoxy cures.

The selection of stainless steel for these clamp collars and for the surrounding cryostat takes some care. Most stainless steels, especially at low temperature, can turn slightly magnetic. This happens when portions of the alloy revert from the austenite phase to the magnetic ferrite phase. Normal iron exhibits this phase change at about 1200°F. Some alloying elements, such as nickel, nitrogen and carbon, eliminate this transformation or force it to lower temperatures. Others, such as chromium, tend to raise it. Too much nickel, as in Inconel and 310, causes magnetic properties stemming from the nickel itself, even though the material never transforms. Many of the "good" elements like carbon and nitrogen are subject to a large manufacturing tolerance. One composition of 304 will transform and another will not.

Another variable is treatment of the material. Cold working tends to raise the transformation temperature. Certain high temperatures can cause the elements to segregate, allowing transformation of some lean crystals. Higher temperatures and a rapid quench cause frozen-in homogeneity and non-magnetic properties. In welding, however, magnetic ferrite is desirable in the weld bead because it aids hot ductility and prevents microcracks. Alloy 310 and 205 do not form this ferrite in the weld bead.

The alloy we have chosen is Armco Nitronic 33. (Its composition percentages are 18 chrome, 3 nickel, 13 manganese and 0.04 nitrogen.) It has the lowest natural permeability of the stainless steels, approximately 1.001. Its cost is the same as that of 304L. It is low in carbon, so weld segregation is minimized. In its natural unworked state, it never transforms to ferrite. Only after fracture does it show any signs of ferrite formation and that only at the fracture point. To prevent weld cracks, it does deposit ferrite at a weld. It has a yield strength of 60,000 psi, double that of 304L. Comparisons of this material to other steels are shown in VI-1 and VI-2. Figure VI-1 shows a comparison at room temperature of the permeabilities of the various stainless steels. Figure VI-2 shows the austenitic stability tolerance for Nitronic 33 and some other common stainless alloys.

The coil bundle ends with an end ring fastened to the laminations squeezing the end fillers into the coil. Three pairs of leads stick out from between the illers, two sets at the lead end, and one set at the return end. One pair at each end is used for the coil terminals. The extra pair at the lead end is lapped and soldered to form the splice between top and bottom coils. The enclosing splice block, which is a copper channel, is mounted against the end plate with suitable helium-ventilated insulation.

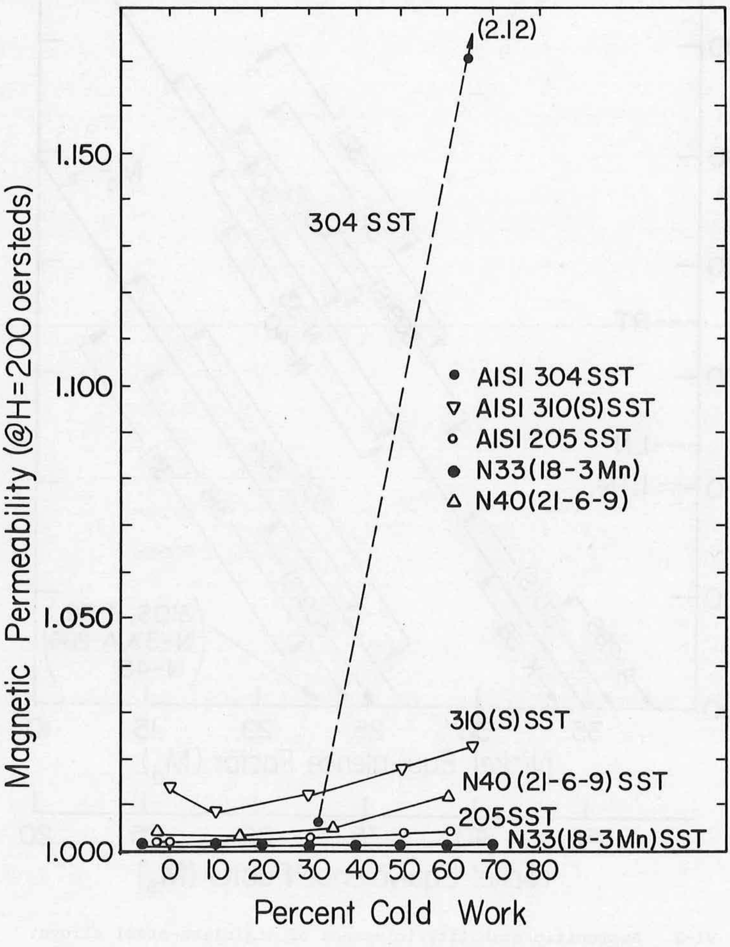

Fig. VI-1. Permeability as a function of cold work.

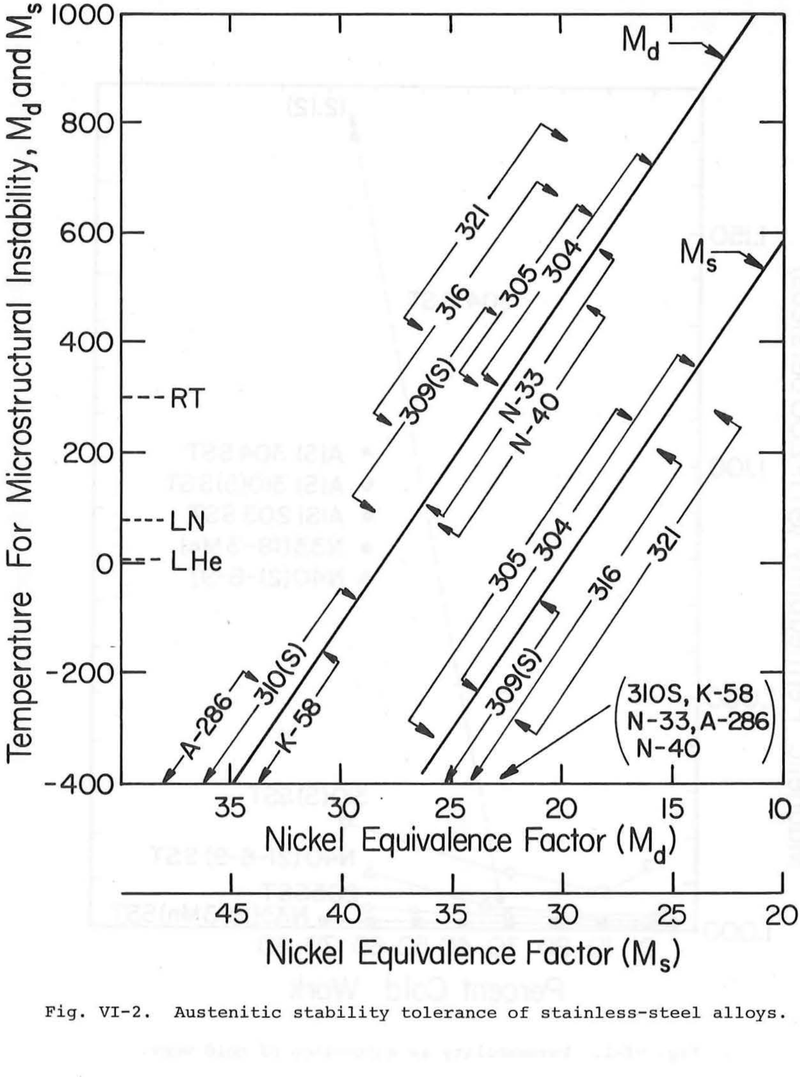

Fig. VI-2. Austenitic stability tolerance of stainless-steel alloys.

The splice mentioned above is the only splice in the dipole. The two double-layer coils are wound with a continuous length of wire. Current flow across a splice between wires cannot be made superconducting, because the superconducting filaments cannot be directly joined. If the copper is etched away to expose the strands, the oxide film that immediately forms on the filaments is more resistive than the original copper. Welding and silver soldering are not possible because the high temperatures destroy the superconducting properties in the joint vicinity. The least-resistive alternative is a soldered lap joint. We make this lap joint by squeezing the wires together during soldering. A heat generated at 5000 A is 0.0325 watts in a 4-in. splice, which can easily be dissipated to the surrounding helium.

Cryostat. Each coil bundle is immersed in one-phase (bubble-free) supply liquid helium contained in an annular cryostat. The inner tube of this annulus allows heat transfer to a second inner annular space filled with the colder, boiling, two-phase return helium. Each triple-tube package with coil is suspended within the thermal-insulating vacuum space by roller suspensions of fiberglass-epoxy composite. A thermal-radiation shield operating at 20K is also suspended in this space. Dimplar multilayer insulation between the shield and room temperature vacuum wall intercepts the bulk of the radiation heat load. The warm-iron magnetic shield is clamped around the outer vessel. The enlarged ends of the vacuum tube called the junction box use a large bellows as an access cover to expose the Conoseal service connections.

The cross-sectional features of the magnet can all be seen in Fig. 2 of the main text. In giving further component detail, the parts will be discussed from inside to out. The beam tube is an approximation to an ellipse with a horizontal major axis of 2.900 in. and a vertical minor axis of 2.0 in. It is made of rolled strip, seam-welded and drawn to shape. The weld is annealed to remove magnetic properties. The inside is Diversy-cleaned for better vacuum properties. The elliptical shape is useful for extraction aperture. Since it is directly in contact with two-phase helium, beam-heating effects are shielded from the coils.

An annular space is formed between the beam tube and the next tube out, the two-phase tube. The space is sized to maintain the two-phase helium in froth flow rather than slug or separated flow. The outside wall of this space, known as the two-phase tube, is again an elliptical approximation and of the same construction as the beam tube. The two tubes are made this thin to minimize eddy-current heating. Vacuum collapse is prevented by making the tubes into a unit by spot welding them together at their major axis.

The space between the two-phase tube and the coil bundle is used to transmit the bulk of the one-phase flow. It is sized to minimize pressure drop along the string. An insulation strip along the major axis electrically isolates the tube and coil bundle surrounding it.

A thin-wall tube of identical construction sheathes the outside of the coil bundle. Just enough space is left between the coil-clamp collar outer surface and the tube to allow the tube to be slipped on during assembly. The wall is thick enough to withstand the pressures encountered in service but is thin enough to allow the suspension rollers to deform it into contact with the coil collars.

The 20 K shield is the next concentric shell encountered; it is made of five Nitronic 33 tubes. Stand-offs of NEMA G-10 fiberglass-epoxy composite space the shield from the outer cryostat. The shield tube also acts as a mount for the brackets holding the roller suspensions. Cooling is provided by a helically wrapped, flattened stainless tube containing 20 K helium gas. Heat is conducted from the tube to the shield by copper braids soldered to both. A phosphoric-acid based flux is used in the soldering to eliminate any chloride-flux stainless-steel corrosion problems.

Dimplar multilayer insulation fills the gap between the shield and the outer vacuum-vessel wall. It is crinkled, aluminized Mylar insulation. It was chosen over Mylar-and-glass paper because of the good pumping characteristics of its large spacings and because the glass paper tended to shred during handling. Glass-felt buffer material is used at all edges to prevent thermal-radiation entry to the inner layers. Quartz felt is used under weld points to prevent burning the Mylar.

Any displacement error of the coil from the center of the iron shield leads to forces attracting the coil toward the shield. The larger the error, the greater the force. Accordingly, a strong but low heat-loss suspension mechanism must be interposed between the coil bundle and the iron shield. This off-center force is the dominant factor in determining the conductive heat leak from the outside world to the helium vessel.

The rate of force increase with error for the C Series is 1 lb for every inch of length. Our suspensions, spaced every 24 in., are designed to react at 3-1/2 times this rate or 84 lb per 0.001 in. deflection. For example, with an initial error of 0.005 in. in centering, the force per suspension at peak field is

120 lb. This is enough to defelct the suspensions an additional 0.0014 in., at which a force equilibrium is reached at 154 lb and the error from center increased to 0.0064 in. Such errors in placement do not cause significant field-quality problems.

Ideally, the suspensions should be put at the end of the coils to simplify construction, but the coil bundle is not stiff enough and would sag over the 22-ft length. Thus the suspension system must consist of 11 units and must fit within the iron. Each unit consists of four rollers placed at 45° to the horizontal. They are in essence compression pegs that have been converted to rollers to allow 0.75-in. longitudinal shrinkage of the cryostat. They are compressed at room temperature so as to be exactly to size at low temperature when the coil bundle has shrunk across its diameter. The rollers are made stiff enough and are spaced close enough that the total coil off center error is never greater than 0.010 in. One roller is replaced by a NEMA G-10 tube at the magnet center. This tube acts as an anchor to maintain rotational and longitudinal alignment.

The iron shield is made of laminations because they are easily stamped and stacked to the tolerances required. It forms an approximate cosine distribution about a circular bore. It is split into two half yokes along the vertical plane. The laminations are held into a pack by tie angles running along the magnet length at the corners and welded to stiff end plates. The cores are to be impregnated with epoxy that acts as the beam shear web. The cores are stacked curved to a precamber to produce an eventual straight magnet under gravity load. In addition, it is possible to curve the magnet in the horizontal plane to approximate the 1/4-in. sagitta correction to increase the beam aperture.

If the steel shield were to extend over the magnet ends, the highest field applied to the superconducting material would occur in the end region. To counteract this field enhacement, the dipole steel shield stops somewhat short of the coil ends.

In the end junction boxes of the magnet, provision must be made for connection to its neighbor of (i) the beam tube, (ii) the two helium vessels, (iii) the two current leads (the internal bus conductor results in the magnet becoming a four-terminal device), (iv) the outer insulating vacuum chamber, and (v) the intermediate heat-shield cooling tube.

The outer vacuum insulation space is connected from magnet to magnet by an enlarged outer vacuum tube connected by a very flexible bellows and a Marmon type

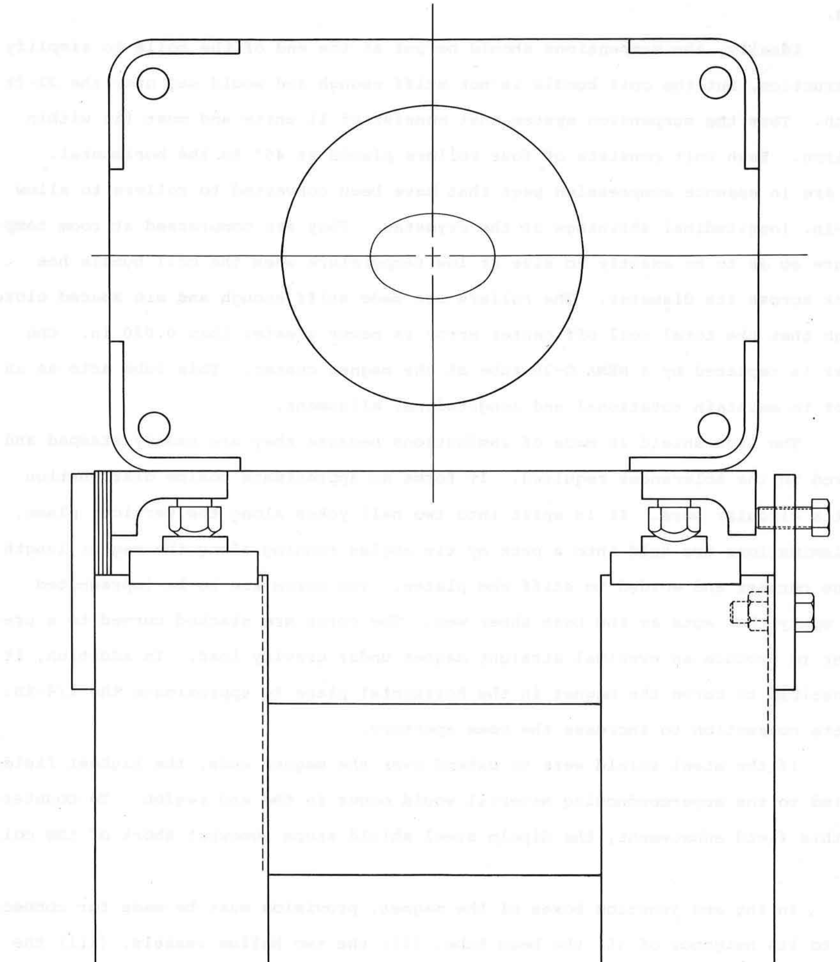

Fig. VI-3. Magnet stand.

O-ring flange. Inside at the beam tube, a bellows with an internal cryosorption vacuum pump spans the beam tube. To the aisle side and underneath are the single- and two-phase helium connections using Aeroquip Conoseal joints and bellows for flexibility. The single-phase connection containing the electrical terminals may be flexed back into the vessels to allow the terminal joints to be made. To the top of the beam bellows is the crossover connection of the shield tube. Connecting to one single-phase vessel end is the insulated, combination relief-valve tube and safety lead with its thermal-oscillation-preventing check valve. We are adapting production sheet-metal techniques to the fabrication of these end parts in order to minimize their cost.

D. Quadrupole

The present quadrupole design is shown in Fig. 3 of the main text. Its design reflects many of the solutions we have developed for the dipole. Its three-shell design makes it different from the dipole, but we believe we can still wind it from two continuous wire lengths. It will share its cryostat with the trim magnets discussed below.

E. Trim Magnets

Trim magnets are planned to be wound as air-core magnets. All correction elements will be housed within every package with the proper leads being connected as needed. This integration is possible because the windings can be wound as concentric shells made from single strands of our superconducting wire. The shunted main-current bus will be shielded from the beam by an iron sleeve placed over the trim windings.

F. Magnet Stands

The magnet stand is shown in Fig. VI-3. The stands are placed at the fifth points of the dipoles to keep magnet deflection to a minimum. Shims are used to produce the main adjustments rather than screws. This simplicity follows the philosophy used in the Main Ring, where minimum adjustment worked successfully. The new magnet's position necessitates removal of a portion of the Main Ring magnet stand. A cross piece will be added to this stand to maintain its original strength. The position of the new magnets allows them to be easily threaded through the Main-Ring stands for rapid installation.

APPENDIX VII. THE MAGNET TEST PROGRAM

A. V. Tollestrup

A. History and Purpose of the Program

In July, 1975, an extensive test program of two-shell magnets was started at Fermilab. The extent of this program can be judged by the following list of magnets that have been constructed between that date and May, 1976.

D SERIES		E SERIES			
1 Ft	10 Ft	1 Ft	5 Ft	10 Ft	22 Ft
D1-1	D10-1	E1-2	E5-1	E10-1	E22-1
1-2	10-2	1-3	5-2	10-2	22-2
1-4	10-3	1-6		10-3	22-3
1-6		1-7		10-4	
1-7		1-8			
1-8		1-10			
1-10		1-11			
		1-12			
		1-14			
		1-15			
		1-16			
		1-17			
		1-18			
		1-19			
		1-20			

The D series magnets had an inner 2.5-in. bore and were made with 17-strand superconducting wire with individual strands 25 mils in diameter. The success of this program led to the start of the E series magnets, which had a 3-in. bore diameter and were constructed of 23-strand wire with a diameter of 27 mils.

The object of this extensive magnet-test program was to find out how the structure of the magnet affects its performance. The structure of the magnet was varied in many ways, such as changing the method of insulating the wire, changing the mechanical support of the wire, and changing the cooling. Performance was measured by running test curves on the magnet after it had been constructed. The information obtained in these tests is summarized in the following:

1. The ultimate field reached by the magnet,
2. Training curves,
3. Ramp-rate sensitivity curves,
4. Deformation of the magnet under the magnetization forces,
5. Temperature dependence of the magnetic properties,
6. Measurements of the accuracy and reproducibility of the magnetic field.

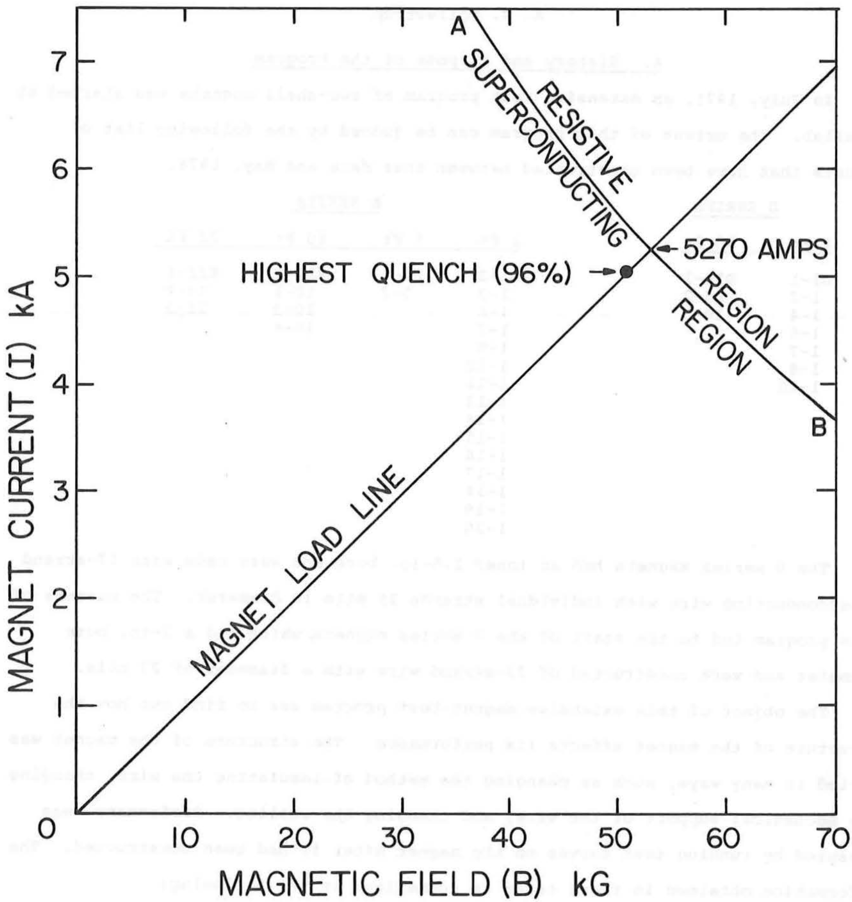

Fig. VII-1. Superconducting and resistive regions.

In addition to the above data, we studied the extraction of energy from a magnet when it quenched. A 22-ft magnet at full field stores approximately 0.5 MJ, which must be extracted in a time sufficiently short that the wire does not heat excessively before the energy is removed. At the same time, the insulation of the magnet must be sufficient to withstand the voltages that are developed during a quench. This is a complicated problem because increasing the electrical insulation of the wire reduces the ability to extract heat from the wire through the liquid-helium cooling.

This test program has been exceedingly fruitful. It has taught us a considerable amount about the support structure, about how magnets quench, and most important, it has led to the successful development of the 22-ft magnet. It was not at all obvious at the start of this program that what was learned from a 1-ft magnet could be successfully applied to the construction of a 22-ft magnet. This result must be viewed as one of the major discoveries of this program. We will now summarize the results obtained from this test program.

B. Ultimate Field

The superconducting wire as supplied by the manufacturer has an I-B relationship such that if the current is less than the critical value, the wire is superconducting and if it is greater than the critical value, the wire is resistive. The critical value of the current is a function of the magnetic field. Figure VII-1 shows such a relationship in the curve A-B. These data are obtained from a piece of wire about 12 in. long in an external magnetic field normal to the direction that the current is flowing. Using these data, it should be possible to predict the performance of any given magnet. In order to do this, one must pick the point in the magnet where the field is highest. Since the maximum field is a linear function of current in the magnet, one can draw a load line for the magnet on the I versus B axis. This is shown also in Fig. VII-1. The load line drawn is the maximum field versus current in magnet E1-17. The field on the bore of the magnet, of course, is somewhat less than the maximum field of the conductor. In the E-series magnets, the high-field point occurs at the center of the inside-shell inner turn, where it is 19% higher than the bore field. Thus we see that magnet E1-17 should have reached a peak current of about 5270A at the short-sample limit. The highest quench current of this magnet is shown as a point on this line and it is seen that it reached 96% of the predicted short-sample limit.

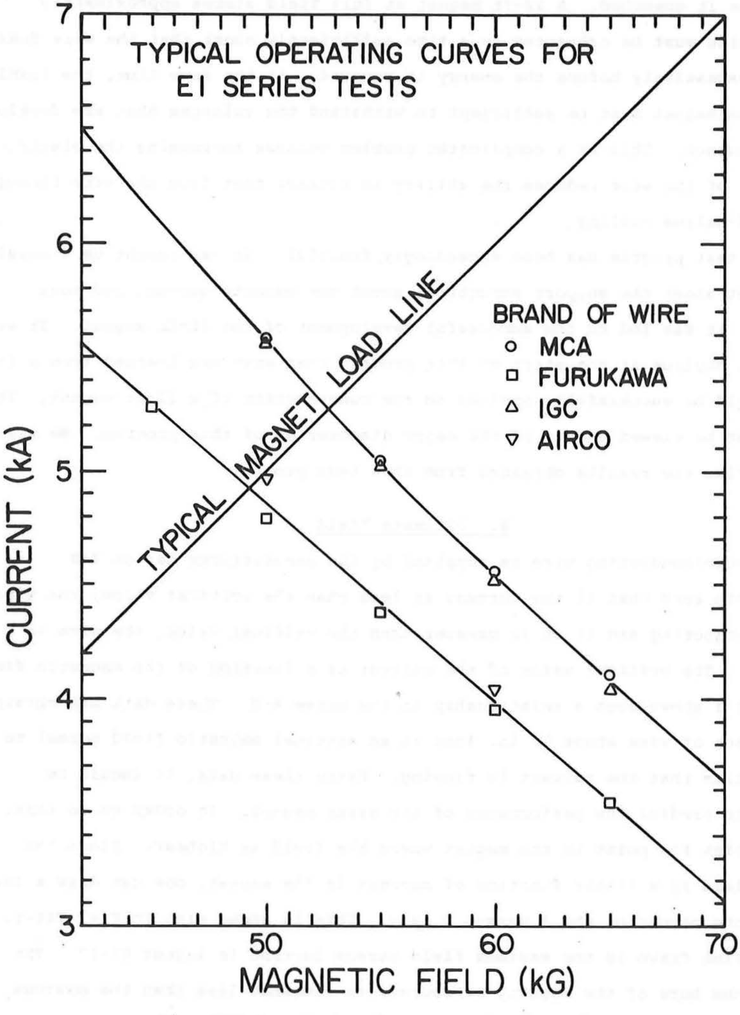

Fig. VII-2. Tests of superconducting wires.

Consider what would have happened if this magnet had been wound with wire that had a higher critical current at each value of B. In that case, it should have quenched at a higher field and the field should have increased in the proportion that the critical current increased.

We have received wire from four different manufacturers. Some of these data have been selected and plotted in Fig. VII-2 for the wire that was used in the 1-ft E series test magnets. Note that there is a suppressed zero so that the test results are spread out. It can be seen that the wire that we have used groups itself around two separate I versus B curves. A load line for a typical magnet is also shown on this graph. Knowing what wire was used in the magnet and what its load line was like, one can plot for each magnet the actual current at which it quenched versus the percentage of the short sample limit that it reached.

Figure VII-3 is such a plot. The two sloping lines correspond to the two different groups of superconducting wire. The individual points plotted on the line indicate the maximum current that the magnet reached and hence are indicative of the maximum field that the magnet achieved. It is seen that all of the magnets fall between 92 to 100% of the short-sample limit. It is also interesting to observe up till now, when the wire is improved by making its critical current higher, we do not correspondingly increase the quench current of the magnet by a proportional amount.

The above data assumed that the quench starts at the high field point in the magnet. This has been verified for a completely trained magnet. This was done by placing a series of probes on the inside turn of the inner shell of a 1-ft magnet. These probes picked up the quench wave along the conductor; by measuring its arrival time at different points along the conductor, it was possible to pinpoint its origin. A histogram of this point is shown in Fig. VII-4.

In any case, we see that the magnets that we are now constructing come very close to the short-sample limit imposed by the wire. We have also verified that the quench point occurs at the high-field point in the magnet. Hence we feel that we understand the gross features of how the wire affects a magnet performance. Some small questions remain but these are certainly not an obstacle to the construction of successful magnets.

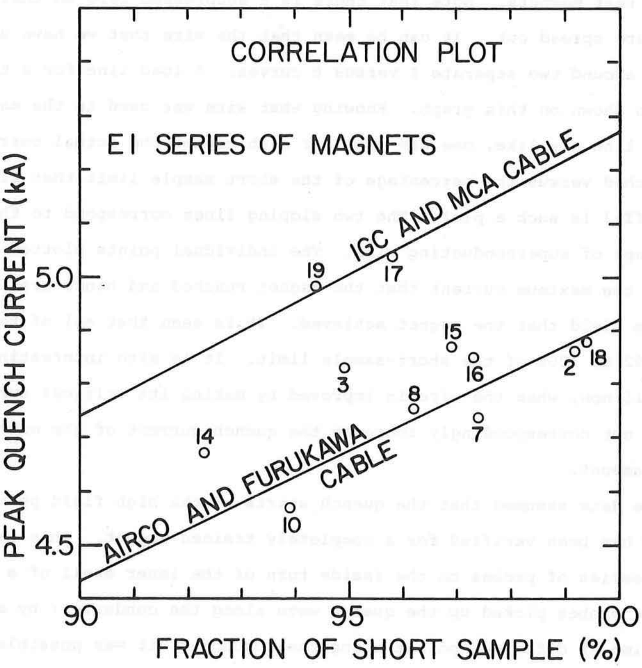

Fig. VII-3. Wire performance.

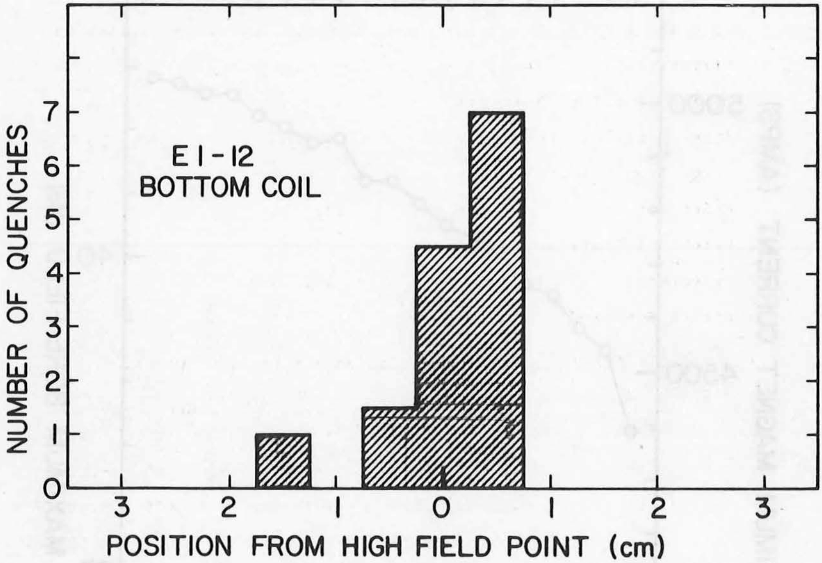

Fig. VII-4. Distribution of quench position.

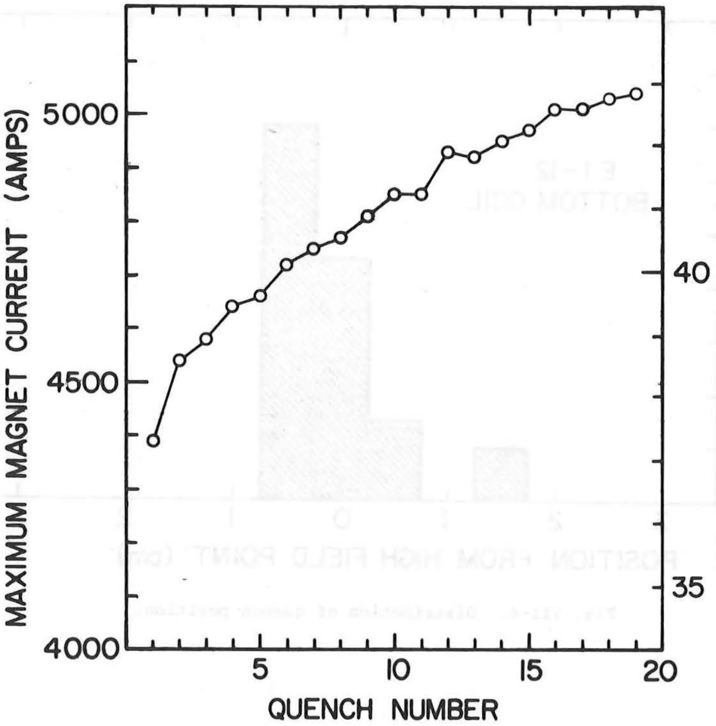

Fig. VII-5. Training curve for magnet E1-17.

C. Training

When a magnet has been constructed and it is energized for the first time, a new phenomenon occurs. As the current is slowly increased, a point is reached where the magnet suddenly goes normal. In the last section, we saw that this point should be determined by the critical current of the wire in the magnetic field. The first time a magnet is energized it may quench itself at currents as low as 30 to 40% of this peak value. If the energy is removed and the magnet again energized, the next time it quenches the current will be slightly higher. The curve that one gets by plotting the quench current versus the number of the quench is called a training curve and Fig. VII-5 shows such a curve for magnet E1-17. Notice that this 1-ft magnet trained in a relatively few number of quenches. In contrast with this, Fig. VII-6 shows a training curve for E1-3, which even at the end of 100 quenches had not been fully trained.

Four main questions arise here:

1. Does it remember its training?
2. Does it take an excessive number of quenches to train?
3. Do long magnets train the same as short ones?
4. Why do magnets train at all?

To answer the last question first, the evidence seems to indicate that magnets train because the support structure is allowing the wires to slightly move and shift at the high-field point. The frictional forces accompanying this motion pump enough heat into the superconducting wire to make it go normal. If we assume that this analysis is correct, then we can understand the major features that we observe. First, magnets do remember their training, even over periods of months provided the basic support structure has not been disturbed. If the banding around a magnet is removed, for instance, then the magnet seems to train as though it were a newly constructed coil. On the other hand, if the magnet is temperature-cycled or left sitting around the laboratory at room temperature for long periods of time, it seems to remember its previous training history.

The magnets as constructed at present do not take an excessive number of quenches. They are generally fully trained in approximately 10 to 15. Figure VII-7 shows a 1-ft magnet in comparison with a 10-ft magnet and Fig. VII-8 shows a comparison between a 10-ft and a 22-ft magnet. It is planned that each magnet would be tested before it is installed in the tunnel. During this test, vacuum

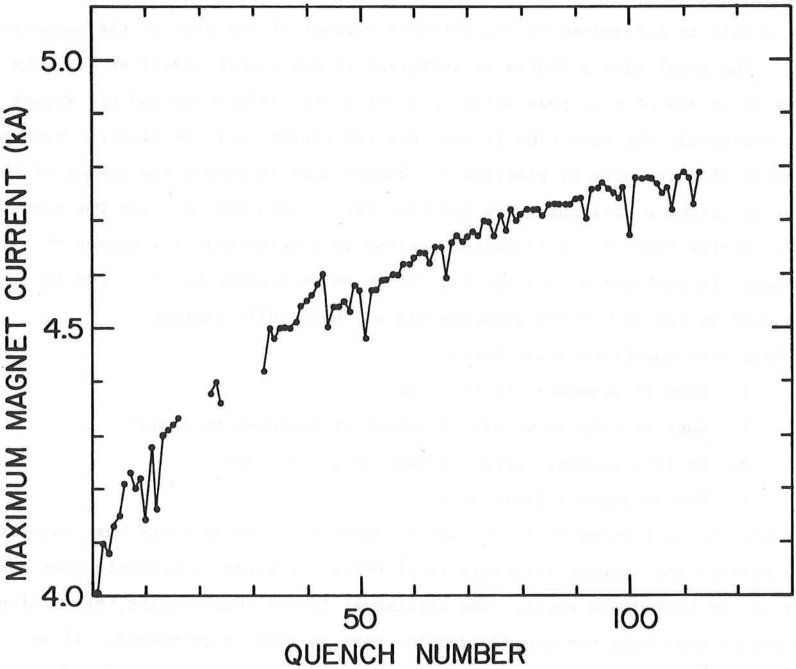

Fig. VII-6. Training curve for magnet El-3.

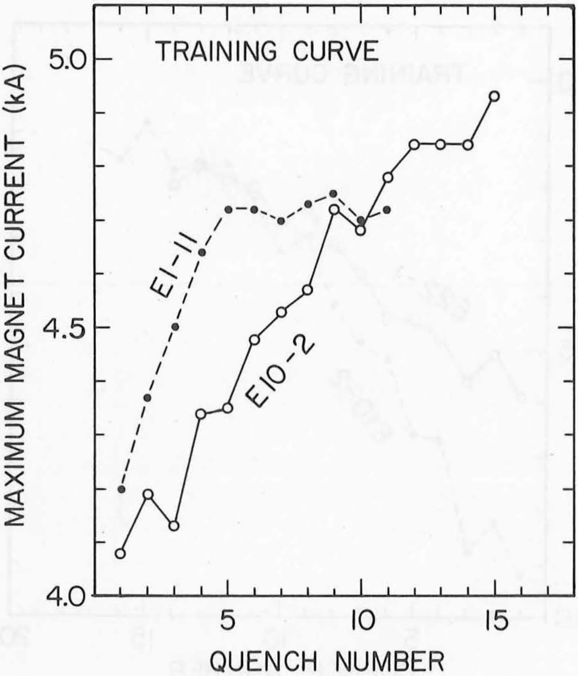

Fig. VII-7. Training curves of 1-ft and 10-ft magnets.

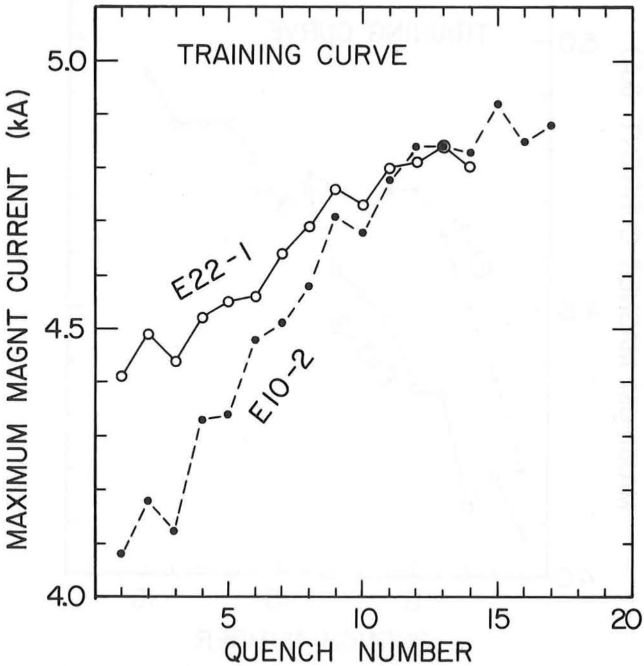

Fig. VII-8. Training curves for 10-ft and 22-ft magnets.

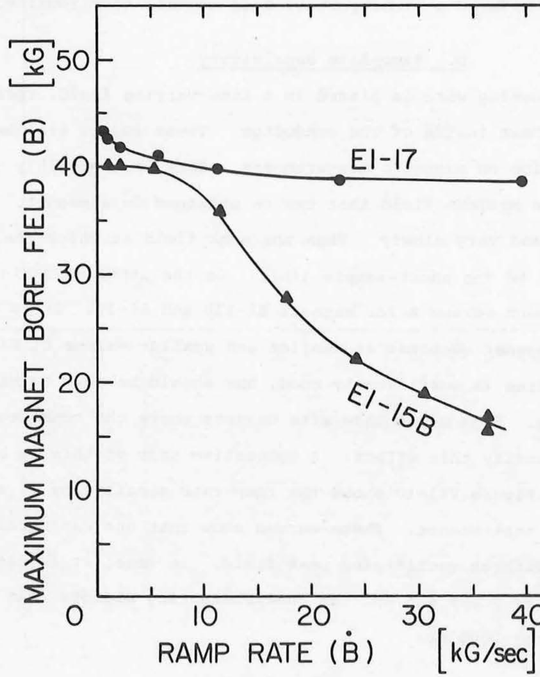

Fig. VII-9. Dependence of peak field on ramp rate for 1-ft magnets.

measurements would be made, the coil would be trained, it would be verified that it is magnetically accurate and survey marks would be placed on the cryostat to indicate where the coil is located inside. The few quenches that it takes to train a magnet are considered a minor part of this overall test routine.

D. Ramp-Rate Sensitivity

When a superconducting wire is placed in a time-varying field, there are ac losses that generate heat inside of the conductor. These losses are measured and discussed in the section on magnetic measurements. Here we are mainly interested in their effect on the maximum field that can be obtained in a magnet. Suppose the current is increased very slowly. Then the peak field at which the magnet quenches can be close to the short-sample limit. On the other hand Fig. VII-9 shows a plot of B-quench versus $\dot{B}$ for magnets E1-15B and E1-17. It is seen that as $\dot{B}$ increases, the magnet quenches at smaller and smaller values of field. If the cooling of the wires is sufficiently good, one should be able to minimize the ramp-rate sensitivity. Some tests made with magnets where the conductor was not well-cooled seem to verify this effect. A quantative test of this is being planned at present. Figure VII-10 shows the ramp-rate sensitivity of a 22-ft magnet and of a 5-ft test magnet. These curves show that one can obtain very rapid rates of rise without sacrificing peak field. In fact, it is clear that it will probably be the rf power and not the superconducting magnets that limit the maximum $\dot{E}$ of the Energy Doubler.

E. Temperature Dependence

The critical current of the superconducting wire is a function of temperature, decreasing as T increases. We have investigated this in detail on several magnets. Figure VII-11 shows the temperature dependence of B-quench for magnet E1-18. It is seen that the peak B decreases by about 15% per K.

F. Wire Comparison

Magnets E1-17, E1-18, E1-19, and E1-20 were constructed to be identical except for the wire, which was made by four different manufacturers. Figures VII-12 through VII-14 show the results obtained with these four magnets for training, ramp-rate sensitivity at two temperatures, and temperature dependence of B-quench.

Notice that the shape of the ramp-rate sensitivity curve remains unchanged as T is varied. There is indication in this series of magnets also that the

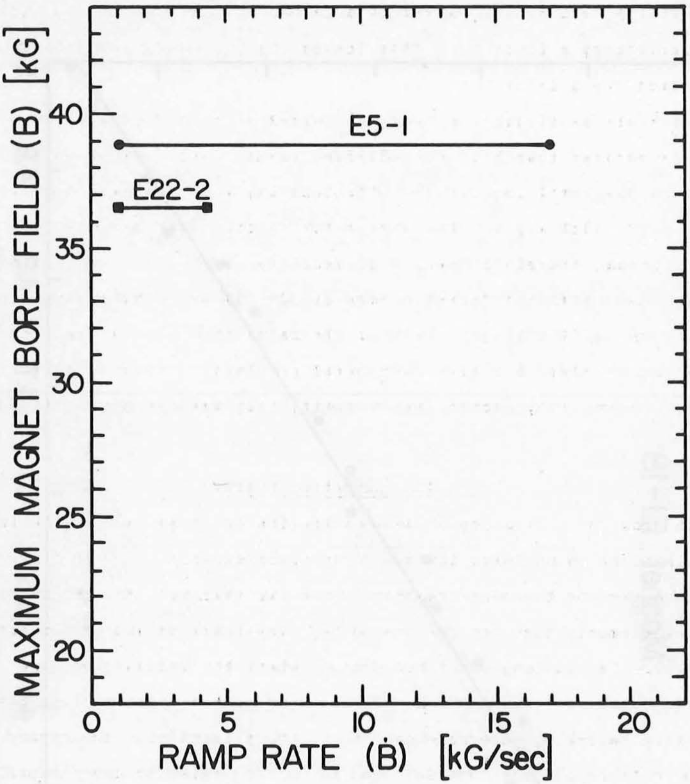

Fig. VII-10. Dependence of peak field on ramp rate for 5-ft and 22-ft magnets.

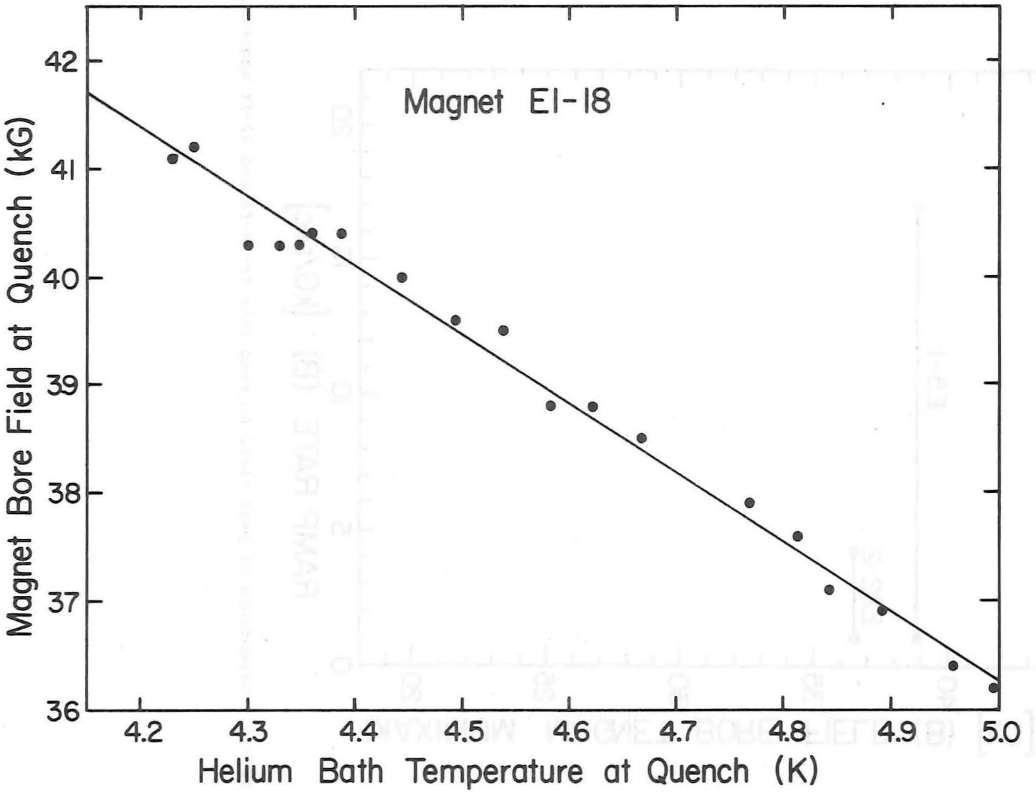

Fig. VII-11. Dependence of peak field on temperature of magnet E1-18.

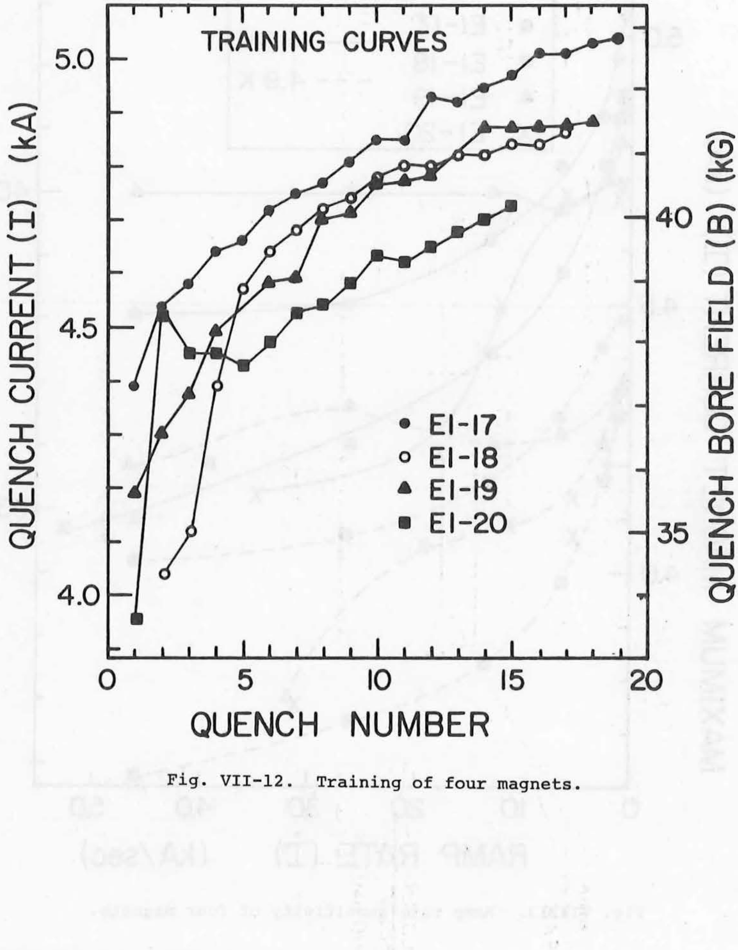

Fig. VII-12. Training of four magnets.

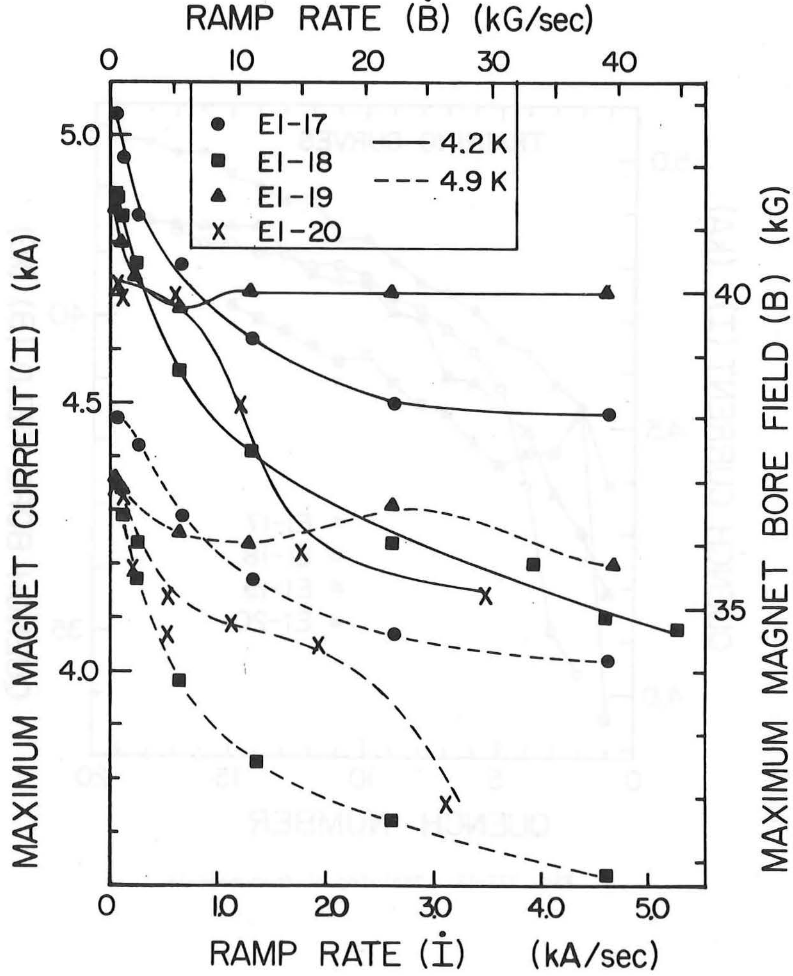

Fig. VII-13. Ramp rate sensitivity of four magnets.

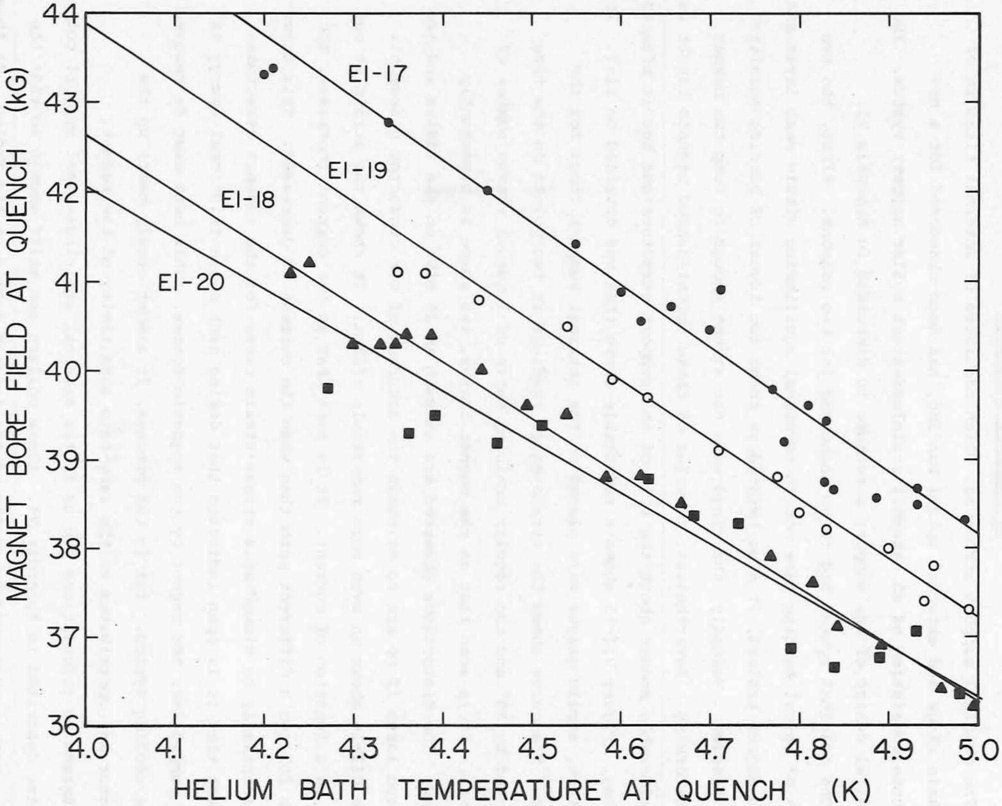

Fig. VII-14. Temperature dependence of four magnets.

fabrication of the wire effects the characteristics of the finished magnet, particularly in the $\dot{B}$ dependence. This will require further investigation.

G. Support Structure

The original support structure, which consisted of internal titanium or porcelain rings and external spiral banding, has been abandoned for a new structure consisting of an external stainless-steel collar support system. The mechanical design of the support structure is discussed in Appendix VI.

The original system had to be abandoned for two reasons. First, the two layers of spiral banding were not in torsional equilibrium within each layer and, as the magnet trained, it also twisted as these two layers of banding equalized their tension. Secondly, the rings were not strong enough to keep the magnet from deforming. Nevertheless, a series of these spiral-banded magnets taught us a considerable amount about the role of the support structure and how it affects training. Figure VII-15 shows a remarkable curve that was obtained on E1-7. In this test, strain gauges were placed on the internal support rings for the magnet. The curve shows the strain-gauge readings at two points on the ring separated by 90^0 and the regular training curve of I quench versus number of quenches. It is seen that as the magnet trains, its shape is permanently altered. The distortions observed are as much as 25 mils on the radius and are much too large if we are to maintain the accuracy of our conductor placement. Figure VII-16 shows an even more remarkable effect. It shows the strain at one point as a function of current. It is seen that as the current increases, the strain follows a different path than when the current is decreased. This curve can essentially be viewed as a stress-strain curve for the support structure. The fact that it is open indicates that during each cycle frictional energy is being pumped into the magnet by the magnetic forces. This heat must be removed by the cooling system. But in the process, it almost surely heats up the conductor and contributes to the ramp-rate sensitivity of the magnet.

Extensive calculations led us to the external stainless-steel support collars that are described in Appendix VI. These collars are stiff enough so that the displacement as measured by strain gauges is only 4 mils on the radius. At this point, we will have to await the magnetic measurements on some real magnets in their cryostat to see if this displacement is enough to generate a sextupole moment that is too large to be tolerable. It is thought that this will not be

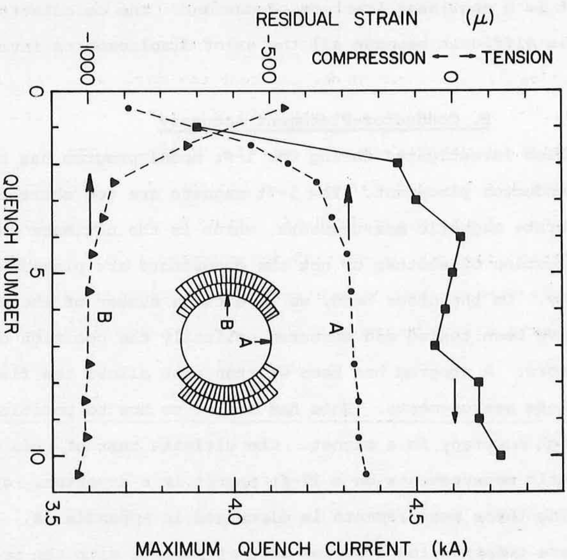

Fig. VII-15. Training and residual strain correlation plot for magnet E1-7.

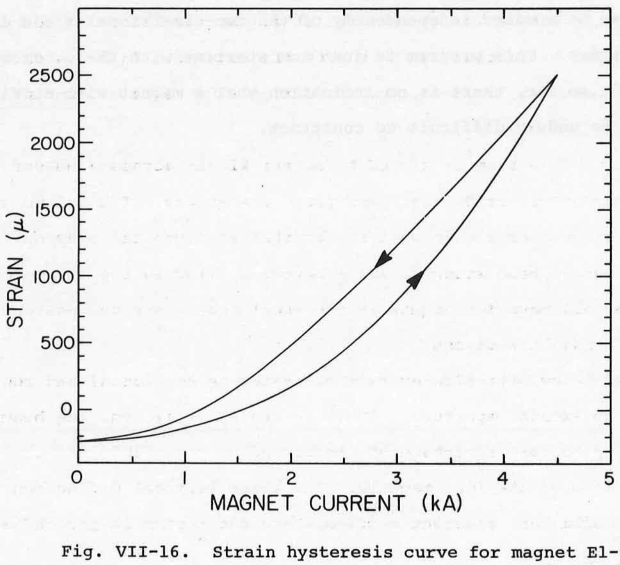

Fig. VII-16. Strain hysteresis curve for magnet E1-7A.

the case, and preliminary measurements on E5-1 do not indicate a significant sextupole moment that is a nonlinear function of current. The calculation of the sextupole moment is difficult because all the exact displacements involved are not known.

H. Conductor-Placement Accuracy

One more problem investigated during the 1-ft model program has been the accuracy of the conductor placement. The 1-ft magnets are too short to lend themselves to accurate magnetic measurements, which is the ultimate way to investigate the question of whether or not the conductors are placed with sufficient accuracy. On the other hand, we have cut a number of the magnets in half after they have been tested and measured optically the position of the individual conductors. A program has been written that allows the field to be calculated from these measurements. This has taught us how to position the conductors with high accuracy in a magnet. The ultimate test of this will be when we make magnetic measurements on a 22-ft magnet in a cryostat. The equipment for making these measurements is discussed in Appendix IX. Parallel to this program, we are constructing a series of 5-ft magnets with the most accurate techniques that we have. These 5-ft magnets will be placed in a small reusable cryostat and measured magnetically. A 5-ft magnet is long enough so that the end configuration can be studied independently of the two-dimensional field in the center of the magnet. This program is just now starting with E5-1. From the measurements made so far, there is no indication that a magnet with sufficient accuracy should be unduly difficult to construct.

APPENDIX VIII. TOOLING AND PRODUCTION PLANNING

W. Hanson

A. Introduction

As the design of the Doubler magnet has evolved, the way in which the components could be economically fabricated has always warranted prime consideration. For instance, the nesting of stamped laminations to minimize material usage was thoroughly explored. The 22-ft length of magnet was partly selected on the available stacking fixtures, maximum conductor length, tube lengths available, and edge-iron lengths available.

B. Tooling

The design of tooling was based upon the short-run needs to prove the concept being explored and the long-term requirements to build 1000 22-ft magnets. The initial tools used usually were adaptable to modification to meet the high-speed requirements of future production.

Coils. The general design of the coils has been fixed for some time and therefore the level of production tooling has developed to the greatest extent. Normal coil winding is done on a rotating table upon which a coil-winding mandrel is mounted. With a 22-ft magnet, the floor space required for such a machine is considerable. In order to meet the production requirements, a bank of these machines will be required. Therefore, a concept of winding was devised that requires much less floor space. The mandrel is stationary and the reel of conductor "walks" around the mandrel. This concept has the further advantage of allowing very rapid traversing along the length and slowing up only at the ends where shaping of the coil is more difficult. To accomplish this, the mandrel oscillates about its longitudinal axis while the conductor is coming around the ends. The winding operation is shown in Fig. VIII-1.

After winding, the coil is "packaged" and molded into a rigid component to place each conductor permanently to its correct position within a few mils. This is done by precision molds and extremely high packaging pressure (approximately 10,000 psi). For initial production, these molds are closed with heavy high-strength bolts, but the design provides for conversion to hydraulics for final high-speed production. Figure VIII-2 shows the important "packaging" of the coil, which places the conductor near its final position in preparation for the application of the high pressure.

Final Assembly. The finished coils are assembled together onto a mandrel and the coil-clamping half rings are pressed on in an interleaving manner to form a solid laminated shell to support the coil. Currently this is mainly a hand operation, with the use of special hand tools to make it a reasonably fast operation (approximately 1 ft per hour). As the exact design of these collars becomes frozen, automated equipment for coating, stacking, and meshing will be acquired that should reduce this time to a fraction of its present value.

Compressing the laminated shell to support the coil assembly tightly also requires high pressure in order to provide intimate contact with the coil. Hydraulic rams provide this pressure, whereas bolted construction holds the pressure during the curing cycle. For final high-speed production, hydraulic rams could be provided for the entire length of each magnet and held during the cure cycle, thus further speeding the operation.

C. Production Planning

In addition to perfecting the tooling for production, space is being provided. The Magnet Facility, which consisted of two large industrial buildings used for the fabrication of the original Main-Ring magnets, has now expanded into a third building. Two of these buildings are planned to be used exclusively for the Energy-Doubler fabrication project. The third building is primarily for conventional-magnet fabrication, but also houses the fabrication of the magnet yokes. These areas are separated and are being partitioned according to the cleanliness and criticality of the various operations. The coil-winding itself, up to the stage of the initial cure, is the most critical from the standpoint of contamination with dirt and chips. This area is therefore being prepared for the highest level of cleanliness.

Fig. VIII-1. Winding the 22-ft magnet.

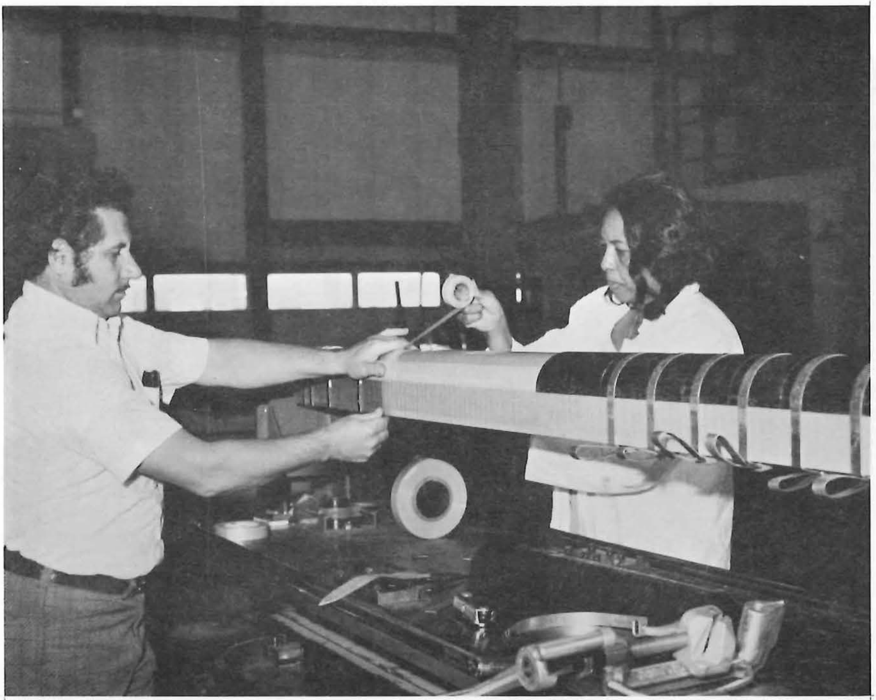

Fig. VIII-2. Packaging of the coil.

APPENDIX IX. MAGNET MEASUREMENTS

R. Yamada

A. Introduction

In the past year, an extensive effort has been made by the Magnet Measurement Group to develop and implement the equipment for the field measurement of Energy-Doubler magnets. An on-line data acquisition system was built for data taking and processing. The ac-loss values of about a dozen magnets were measured by the group. An old D-type 10-ft canned magnet, D10-3, and a new E-type 5-ft canned magnet, E5-1, were tested extensively, using pool-boiling cooling. Their harmonic contents were measured for both dc and pulsed mode, using the newly developed data-acquisition system. The equipment and facility for the production magnet test are installed at the Protomain in the Village.

In addition, methods to measure ac loss and hysteresis loss of superconducting wire were established. A large number of wires were tested for short-sample data and the quality-control testing of production wire is being carried on.

B. Instrumentation and Facility for Production-Magnet Testing

An advanced data-acquisition system using an on-line mini-computer (PDP-11/10) and a CAMAC system was developed and has been in use successfully for testing superconducting magnets. It can be used to investigate many characteristics, including harmonic analysis of magnetic fields, and we can know exactly and instantly how the superconducting magnet system behaves.

The Protomain, which was used for the original design study of Main-Ring magnets and also for the study of the liquid-helium loop, has been converted to test production magnets. There is a complete set of equipment installed, including a set of magnet stands with end boxes for superconducting magnets, a vacuum system, a control system and a power supply. They will be used for extensive study of prototype magnets and production magnets. For the production testing of all magnets, we need at least two sets of test stands for bending magnets and one set for quadrupoles. Liquid helium from a Gardner refrigerator system with a 1000-gallon dewar will be force-circulated through a 50-ft transfer line and a 200-ft loop

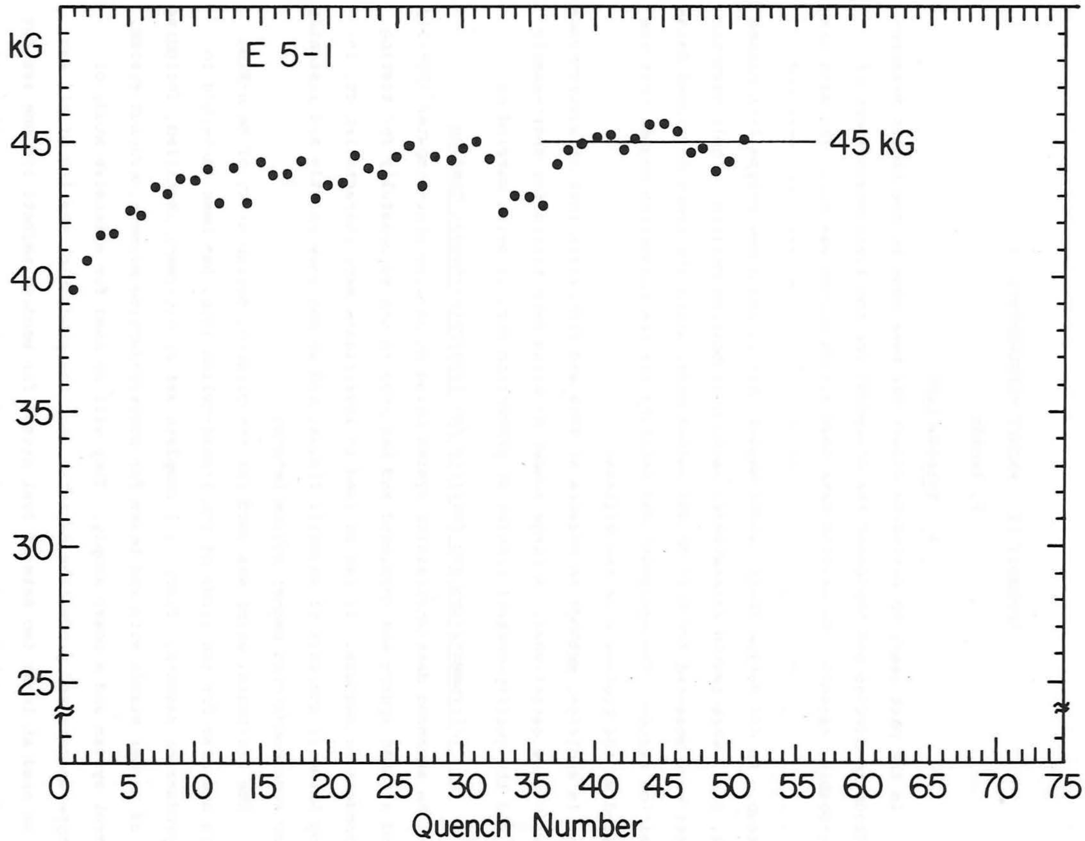

Fig. IX-1. Training curve of E5-1 magnet.

line. The temperature of the liquid helium can be varied downward from the standard 4.7K.

C. Procedures for Production-Magnet Tests

After a magnet is finally assembled with canning and lamination cores, it will be tested using the equipment and facility above. The following procedure will be used for production tests of a magnet after simple vacuum-leak tests:

1. The magnet will be trained up to maximum field.
2. Ramp-rate dependence of the magnet will be measured.
3. AC loss of the magnet will be measured.
4. The integrated field value of a bending magnet or the integrated-gradient value of a quadrupole magnet will be measured in pulsed operation from injection field to the maximum field.
5. The magnetic median plane of the magnet will be determined electronically by finding a vertical magnetic symmetry plane, and survey marks will be put on the outside surface.
6. Heat loss of the magnet will be measured.
7. Remanent field and some low fields will be measured.
8. Harmonic analysis of the field distribution will be done for both dc and pulsed operation on some sample magnets.

D. Prototype Model-Magnet Test

Extensive magnet tests and field measurements were done on the D10-3 and E5-1 magnets.[1] These magnets were canned and provided with lamination cores. They were tested with pool-boiling cooling. The training curve of the E5-1 magnet is shown in Fig. IX-1, and its central field value exceeded 45 kG after some training.

Training curves, ramp-rate dependence, quench behavior and ac loss were measured on these magnets. Field shapes were measured with a Hall-probe gaussmeter for general features. For precision field measurement, a harmonic-analysis method was carried out.

A special method using an NMR circuit and signal averaging was used to measure the absolute field value. The NMR signals obtained are shown in Fig. IX-2. The signal at 20 kG is from protons without signal averaging. The ones at 30 and 44 kG are from ^{7}Li and obtained with signal averaging. The transfer function is shown in Fig. IX-3, which shows the saturation effect of iron beyond 35 kG. The lamination used for the E5-1 magnet was smaller than the final one, and we should

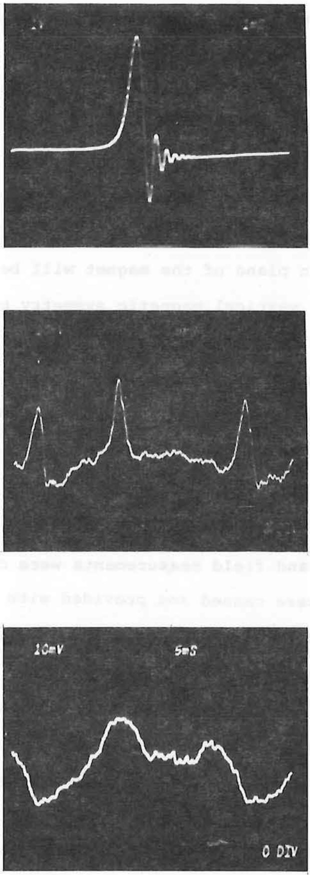

Proton

2000 A (~20 kG)
85.661 MHz
= 20.12 kG

^{7}Li

3000 A (~30 kG)
49.953 MHz
= 30.19 kG
After signal averaging

^{7}Li

4400 A (~44 kG)
72.954 MHz
= 44.09 kG
After signal averaging

Fig. IX-2. NMR signals in E5-1.

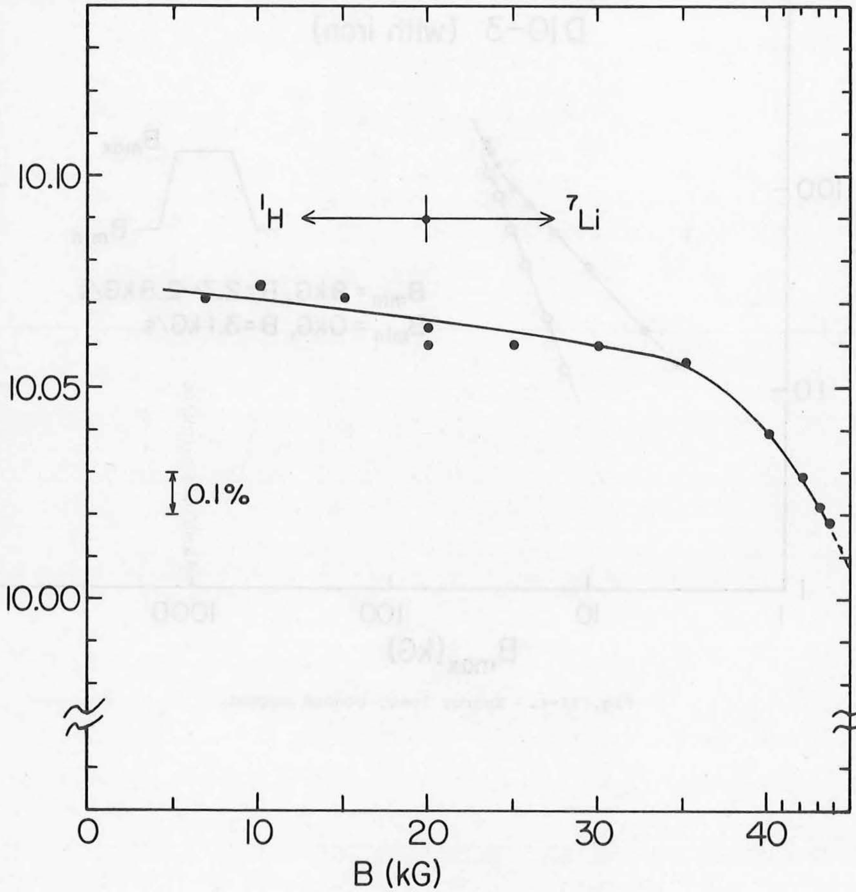

Fig. IX-3. Transfer function using NMR.

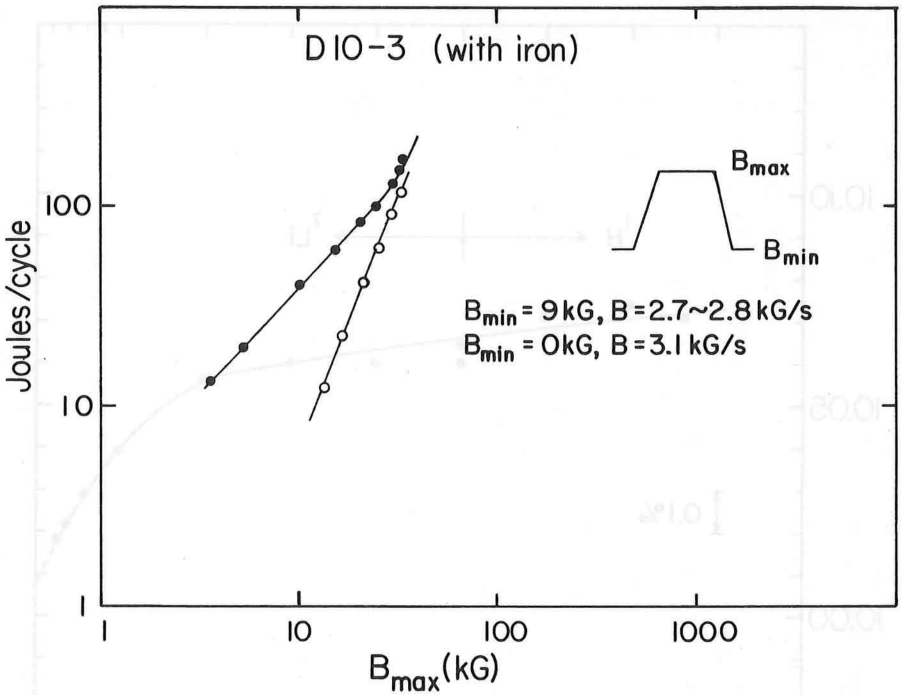

Fig. IX-4. Energy loss, banded magnet.

expect less saturation effect for the final design of the lamination.

E. AC-Loss Test on Magnets

The total energy used during a cycle can be measured electronically using the on-line data-acquisition system. This is an excellent diagnostic method to test a magnet. If the magnet structure is not adequate for strong magnetic forces at high field, we can infer from this measurement that the wire is moving and causing an excessive extra energy loss. We can also tell whether the superconducting wire is within specification.

A half-dozen 1-ft magnets, one 5-ft magnet, three 10-ft magnets, and one 22-ft magnets have been measured for their ac loss.[2] The ac-loss curves of the D10-3 magnet, (banded structure) and E5-1 (collared structure) are shown in Figs. IX-4 and IX-5 respectively. The ac-loss curves of all banded magnets show a bend around 20 or 30 kG, as shown in Fig. IX-4, reflecting a rapid increase in ac loss at higher field. This fact is attributed to wire movement inside a magnet caused by the structural deformation under strong magnetic force. Also shown in Fig. IX-4 is a curve of ac loss for operation starting from 9 kG.

The newly developed collared magnet, E5-1, does not show a high-field bend in its ac loss, as shown in Fig. IX-5. This means that the collared structure is strong enough to hold the wire in place. This implies there is no additional ac loss or extra field distortion caused by wire movement. The circle at 45 kG is the calculated value for a 5-ft magnet from wire data. They are in good agreement. The low-field bend around 3 kG is caused by the penetration of field into the superconducting filaments.

F. Harmonic Analysis of Magnetic Fields

The on-line data acquisition system was used successfully for harmonic analysis of magnetic field measurement of the D10-3 and E5-1 magnet.[2] It was used for both dc and pulsed-mode operation. The data were taken automatically using Morgan coils. The sextupole component of E5-1 magnet during pulsed-mode operation is shown in Fig. IX-6, which is taken at 0.75 in. radius. It shows a hysteresis curve caused by magnetization of the superconductor. The various measured coefficients of the E5-1 magnet up to octupole are shown in Fig. IX-7, where b_1 and b_2 are normal quadrupole and sextupole coefficents and a_1 and a_2 are the corresponding skew coefficients. The measurements were made up to 40 kG. In addition, quadrupole and sextupole terms were measured at the ends.

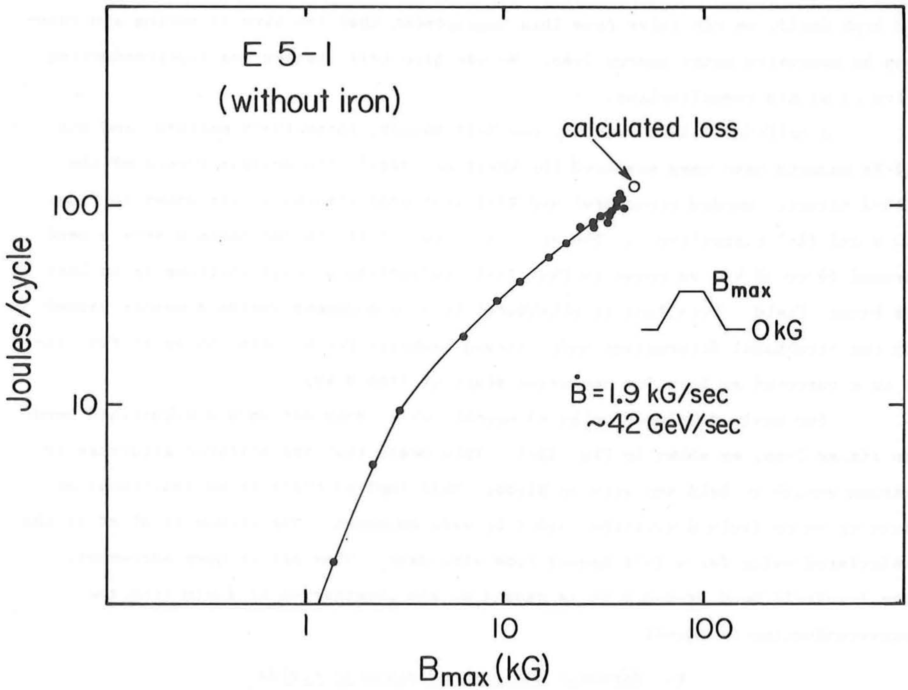

Fig. IX-5. Energy loss, collared magnet.

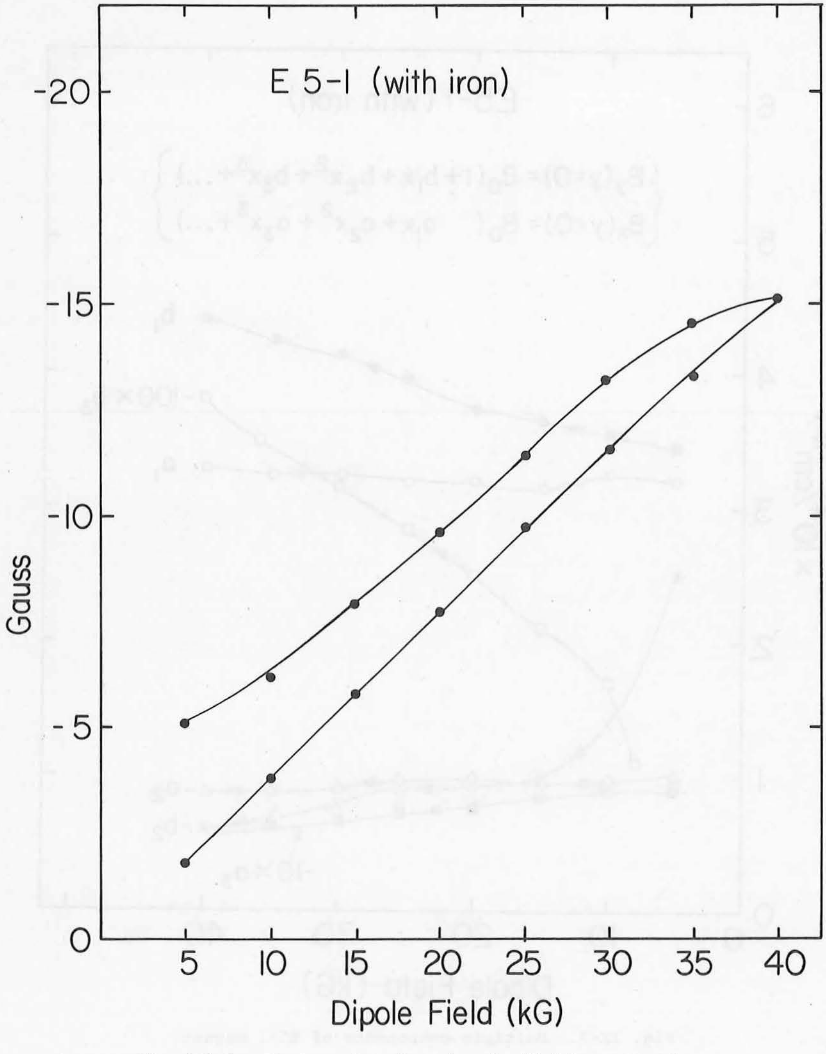

Fig. IX-6. Hysteresis of sextupole field components.

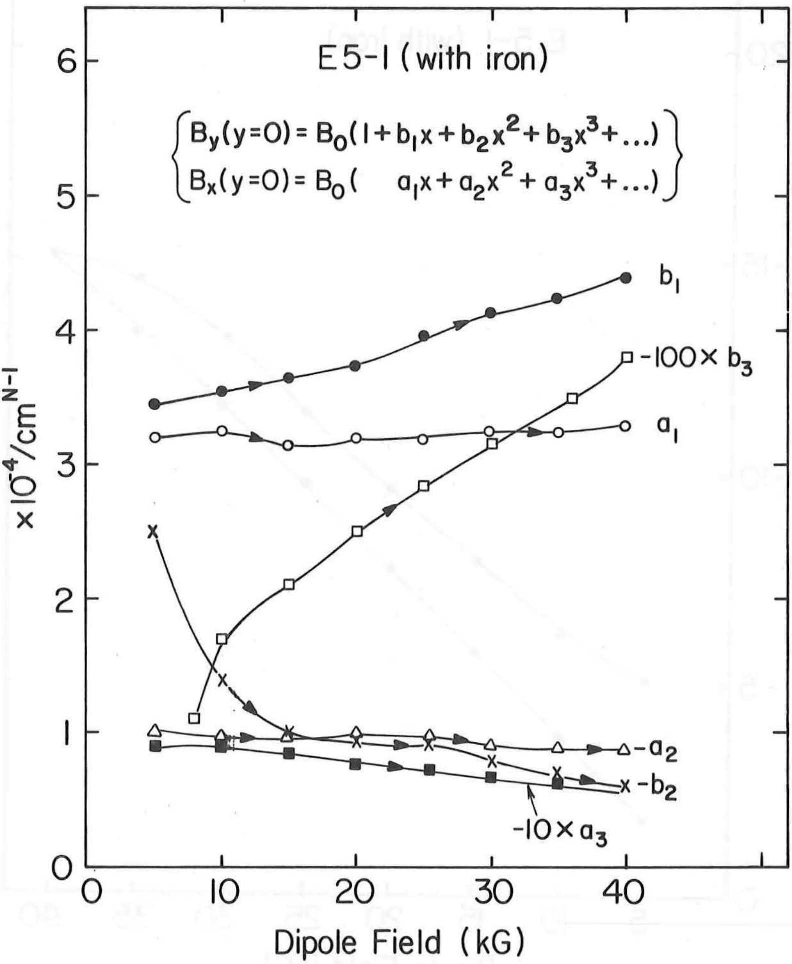

Fig. IX-7. Multiple components of E5-1 magnet.

G. Superconducting-Wire Tests

The NbTi superconducting cables that are being used for Energy Doubler magnets have been investigated extensively. The ac-loss, hysteresis loss and short-sample data of wire were measured both in the short-sample form and in solenoidal form.[3] These measurement methods were established and permanent equipment is set up. The ac-loss and maximum-field values in real magnets are interpreted in light of thse data from wire samples, which have proven to be essential for the understanding of magnet operation.

The electronic-magnetization method was used to measure the ac-loss of wire.[4] Field-orientation effects on the ac loss was measured for soldered and unsoldered cable. For the perpendicular field, the ac loss of soldered cable strongly depends on ramp rate, because of coupling between strands. For this reason, soldered cable was abandoned. The hysteresis losses of short pieces of cable are measured at very slow ramp rates in three different orientations relative to the magnetic field.[5]

The short-sample data are measured in external fields of 30 to 60 kG for both single-strand wire and cabled wires. Quality control of production wires of single-strand and 23-strand varieties is now routinely being conducted. Resistivity tests of copper are also being done.

References

[1]R. Yamada et al., Operational Test and Field Measurement of D10-3 Magnet, TM-651, 0428.000, March 26, 1976.

[2]R. Yamada et al., AC Loss Test of D10-3 Magnet, TM-638, 1600.000, December 30, 1975.

[3]R. Yamada et al., Superconducting Wire Test at Fermilab, TM-598, 1600.000, July 1975.

[4]H. Ishimoto et al., AC Loss in Flat Transposed Superconducting Cable, TM-636, 1600.000, October 28, 1975.

[5]M. E. Price and R. Yamada, Hysteresis Loss Test of Superconducting Wires, TM-639, 1600.000, December 15, 1975.

APPENDIX X. CRYOGENIC MEASUREMENTS

M. Kuchnir

A central part of the Fermilab effort on superconducting magnets has been the development of measurement methods at very low temperatures. As part of this effort, many instruments have been constructed and many studies have been carried out. Among these are:

1. A carbon-resistor calibration mini-cryostat which permits the simultaneous calibration of eight resistors over the range 4.2K to 300K to be done inside a regular storage dewar.[1] This device allows us to instrument magnet cryostats with non-recoverable thermometers.
2. A device for measuring thermal contraction of solid components when immersed in liquid nitrogen or liquid helium with a sensitivity of 5×10^{-6} cm.
3. A setup for measuring the thermal-conductivity integral of solid or layered material from 4.2K or 78K to 300K. Preliminary measurements on fiberglass-epoxy composites, as well as stacks of dusted stainless foils, alumina chips, and superinsulation[2] have been made. The capability now exists for doing such measurements as functions of load.
4. A computer program for estimating the refrigeration load of a given magnet-cryostat design.
5. A procedure for simple fabrication of electrical vacuum feedthroughs for up to 40 or more wires that withstands thermal shocks as well as liquid-helium temperatures.[3] These feedthroughs are known to be vacuum tight for superfluid-helium containment.
6. Set of measurements[4] of Baushinger-effect heat developed in superconducting wire and cable under application or release of tensions at cryogenic temperatures.
7. An experimental study of the efficiency of a heater discharging a capacitor as a quench-provoking element in a superconducting wire. This study and a program that calculates the temperature of a 1-cm

length of superconducting cable as a function of time and current, developed into a more complete study[5] of quench-propagation velocity in our magnets.

References

[1]M. Kuchnir and J. L. Tague, Carbon Resistance Thermometers, TM-647, March 9, 1976.

[2]M. Kuchnir and R. J. Houkal, Measurements of Thermalconductivity Integrals, TM-583, June 1975.

[3]M. Kuchnir, Fabrication of Cryogenic Electrical Feedthroughs, TM-596, August 8, 1975.

[4]M. Kuchnir, Stress Heating of a Thermally Insulated Superconductor, presented at the 3rd NBS-ARPA Workshop, Vail, Colorado, April 1976.

[5]R. H. Flora et al., Quench Development in Magnets Made With Multifilamentary NbTi Cable, to be presented at the 1976 Applied Superconductivity Conference, Stanford, August 17,21, 1976.

APPENDIX XI. COOLING SYSTEM

C. Rode, P. VanderArend and R. J. Walker

A. Development of the Cooling System

Conceptual work was started in the fall of 1972 on a refrigeration system to provide cooling to a complete ring of approximately 20,000 ft length. At that time, a basic decision was made that warm iron would be used. This decision determined to a great extent the space available for coolant passages in the magnets; as a result, a limited cross section was available for flow of liquid helium.

Since 1972, several different methods of supplying and distributing this refrigeration have been studied. All these methods are characterized by a system that puts liquid helium through the region containing the coil windings. This liquid is in a state in which the static pressure on the liquid is higher than the saturated vapor pressure at the temperature of every point. Liquid in this condition is referred to as subcooled liquid. It could also be said to be at overpressure, the term which is used in bubble-chamber operation.

B. Magnet Cooling

A magnet vessel filled with subcooled liquid will be completely full of liquid; no gas will be present. This kind of filling has many advantages and appears to be the only practical way of operating very large magnet systems. One advantage is that flowing of fluid through the magnets and piping can be controlled and predicted exactly because the density and flow resistance vary only slightly with position throughout a given flow system. This flow, referred to as "one-phase", has the highest cooling capacity attainable, as well as the highest heat capacity to compensate for any local surges. All these facts contribute to the stability and reliability of the superconducting system.

The earliest concept of cooling was a continuous flow of liquid helium around the ring, with booster pumps providing the necessary driving force. At the booster-pump stations, the liquid would be recooled by means of heat exchange with boiling liquid helium. Figure XI-1 is a schematic representation of such a

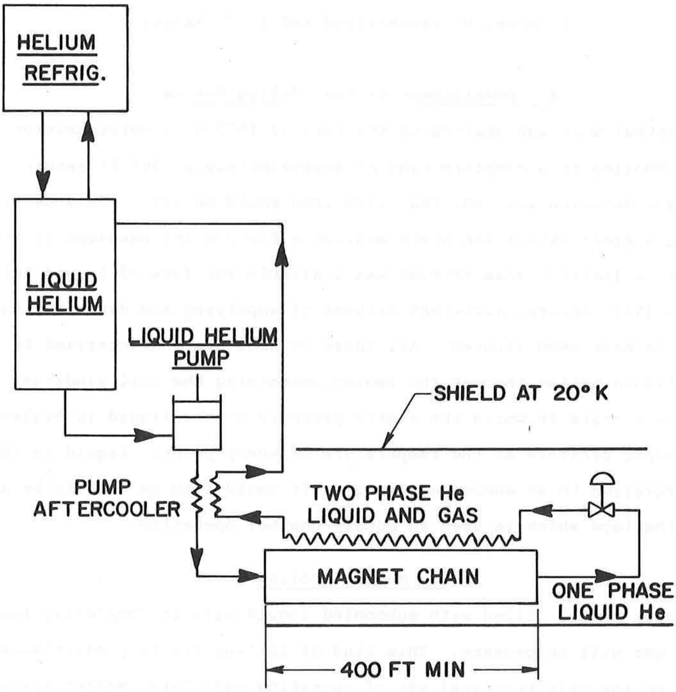

Fig. XI-1. Schematic of magnet cooling concept.

system. The flow of liquid through the magnet structure is one-phase, primarily because control of two-phase flow in the magnet structure is difficult. When flowing a two-phase mixture through the magnet structure, the cooling channels inside the windings of the magnet can by definition contain a fluid with a density somewhat less than that in the longitudinal flow channels, because generation of heat will vaporize the liquid; to drive this mixture through the magnet structure, a density difference is required. The quality of the two-phase mixture will thus change between pumping stations and cooling of the windings of magnets at the beginning of the string will be much different from that of the end of the string.

In order to provide uniform cooling independent of the position of the magnet along the string, it is believed that one-phase fluid cooling is necessary. To increase the mass of the fluid in the cavities of the magnets, liquid is the preferred phase. The minimum flow rate is determined by the heat load, distance between heat exchangers and allowable temperature rise of the helium in passing through the string between heat exchangers. Doubling the distance means doubling the flow rate. This, in turn, means an increase of pressure drop by a factor eight.

The concept described above has several disadvantages. The major one is a temperature rise along the flow path. In addition, liquid needs to flow all the time through the complete ring and it is impossible to deactivate a section of the ring while maintaining the rest of the ring at operating temperature.

The solution to the problem of temperature variation is to replace the cooling at discrete heat exchangers by a system that cools all along the path at approximately a constant temperature. This can be accomplished by employing a return channel filled with boiling helium, surrounding the magnet vessel. This system will maintain a string of magnets between heat exchangers at essentially a constant temperature. It also separates the total ring into 6, 12, or 24 separate systems, each of which forms an independent module. At present, this counterflow method appears to be superior.

Figure XI-2 is an illustration of a counterflow system. The pressure in this case is provided by a liquid pump. Another option under consideration is to use flow directly out of the liquefier and eliminate the pump. The pump increases the cost, but adds greater reliability. Figure XI-3 shows a typical distribution system.

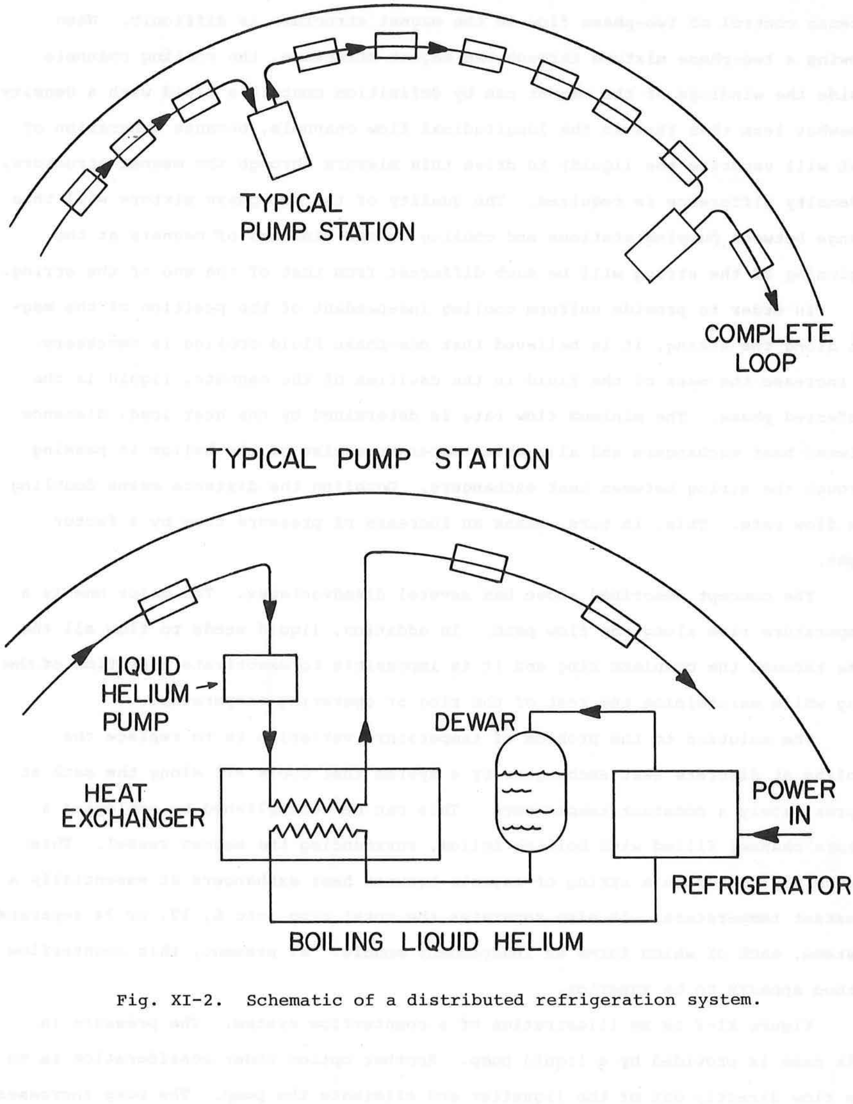

Fig. XI-2. Schematic of a distributed refrigeration system.

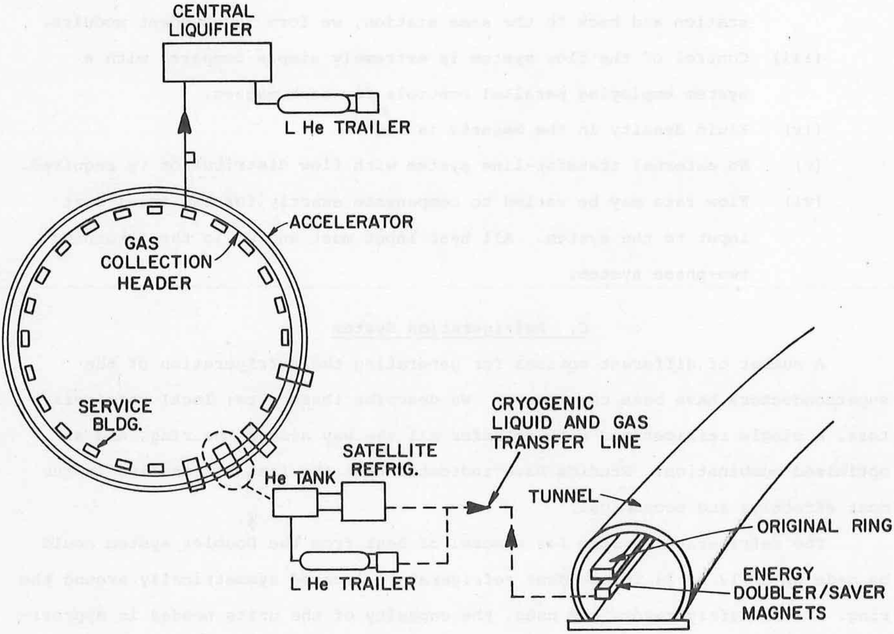

Fig. XI-3. Schematic layout of cooling system.

The system has the following advantages:

(i) Magnets operate at a constant temperature independent of location in the ring, except for the small temperature gradient caused by pressure drop in the two-phase flow channel.

(ii) By directing the flow away from a heat exchanger or refrigerator station and back to the same station, we form independent modules.

(iii) Control of the flow system is extremely simple compared with a system employing parallel controls for each magnet.

(iv) Fluid density in the magnets is high.

(v) No external transfer-line system with flow distribution is required.

(vi) Flow rate may be varied to compensate exactly for the total heat input to the system. All heat input must end up in the returning two-phase system.

C. Refrigeration System

A number of different options for generating the refrigeration of the superconductors have been considered. We describe three here; local refrigerators, a single refrigerator with transfer all the way around the ring, and an optimized combination. Studies have indicated that the last alternative is the most effective and economical.

The refrigerator system for removal of heat from the Doubler system could be made up of 12 or 24 independent refrigerators located symmetrically around the ring. If 12 refrigerators are used, the capacity of the units needed is approximately 950W at 4.5K and 1,250W at 20K. To enhance reliability of the units, turbo machinery would be used. As a consequence, each unit would require approximately 1,000 bhp of connected compressor capacity. The large requirement for power along the ring is the major disadvantage of this proposed system.

A system employing a centrally located refrigerator with distribution of cryogenic fluids is possible, but it requires a large vacuum-jacketed transfer-line system paralleling the complete ring for the following fluids:

a) Liquid helium at 4.5K at a rate of 5,280 lb/hr.

b) Gaseous helium at 4.5K at a rate of 5,000 lb/hr.

c) Gaseous helium at 15K at a rate of 2,280 lb/hr.

d) Gaseous helium at 25K at a rate of 2,280 lb/hr.

The gaseous helium streams are at high pressure (approximately 20 atm). In order to provide a line of this type, the refrigeration load at 20K of the system may increase by 50 to 100%, unless liquid-nitrogen shielding is used in the line. The line will be very large, with a jacket diameter of approximately 16 in. at the point where the central liquefier-refrigerator connects. Its cost has not been determined, but is expected to be at least $4 million.

A system of central liquefier and satellites will reduce the demand for power along the ring. The system is a hybrid between the initial system of local refrigerators and a system using only a centrally located refrigerator. It is the kind of refrigeration that matches the distribution system illustrated in Figure XI-3.

The system of satellite refrigerators with a central liquefier reduces the demand for liquid helium from the central facility from 5,280 to 600 lb/hr and the demand for gaseous helium for shield cooling from 2,280 lb/hr to nothing. As a consequence, liquid helium from the central facility may be distributed either by semitrailer of 10,000 gallon capacity or by a small-diameter liquid-helium transfer line of simple construction.

The total power requirement of the central liquefier with a capacity of 960 lb/hr (approximately 50% excess capacity) and the 24 satellite refrigerators, each capable of providing 700W at 4.5K and 625W at 20K is of the order of 5.2MW compared with 9.8MW for the 12 refrigerator case. In addition to this, it is possible to reliquefy nitrogen at the central liquefier facility at a considerable cost saving over the 12-refrigerator case with each of the 12 refrigerators requiring liquid nitrogen. The satellite refrigerators do not require liquid nitrogen for the proposed operating mode.

D. Central Liquefier

There are many other advantages to a central liquefier. Larger plants are much more efficient, for example in the expanders and compressor. This, of course, enhances the power saving. Maintenance can be in one location, eliminating lost time and extra traveling. There is also less overall equipment to install.

A central helium liquefier to match these requirements is currently in the design and construction phase. This plant consists of three large compressors, a helium reliquefier and a nitrogen reliquefier. The compressors from both the nitrogen and helium reliquefiers and part of the nitrogen reliquefier have been obtained as surplus from an Air Froce liquid-oxygen plant located near Los Angeles, California.

Our plan is to use two of the compressors for helium instead of air service (as they were previously), which will necessitate operating them at one-half of their rated horsepower. The compressor providing flow for the nitrogen reliquefier will run at near full power. Under these conditions, the design output of the plant is approximately 1,100 lb/hr (4000 ℓ/hr) of liquid helium with both compressors running. The design output of the nitrogen reliquefier is 5,000 lb/hr (2800 ℓ/hr) of liquid nitrogen.

The current plan is for the central helium liquefier to be operational in the fall of 1977.

Many possible uses exist for the central liquefier. It can provide refrigeration for beam-line magnets. Depending on the actual heat loads developed by the Doubler system, it may be possible to run only one helium compressor at a time. In the event of future expansion of liquid-helium requirements, it would be possible to rearrange the cylinders on the helium compressors and to approximately double the plant output. This would require an expenditure of approximately $200,000 to buy some additional cylinders.

E. Satellite Refrigerators

The basic operating mode of the satellite refrigerator extracts refrigeration from liquid helium supplied by the central liquefier and amplifies the available refrigeration. Table XI-I provides the design ratings of a satellite refrigerator, of which 24 would be required to cool the Doubler system.

Table XI-I. Satellite-Refrigerator Parameters

Liquid helium supplied by central facility	70-100 ℓ/hr
Refrigeration at 4.5K	700 W
Refrigeration at 20K	625 W

The satellite refrigerator consists of a compressor package that supplies approximately 300 lb/hr of oil-free helium gas at 20 atm to the cold box. The cold box consists of heat exchangers and employs two reciprocating expansion engines. The refrigeration cycle is balanced in such a way that all the refrigeration available in the liquid helium supplied by the central liquefier is extracted. By doing this, the satellite refrigerator produces some 700 ℓ/hr of liquid helium. This liquid vaporizes in the magnet system and is returned as cold vapor for reliquefication by the satellite refrigerator.

Reliability of the satellite refrigerator system is high, for the following reasons:

(i) The compressor package consists of ammonia refrigeration compressors. These machines are commercially produced and have a proven record of reliability.

(ii) The expanders are installed in separate canisters. This allows quick removal and replacement with a spare unit. During the absence of an expander, the satellite refrigerator can produce the same amount of refrigeration through the addition of more liquid helium at a rate of 400 ℓ/hr coming out of storage. While the expander is being repaired, the central liquefier will liquefy the extra gas.

The satellite refrigerator is a versatile unit that can make liquid helium and supply refrigeration without the addition of liquid helium from an external source. It will do this through the addition of liquid nitrogen. Table XI-II shows the capability of the refrigerator under various conditions. This table applies when no liquid helium is being supplied by the central liquefier.

Table XI-II. Performance Characteristics of the Satellite Refrigerator as an Independent Operating Unit

System	Capacity
a) Helium liquefier with liquid-nitrogen consumption (nitrogen consumption is 60 ℓ/hr)	90 ℓ/hr
b) Helium refrigerator with liquid-nitrogen consumption (nitrogen consumption is 25 ℓ/hr)	400 W

The performance listed in Table XI-II may be improved by providing a larger compressor package. The flow rates may be increased by 50% without generating a high pressure drop in the heat exchanger system of the satellite refrigerator. Refrigeration output will be in proportion to the flow rate.

APPENDIX XII. VACUUM SYSTEM

P. Limon

A. Introduction

The decision to use the Energy Doubler as a storage ring to collide beam with the Main Ring places stringent requirements on the vacuum system. In addition, the vacuum system is unconventional because the Energy Doubler is a cold-bore machine. There are many advantages and some disadvantages of a cold-bore machine. Among the advantages are:

(i) Maximum use of the beam-tube aperture. This is an advantage even if the magnetic field is not uniform throughout the aperture, because this space can be used for injection and extraction of beam when the Energy Doubler is operating as an accelerator.

(ii) Cryopumping of all residual gases except for helium and hydrogen. The vapor pressure of hydrogen is approximately 10^{-6} Torr at 4.6K.

The major disadvantages of a cold-bore system are lack of access to the beam tube and lack of experience with cold-bore systems.

B. Pumps

Since liquid helium is readily available, it seems advantageous to use cryosorption pumps throughout the system. These pumps can have a very high pumping speed and capacity for both helium and hydrogen, and can be built into the cryostat in many places. Two possibilities are:

1. To build a small cryosorption pump coaxially with the beam tube between each magnet. This pump can easily be shielded from the beam.
2. To build a larger pump into each quadrupole cryostat. Although this scheme provides lower net pumping speed, it should be more than adequate, provided there are no helium leaks into the tube directly from the liquid-helium regions of the cryostat.

   This last point is worthy of some discussion. Thousands of dewars have been built over the last few years with no leaks. Welded or seamless stainless steel tubes should have no leaks at all, so the requirement is that there be no welds that go through from the beam tube into the liquid helium. In this case, the pumps are installed to dispose of residual hydrogen that desorbs from the walls and small helium leaks into the tube from the insulating vacuum region.

C. Beam-Off Vacuum

If there are no leaks into the beam tube from the liquid, the pumps must still be capable of handling the outgassing of the beam tube and leaks from the insulating vacuum into the tube. The beam tube itself will be chemically treated, vacuum baked, and stored in dry nitrogen before installation. With treatment of that type, outgassing rates at room temperature of hydrogen from stainless steel can be held to less than 10^{-12} Torr-liters cm^{-2} sec^{-1}. At 4.6K, the outgassing should be many orders of magnitude less. The major problem will be small leaks from the insulating vacuum region into the bore tube. A string of magnets will be leak checked when warm and with the pressure in the insulating region at one atmosphere or more. This sets a limit on leaks of $Q_{leak} \lesssim 10^{-9}$ atm-cc/sec. Sensitive regions, such as bellows and feedthroughs, can be cold-shocked to liquid-nitrogen temperatures during the leak-detection procedure. Since the insulating vacuum is between 10^{-4} and 10^{-5} Torr, undetected leaks will be small; i.e., $Q_{leak} \lesssim 10^{-13}$ atm-cc/sec. If we assume a leak rate Q_{leak} of 10^{-12} atm-cc/sec and pumps of speed s of 500 liters/sec at every quadrupole, then the peak gas density at the position of a leak (15 meters from a pump), would be less than 10^{7} helium molecules/cm^{3}, which is equivalent to a room temperature pressure of less than $2x10^{-10}$ Torr. This is clearly adequate for any storage ring, and would give a beam lifetime against multiple scattering and nuclear interactions of many days.

D. Beam-On Vacuum

The most severe limitation to current in the Energy Doubler will be the pressure-bump instability. Dynamically, this is caused by ions made by beam-gas collisions and accelerated to the beam-tube wall by the electrostatic potential of the beam. When the ions hit the wall, they release gas molecules that are adsorbed on the wall causing a local increase in pressure. At some beam current, $I_{critical}$, this becomes a runaway process that destroys the beam. One of the uncertainties of cold-bore systems is the possibility that the desorption coefficient, η = desorbed molecules/incident ion, might be very high. Theory predicts that for a cold-bore system with high sticking probability, the product $\eta I_{crit} \simeq 10^{4}$ amps.

The only data for desorption of hydrogen from cold surfaces have been published by Erents and McCracken.[1] They used protons of a few keV to bombard films of frozen gas and measured η to be approximately $5x10^{4}$ for hydrogen and helium and much less for nitrogen and argon. Since the ions in our case will be a few hundred electron volts, we expect that an η of approximately 5×10^{3} is realistic, giving $I_{crit}\approx10A$. The current in the Energy Doubler at 5×10^{13} proton per pulse is 0.4A if the bunching factor is one, so we believe we are well below the limit for the pressure-bump instability.

E. Warm Regions

The long straight sections will be pumped by cryosorption pumps or titanium getter-ion pumps. This region can and will be baked in situ. A coaxial pumping region with chevron baffles can be installed in the beam tube to decrease the migration of gas into the cold region, and to reduce the heat leak due to radiation. With sufficient pumps, the pressure in the straight sections can be held to 10^{-9} to 10^{-10} Torr.

F. Valves

At the end of each cryogenic string, halfway between service buildings, there is a short (1-m) region for Joule-Thomson valves. This region will have a warm/cold interface, with a fast-acting vacuum valve to isolate the regions.

G. Insulating Vacuum

The vacuum in the insulating region should be between 10^{-4} and 10^{-5} Torr and should be able to be attained quickly. In order to get lateral pumping of the superinsulation, we will use aluminized Mylar with prepunched holes. These holes increase the pumping speed by orders of magnitude over edge pumping, without significantly increasing the effective emissivity. We will use a system similar to the present Main-Ring roughing system (perhaps even share the same one). This system consists of a mechanical pump and diffusion pump at each service building. Experiments are being done to determine the optimum frequency of pumps for quick roughing of the insulating system and beam tube.

Reference

[1]S. K. Erents and G. M. McCracken, J. Appl. Phys. 44, 3139 (1973).

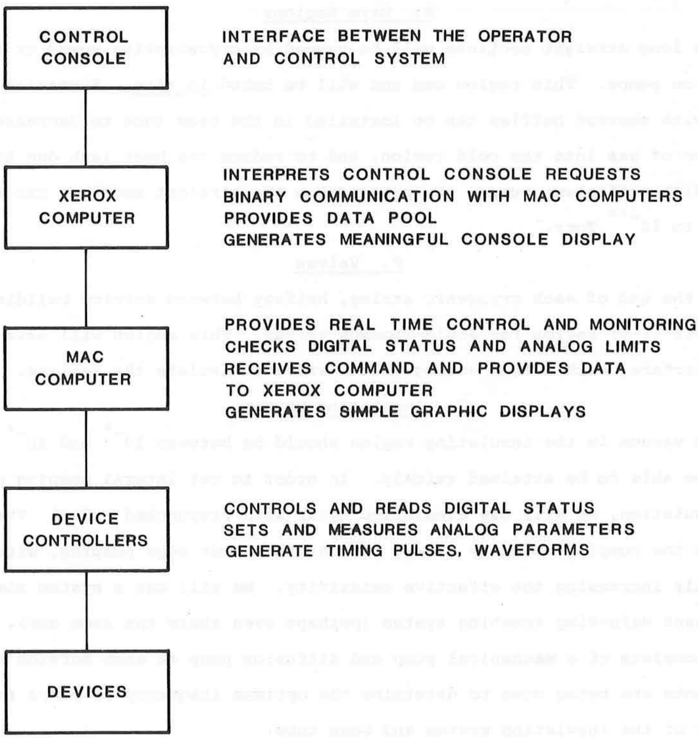

Fig. XIII-1. Control flow diagram.

APPENDIX XIII. CONTROLS FOR THE ENERGY DOUBLER

B. L. Chrisman

A. Introduction

The philosophy followed in the present Fermilab Computer Control and Monitoring System will be continued in the Energy Doubler Controls and Instrumentation. The present system has developed in an historical manner; many things that were done in the early phases of the accelerator are no longer necessary or have been replaced by new installations. Thus, there is considerable redundancy in the existing control system---enough so that the present system is capable of including the initial Doubler control with only minor extensions. Of course, there are modifications and extensions that make for convenience and improvement. These will be incorporated as operating experience is gained. Since the addition of the Doubler primarily impacts the Main Ring and Switchyard control system, a brief description of these segments of the entire system is presented first. Next a discussion of necessary modifications to the existing system is presented, followed by a discussion of new installations.

B. Present Control System

The present system and its components have been described previously.[1] In summary, the system is schematically shown in Figure XIII-1. The total Main-Ring control system is shown in Figure XIII-2.

The control console consists of interactive multicolored text-display terminals, CRT graphic-display unit, and necessary knobs, buttons and keyboard for operator control. The Xerox computer isequipped with 64K of core memory, a 48-Megabyte dual-spindle disc pack, and 12 interrupts. The Xerox RBM (Real-Time Batch Monitor) operating system, which is a relatively powerful system providing foreground/background capabilities, is used. The Xerox computer core assignment and timing cycle are shown in Figure XIII-3. The resident foreground includes the data pool, remote-and-local-console servicing programs, library routines, name tables, continuous plotting routines, etc.

The non-resident foreground is divided into three areas reserved for the application programs associated with three control consoles. The background is

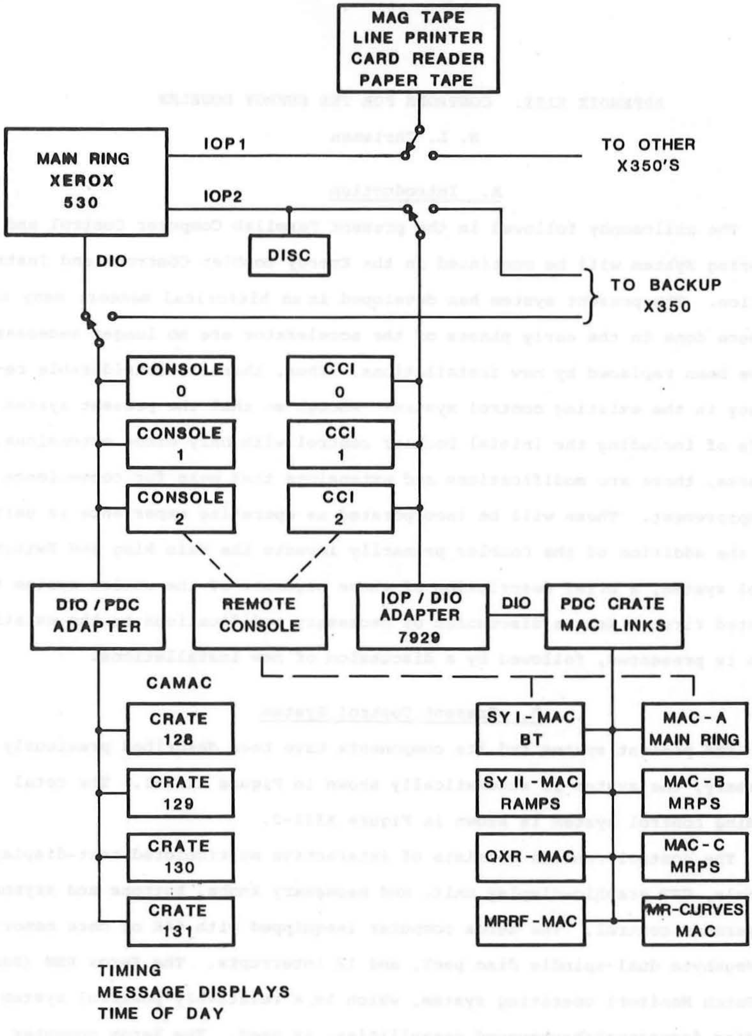

Fig. XIII-2. Main Ring and Switchyard control system.

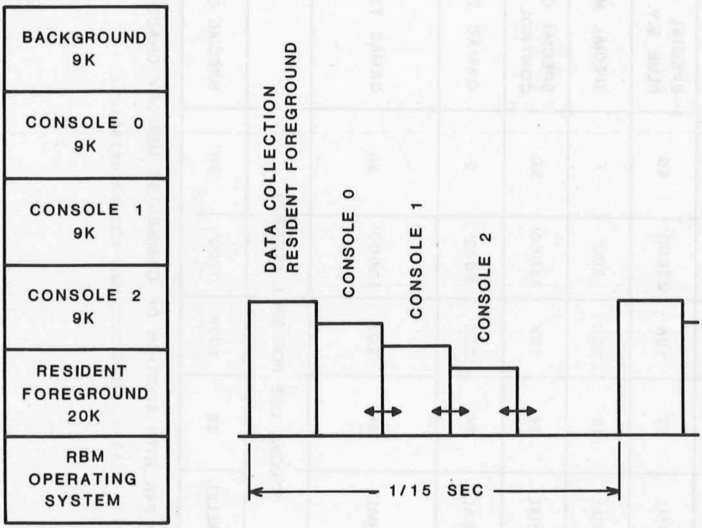

Fig. XIII-3. Main Ring Xerox computer core assignment and timing cycle.

			CONTROLLER LINK					
COMPUTER	PRESENT CORE	MAX CORE	CONTROLLER LINK	BITS PER LINK WORD	WORD RATE	TOTAL LENGTH	NO. CONTROLLERS	COMMENTS
MAC-A	16K	24K	SERIAL	32	10K	23000′	55	SPECIAL CONTROLLER PLUS S.Y. CRATE
MAC-B	8K	* 8K	SERIAL	18	35K	500′	1	SPECIAL MADC CONTROLLER
MAC-C	16K	24K	SERIAL	34	18K	23000′	30	SPECIAL CONTROLLER FOR P.S. CONTROL IN S.Y. CRATE
MR CURVES	8K	* 8K	SERIAL	34	25K	2000′	2	CAMAC TYPE HARDWARE
SY I	32Kc	64Kc	SERIAL	34	20K	10000′	30	CAMAC TYPE HARDWARE
SY II	8K	* 8K						
QXR	32Kc	64Kc	SPECIAL USE FOR SPILL CONTROL					
MR RF	24K	24K	PARALLEL	38	100K	1200′	38	SPECIAL CONTROLLER

* CAN BE EXPANDED TO 64K WITH ADDITION OF CAMBRIDGE MEMORY CHASSIS

Fig. XIII-4. MAC computer characteristics.

used for program development. A relocating loader is used that brings in a core image program from the disc and relocates it before execution. Overlaid programs are relocated into another disc file before execution, so that no overhead is required for overlay loading during execution.

The Xerox computer operates at a 15-Hz rate in serving consoles and communicating with the MAC computers. The 15-Hz rate was chosen because it is the injector pulse rate and provides a good response time to the consoles.

The Main-Ring Xerox computer communicates with eight MAC computers. The MAC computers are responsible for providing real-time control and monitoring, scanning devices for correct status and analog settings, sending alarms to the Xerox computers, generating simple graphic displays, and interpreting the commands and sending data to the Xerox computer. They are also used as software function generators, for making measurements at selected clock times, and for temporary storage of data needed by the Xerox computer.

The MAC computers are assigned particular areas of the accelerator and communicate with a number of device controllers to which the devices are connected. The MAC computers presently on the Main-Ring Xerox computer and the characteristics of their device controllers are shown in Figure XIII-4. Although different hardware schemes exist in the various areas, standard communication exists between the Xerox and all the MAC computers. All device controllers can revert to local control for testing and troubleshooting and are equipped for controlling a 64-channel A/D converter.

Various clocks are used to time the different accelerator areas. All are derived from a Master Clock having a nominal 1-MHz frequency that is synchronized to the 6-Hz line frequency. A selectable 5/10-kHz clock is distributed in the Main Ring and 1 MHz is distributed in Switchyard. These two clocks have a gap of four pulses at the start of the Main-Ring cycle. The Main-Ring rf system uses a 1-MHz booster clock which has various gaps at the booster 15-Hz rate. Device-controller timing modules are used to generate pulses at selected times in the accelerator cycle.

C. Modifications Necessary for Energy Doubler

Independent of the Energy Doubler, but also important to it, operating experience and increased demands on the Main-Ring control system have made it desirable to modify the existing system, which has changed little from the initial installation. In the past, for example, lightning storms and magnet failures have caused the dc-coupled link repeaters in several of the Main Ring service buildings to fail. These are being replaced with transformer-coupled links. In addition, to improve the utilization of cables around the ring, a block-transfer channel and a separate link for the utility crate are being installed without adding additional cables.

The bit rate on the data link will be increased to 1 MHz, decreasing the overall link transmission time by 10%. There are devices in the Main Ring requiring better timing resolution than provided by the present 10-kHz clock frequency, and installation of the 1-MHz clock used in the experimental areas will accomplish this. All these improvements to the Main-Ring system will occur with the replacement for the repeater system that is now being installed.

More directly related to providing a control system for the Energy Doubler is the present spare capacity in the installed Main-Ring control system. Each device slot in the utility crate typically handles one device, such as a power supply, timing modules, etc. Each DI and DO channel on the HLU provides 16 bits of data in or out. The 64-channel multiplexed A/D converter in each of the buildings has approximately 16 channels open. Thus, there is spare capacity available in each service building for use by the Energy Doubler and, if further channels are needed, it would be relatively easy to increase the capacity by the addition of more utility crates.

All 12 channels on both the North and South Main-Ring television systems are used. In fact, the Main-Ring South system, two additional channels, A and B, have been squeezed into the system. When additional channels are needed on the TV systems, new trunk-line amplifiers can be installed, which will provide 27 new channels.

D. New Installations for the Energy Doubler

The necessity of maintaining operation of the Main Ring during Doubler development will place a heavy burden of the existing Main-Ring/Switchyard computer/console system. Recently, work has begun on a network of PDP-11's for control of the external-beam lines. This was initiated to give more local control to each experimental area. In addition, this effort will allow the X530 computer currently used for the external-beam lines to be utilized in the Main Ring, Doubler and Switchyard. The configuration of the system would then

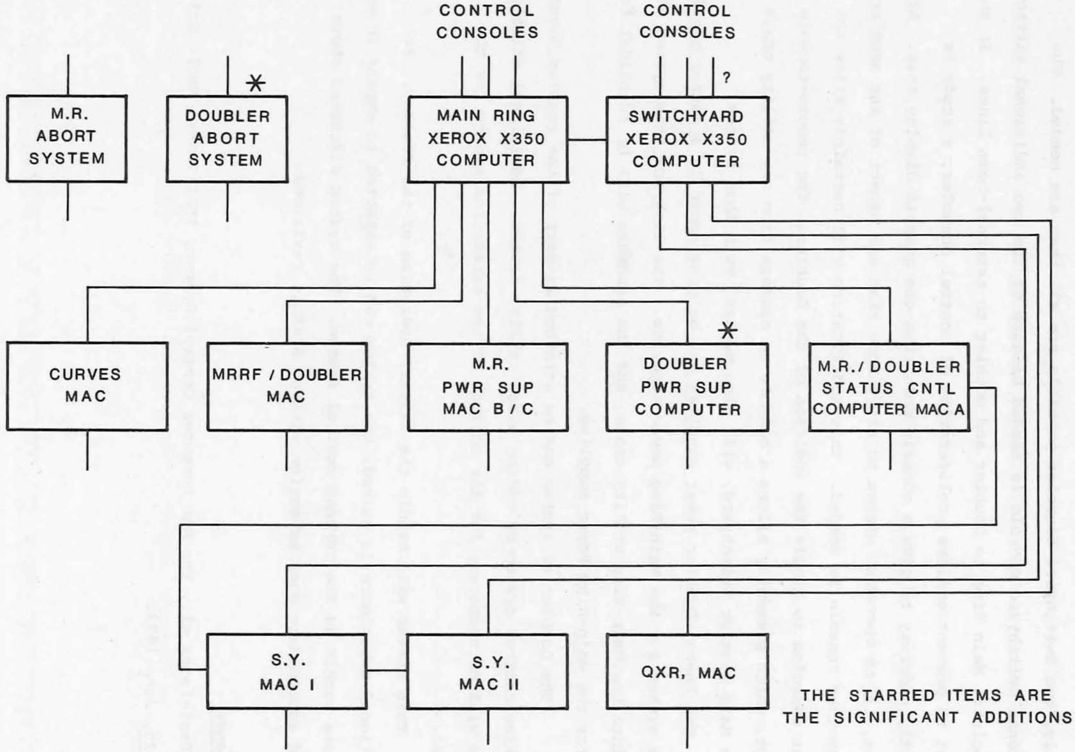

Fig. XIII-5. Proposed control configuration.

be as shown in Figure XIII-5. This configuration would allow three consoles to be shared by the Doubler and Main Ring plus up to three for the Switchyard. Actually, two Switchyard consoles probably are all that are needed. The additional Switchyard console is needed because of the two additional extraction points, Main Ring to Doubler and Doubler to external-beam lines. In an attempt to prevent endless proliferation of control consoles, a study is currently underway to give a console more than one graphic display unit. At present, if an operator wishes to study more than one aspect of the accelerator, another console is needed. This modification will certainly allow the present consoles to handle the addition of the Doubler. The remote-console concept, which presently allows a console to operate from any utility crate in the Main Ring or Switchyard, will also be used with this system.

The Energy-Doubler power supplies can be programmed in a manner similar to the system for the Main-Ring power supplies. The link for this system will plug into the Main-Ring utility crate, and the hardware will be identical to that for the Main-Ring Power supplies.

The Doubler rf system can be attached as part of the regular Doubler/Main-Ring control system by adding a few utility crates. Additional utility crates will be necessary for the control of the extraction system for the Doubler.

This system will handle the initial operation of the Doubler. As operational experience is gained, the system can be expected to expand in much the same manner as the current control system. The system discussed above should accommodate such expansion without drastic revisions.

Reference

[1]R. Daniels et al., The NAL Computer Control System, IEEE Trans. Nucl. Sci., NS 20, June 1973.

APPENDIX XIV. COST ESTIMATE AND SCHEDULE

J. E. Finks, Jr.

The cost of the Energy Doubler is determined by a number of factors and definitions. For example, how fast will it be funded, and what part of the experimental facilities will be defined as Doubler?

In our proposal of June 1975 when we anticipated receiving a "new construction" authorization, we estimated the costs on the basis of a definite schedule and on the scope of the Energy Doubler as specified in that proposal. Our estimate, based on a very rapid schedule of building the Doubler largely in FY 77, would still be \$35 million, and on a slower schedule to be about \$50 million. New data accumulated over the past year shows no reason to change that estimate.

At present the Doubler is being funded as an R&D project. At the rate we can anticipate funding, we are on a slow schedule so the total cost probably corresponds to approximately \$50 million. On the other hand there is a considerable difference between an effort undertaken with stretched-out funding on an R&D basis and the deliberate development of a totally funded new construction project. There are advantages as well as disadvantages to each method, and the total cost may turn out to be smaller - or larger. Clearly the Doubler implemented on an R&D basis will advance in stages that are more narrowly designated and the final scope of the project may be different than presently presented in this report because of developmental results.

As one example of how the program might proceed let us assume that \$10 million will be available in FY 77 and that about \$25 million will be availabale in FY 78. On that basis we should be able to build all of the magnets, to have installed them in the tunnel and to have sought a coasting beam before the end of FY 78. Expected results by fiscal year are as follows. (See also Schedule Table XIV-I.)

Fiscal Year 1976. During fiscal year 1976, extensive progress was made in the development of various models of components for the Energy Doubler. Major accomplishments included perfection of 23-strand, Rutherford-type superconductor cable, fabrication and testing of several 10-ft dipole magnets that reliably achieved the 45-kG design field, installation and operations of model magnets in the Main-Ring tunnel, and design and assembly of the first satellite refrigerator. Production of 22-ft Energy Doubler dipole magnets started on January 20, 1976. We tested the first 22-ft magnet on March 12 and were extremely pleased with this test, because it demonstrated convincingly our ability to produce full-size Energy Doubler magnets that meet performance requirements. By the end of FY 76, we should have fabricated six 22-ft magnets. With the ten magnets planned for the mini-year, this should give us enough dipoles to make up the first string of magnets from Service Building B-1 to the injection line. The first satellite refrigerator is presently being assembled and is scheduled for testing in the Village. Subsequent to testing, it will be moved to Service Building B-1, so that by October 1976 we may expect to have the first magnet string in place and, in addition, to be able to cool it with the satellite refrigerator. We plan to bring 100-GeV beam to B-1 through the Doubler magnets.

The production-magnet field-measurement device for the Energy Doubler development program has been assembled and tested. This includes the necessary magnet stands, a new search-coil system, the existing data-acquisition system, power supplies and junction boxes required by the new cryogenic system. General-purpose search coils, short and long, have been developed foruse with the Energy Doubler magnets.

During the mini-year (July-Sept. 1976), we will be severely limited in Energy Doubler production capability by the $11 million provided to the Laboratory by present financial plans. We will be able to finance a maximum of ten magnets during the mini-year. Not only will our in-house production suffer, but we will be forced to delay industry participation to develop magnet-production capability. Efforts on the satellite refrigerator system will be minimal during this time.

Fiscal Year 1977. The budget submitted by the President to the Congress for FY 77 requests $2 million specifically for Doubler R&D. With the funds requested by the President, some 80 Energy Doubler dipole magnets would be fabricated in-house and installed in the Main-Ring tunnel during FY 77. In addition, initial orders would be placed with three commercial firms for the construction of 25 dipole magnets (eight or nine magnets per firm) to be delivered in FY 78. This would allow qualification of the firms in anticipation of total project funding in FY 78 to allow completion of the Energy Doubler.

We have assumed that an additional $4 million will become available in FY 77, thereby allowing us to increase the production of the Doubler magnets to a total of 270. This corresponds to the example given above and to the entries for FY 77 in Table XIV-I.

The 1500-W helium refrigerator ordered from industry will be delivered and evaluated. Testing of the Fermilab-developed satellite refrigerator system will be completed and final specifications written to allow industry involvement in production of additional systems. Two more satellite refrigerators will be installed during FY 77, making a total of three by year-end.

R&D efforts will be continued to allow extraction of all possible useful information from the prototype systems and test loops until installation of the final magnets starts.

Fiscal Year 1978. During FY 78, we expect to achieve installation and operation in the Main-Ring tunnel of all Energy Doubler magnets, with the achievement of a coasting beam with acceleration at a slow repetition rate. This will allow the beginning of experiments in the new energy range using the Internal Target area. Attainment of a stored beam in the Doubler opens up the possibility of bringing about collisions between protons in the Main Ring with those in the Doubler. This possibility is being intensely evaluated.

About one-half of the satellite refrigerators will be installed by the end of FY 78. These will be adequate for achieving a circulating beam at a slow repetition rate.

Beyond Fiscal Year 1978. Installation of all components for the Energy Doubler will be completed in FY 79. Full-capacity refrigeration equipment will be installed to allow 10^{12} protons per sec accelerated to 1000 GeV. The 1000-GeV proton beam will be extracted and transported to experimental areas for use in physics experiments. Energy Doubler use will be programmed for electrical-power savings.

Table XIV-I. Energy Doubler Cost Estimate*
(to circulating beam)

	FY 77	FY 78
MAGNETS		
Number of 22-ft Dipole Magnets	270	530
Number of Quadrupole Magnets & Correction Elements	0	200
Dipole Magnet Cost	$ 5,400	$11,600
Quadrupole Magnet & Correction Element Cost		1,800
Subtotal - Magnet Cost	$ 5,400	$13,400
OTHER COMPONENTS		
Vacuum	$ 80	$ 300
Controls		300
RF		1,200
Power Supplies		300
Beam Transfer		600
Supports	70	700
Conventional Utilities		1,000
Subtotal - Other Components	$ 150	$ 4,400
ANNUAL R&D	$ 4,000	$ 5,000
SATELLITE REFRIGERATOR SYSTEM	$ 450	$ 2,200
TOTAL - Energy Doubler/Saver (less Central Helium Liquefier, and Contingency)	$10,000	$25,000

*In thousands of dollars

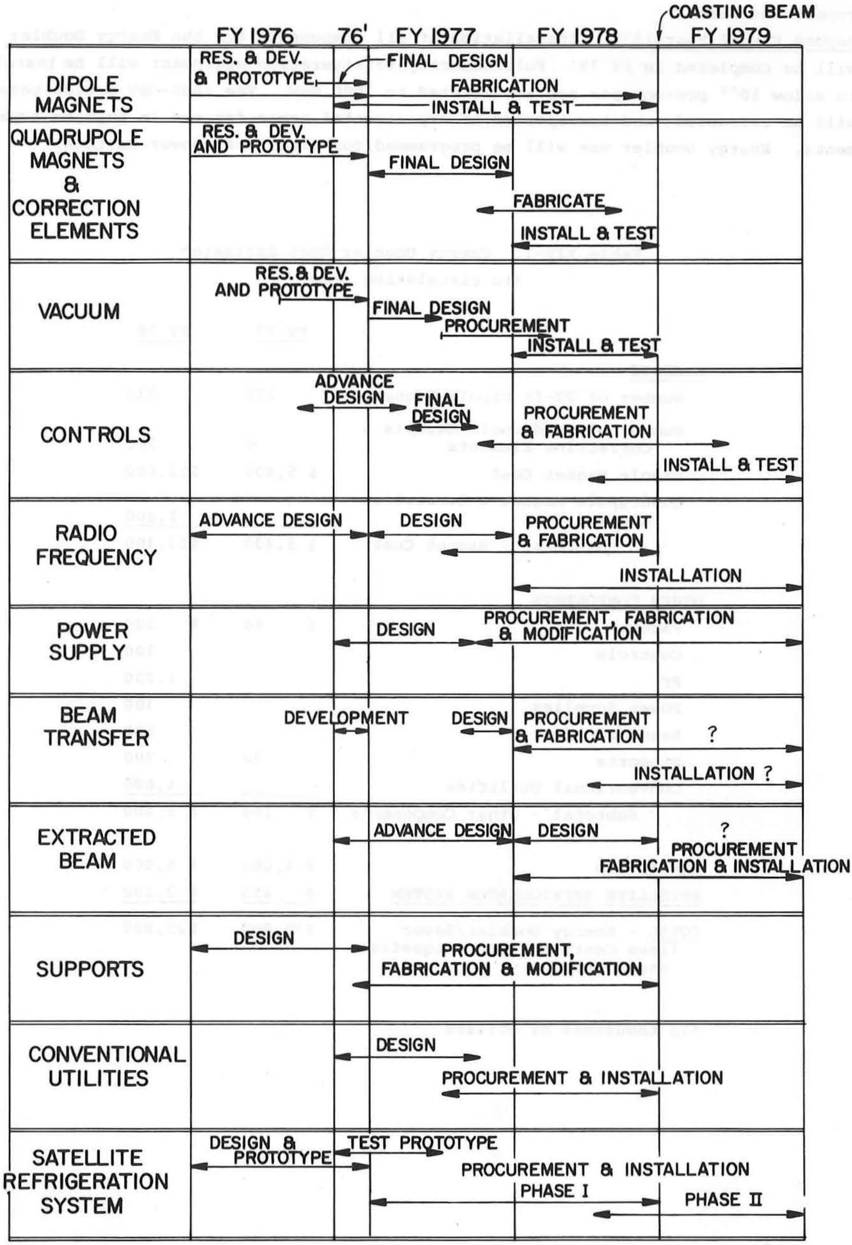

COASTING BEAM
FY 1976
76'
FY 1977
FY 1978
FY 1979
DIPOLE MAGNETS
RES. & DEV. & PROTOTYPE
FINAL DESIGN
FABRICATION
INSTALL & TEST
QUADRUPOLE MAGNETS & CORRECTION ELEMENTS
RES. & DEV. AND PROTOTYPE
FINAL DESIGN
FABRICATE
INSTALL & TEST
VACUUM
RES. & DEV. AND PROTOTYPE
FINAL DESIGN
PROCUREMENT
INSTALL & TEST
CONTROLS
ADVANCE DESIGN
FINAL DESIGN
PROCUREMENT & FABRICATION
INSTALL & TEST
RADIO FREQUENCY
ADVANCE DESIGN
DESIGN
PROCUREMENT & FABRICATION
INSTALLATION
POWER SUPPLY
DESIGN
PROCUREMENT, FABRICATION & MODIFICATION
BEAM TRANSFER
DEVELOPMENT
DESIGN
PROCUREMENT & FABRICATION
?
INSTALLATION ?
EXTRACTED BEAM
ADVANCE DESIGN
DESIGN
?
PROCUREMENT FABRICATION & INSTALLATION
SUPPORTS
DESIGN
PROCUREMENT, FABRICATION & MODIFICATION
CONVENTIONAL UTILITIES
DESIGN
PROCUREMENT & INSTALLATION
SATELLITE REFRIGERATION SYSTEM
DESIGN & PROTOTYPE
TEST PROTOTYPE
PROCUREMENT & INSTALLATION
PHASE I
PHASE II

APPENDIX XV. ENERGY DOUBLER PARAMETERS

L. C. Teng

A. Principal Parameters

1.	Final energy	1000 GeV
2.	Intensity	5×10^{13} protons/pulse
3.	Circumference	6283.185 m (20614.13 ft)
4.	Magnetic radius	788.49 m (2586.9 ft)
5.	Lattice type	Separated function with matched long straight sections
6.	Injection energy	100 GeV
7.	Betatron-oscillation wave number	19.4
8.	Synchrotron-oscillation wave number	$(2.4 \text{ to } 1.1)\times10^{-13}$
9.	Transition kinetic energy	16.7 GeV
10.	Rise time (Fall time)	24 sec
11.	Flat-top time	10 sec
12.	Repetition rate	1 pulse/min
13.	Duty factor	1/6
14.	Beam emittance at 1000 GeV	0.02π mm-mrad
15.	Momentum resolution	10^{-4}

B. Lattice Structure and Orbit Parameters

1.	Normal cell (C)	
	a. Length of dipole (B)	252 in.
	b. Length of cell quadrupole (QF and QD)	53 in.
	c. Length of separation between magnets (S)	12 in.
	d. Length of mini straight section (SS)	62 in.
	e. Cell structure	(QF)SS(B)S(B)S(B)S(B)S (QD)SS(B)S(B)S(B)S(B)S
	f. Length of cell	2342 in.
	g. Number of normal cells	84
2.	Cell with medium straight section (M)	
	a. Length of medium straight section (MS)	590 in.
	b. Cell structure	(QF)MS(B)S(B)S (QD)SS(B)S(B)S(B)S(B)S
	c. Length of cell	2342 in.
	d. Number of cells with MS	6
3.	Cell with matched long straight section (L)	
	a. Length of cell	6098.25 in.
	b. Number of cells with LS	6
4.	Sector	
	a. Structure	LCCMCCCCCCCCCCC
	b. Length of sector	41228.25 in.(1047.198m)
	c. Number of sectors	6
5.	Pulse form	
	a. Rise and fall time between 100 GeV and 1000 GeV	24 sec
	b. Flat-top time	10 sec
	c. Bottom turn-around time	2 sec
	d. Total cycle time	60 sec

C. Magnet System

1.	Rise time (fall time)	24 sec
2.	Flat-top time	10 sec
3.	Dipole	
	a. Number of unit	774
	b. Effective field length	252 in.
	c. Coil length	258 in.
	d. Gross length	264 in.
	e. Coil ID	3.0 in.
	f. Aperture diameter	2.25 in.
	g. Field at 1000 GeV	42.344 kG
	h. Number of coil turns per pole	34 + 21
	i. Current at 1000 GeV	4343 A
4.	Normal-cell quadrupoles	
	a. Number of units	180
	b. Effective gradient length	53 in.
	c. Coil length	59 in.
	d. Gross length	65 in.
	e. Coil ID	3.25 in.
	f. Aperture diameter	2.5 in.
	g. Field gradient at 1000 GeV	24.1 kG/in.
	h. Number of coil turns per pole	16 + 13 + 10
	j. Current at 1000 GeV	4343 A

D. Refrigeration System

1.	Heat load per dipole	13 W (2W/m)
2.	Heat load per quadrupole	3 W (2W/m)
3.	Total heat load	10.8 kW
4.	No. of satellite refrigerators	24
5.	He circuits	48
6.	Magnets in each circuit	

Circuit	B	Q7	Q4
I-U	16	4	4
I-D	18	5	-
II-U	16	4	-
II-D	16	4	-
III-U	16	4	-
III-D	16	4	-
IV-U	16	4	-
IV-D	15	3	4

7. Capacity per satellite refrigerator 450 W (150 ℓ/hr.)

E. Vacuum System

1.	Vacuum-enclosure temperature	4.2 K
2.	Vacuum pressure (at 4.2 K)	10^{-8} Torr (10^{-11} Torr for Storage Ring mode)

F. Radio-Frequency System

1.	Injection energy	100 GeV
2.	Final energy	1000 GeV
3.	Acceleration Cycle Time	
	a. Rise or fall time	24 sec
	b. Flat-top time	10 sec
	c. Bottom turn-around time	2 sec
	d. Total cycle time	60 sec
4.	Field rise-rate	1.59 kG/sec
5.	Energy Gain per turn	0.786 MeV/turn
6.	Synchronous phase	42°
7.	Peak rf voltage per turn	1.175 MV/turn
8.	Harmonic number	2226
9.	Injection frequency	106.2056 MHz
10.	Final frequency	106.2102 MHz
11.	Relative frequency range	4.28×10^{-5}
12.	Number of cavities	1

13.	Cavity type	Cylindrical 140° double gap drift-tube cavity
14.	Cavity length	45 in.
15.	Cavity diameter	30 in.
16.	Beam current ($5x10^{13}$ protons)	0.382 A
17.	Power to beam	300 kW
18.	Cavity shunt impedance	1 MΩ
19.	Power to cavity	100 kW
20.	Total rf power	400 kW
21.	Future addition	3 cavities will accelerate at 100 GeV/sec

G. Beam Transfer System

1.	Extraction kicker in MR	
	Location	A46
	Length	1.5 m
	Field	1 kG
	Rise time	<0.2 μsec
	Kick angle (horizontal out)	0.44 mrad
	Horizontal beam displacement from central orbit at A50	30 mm
	Horizontal beam angle at A50	0.13 mrad
2.	Extraction Lambertson	
	Length	8.0 m
	Location	A50 (-25 m to -17 m from B0)
	Septum position	25 mm outward from central orbit
	Field	9.16 kG
	Bend angle (vertical down) (skewed slightly to take out the horizontal beam angle of 0.13 mrad)	21.8 mrad
	Horizontal beam displacement from central orbit	30 mm
3.	Injection Lambertson	
	Length	8.0 m
	Location	B0 (-4 m to +4 m)
	Septum position	20 mm outward from central orbit
	Field	9.16 kG
	Bend angle (vertical up) (skewed slightly to produce a horizontal beam angle of -1.32 mrad)	21.8 mrad
	Vertical beam displacement from MR orbit	-457 mm = 18 in. (beam vertically on ES/D orbit)
	Horizontal beam displacement from central orbit	30 mm
4.	Injection kicker in ES/D	
	Length	4.5 m
	Location	B10 (20.5 m to 25 m)
	Field	1 kG
	Fall time	<0.2 μsec
	Kick angle (horizontal out) (after kick beam on ES/D orbit)	1.32 mrad

H. Extraction System

1.	Extraction Channel	
	a. Location	Long Straight A
	Entrance	F50 (-25.4 m from A0)
	Exit	72.375 m (from A0)
	(at exit the beam follows the present EPB line)	
	b. Lambertson (vertical up)	
	Length	20 m
	Location	-25.4 m to -5.4 m

Field	8.937 kG
Bend angle	5.35 mrad
Septum position	11 mm outward from central orbit
Septum thickness	2 mm
Beam vectors	Entrance / Exit
Horizontal:	$\begin{pmatrix} 15\text{ mm} \\ 0\text{ mrad} \end{pmatrix}$ $\begin{pmatrix} 15\text{ mm} \\ 0\text{ mrad} \end{pmatrix}$
Vertical:	$\begin{pmatrix} 0 \\ 0 \end{pmatrix}$ $\begin{pmatrix} 53.5\text{ mm} \\ 5.35\text{ mrad} \end{pmatrix}$

c. Superconducting dipole (horizontal out)

Length	20 m
Location	4.6 m to 24.6 m
Field	40.017 kG
Bend angle	23.97 mrad
Beam vectors	Entrance / Exit
Horizontal:	$\begin{pmatrix} 15\text{ mm} \\ 0\text{ mrad} \end{pmatrix}$ $\begin{pmatrix} 254.7\text{ mm} \\ 23.97\text{ mrad} \end{pmatrix}$
Vertical:	$\begin{pmatrix} 107.1\text{ mm} \\ 5.35\text{ mrad} \end{pmatrix}$ $\begin{pmatrix} 214.1\text{ mm} \\ 5.35\text{ mrad} \end{pmatrix}$

d. Skew superconducting dipole (in and down)

Length	4.76 m
Location	67.62 m to 72.38 m
Skew angle	Bending direction 20.2° from vertical
Field	-40.016 kG
Bend Angle	-5.70 mrad (horizontal -1.97 mrad) (vertical -5.35 mrad)
Beam vectors	Entrance / Exit
Horizontal:	$\begin{pmatrix} 1285.9\text{ mm} \\ 23.97\text{ mrad} \end{pmatrix}$ $\begin{pmatrix} 1395.4\text{ mm} \\ 22.0\text{ mrad} \end{pmatrix}$
Vertical:	$\begin{pmatrix} 444.5\text{ mm} \\ 5.35\text{ mrad} \end{pmatrix}$ $\begin{pmatrix} 457.2\text{ mm} \\ 0\text{ mrad} \end{pmatrix}$

(at exit beam follows present EPB line)

e. Overall geometry

2. Slow extraction (horizontal $\frac{1}{3}$-integer resonance)

a. Sextupole

Location	10 m downstream of D0
Length	2 m
Strength	$B'' = 1.22$ kG/cm^2

b. Electrostatic wire-septum

Location	F10 (downstream end of long straight F)
Septum position	20 mm outward from central orbit
Thickness	0.05 mm
Length	6 m
Field	100 kV/cm
Deflection angle	0.06 mrad
Aperture	1 cm^2

c. Extraction channel

Entrance location	F50 (upstream end of long straight A)
Entrance septum thickness	2 mm

(For details see Extraction channel)

d. Beam behavior

Extraction starts	$\nu_h = 19.3364$
Extraction completes	$\nu_h = 19.3333$

(Long-spill mainly by momentum pealing)

Step-size at ES septum	9 mm

	Horizontal Vectors: Just inside ES-septum	Just outside ES-septum	Extreme outside
Entrance to ES-septum	(20.0 mm, 0.21 mrad)	(20.0 mm, 0.21 mrad)	(29.0 mm, 0.30 mrad)
Exit from ES-septum	(21.3 mm, 0.21 mrad)	(21.5 mm, 0.27 mrad)	(31.0 mm, 0.36 mrad)
Entrance to channel	(9.3 mm, -0.16 mrad)	(12.5 mm, -0.08 mrad)	(16.7 mm, -0.16 mrad)
Gap to clear channel septum		3.2 mm	

Width of beam entering channel	4.2 mm
Average vector of beam entering channel (with orbit tilt)	(15 mm, 0 mrad)

3. Fast extraction (horizontal one-turn)
   a. Fast kicker

Location	A10 (downstream end of long straight A)
Length	3 m
Field	1 kG
Kick angle	0.09 mrad
Rise time	<0.2 μsec

   b. Beam at entrance to channel (F50)

Displacement kicked	6.6 mm
Width of beam	2.2 mm
Gap to clear channel septum	4.4 mm